AD-A130 021 MEASUREMENT AND THEORY OF THE HALL SCATTERING FACTOR AND THE CONDUCTIVITY..(U) DAYTON UNIV OH RESEARCH INST F SZMULOWICZ ET AL. APR 83 AFWAL-TR-83-4043 1/2

UNCLASSIFIED F33615-81-C-5095 F/G 20/12 NL

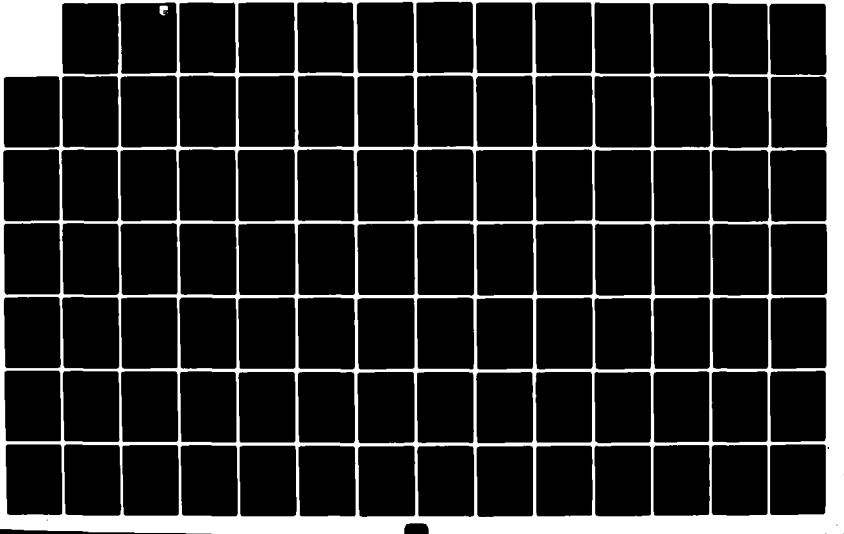

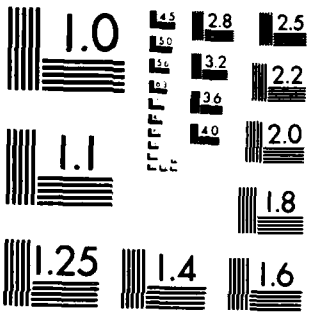

AFWAL-TR-83-4043

MEASUREMENT AND THEORY OF THE HALL SCATTERING FACTOR AND THE CONDUCTIVITY MOBILITY IN ULTRA PURE p-TYPE SILICON AT LOW TEMPERATURES

F. Szmulowicz
University of Dayton
Research Institute
Dayton, Ohio

W. Mitchel
Materials Laboratory
Air Force Wright Aeronautical Laboratories
Wright-Patterson Air Force Base, Ohio

F. Madarasz
University of Dayton
Research Institute
Dayton, Ohio

P. Hemenger
Materials Laboratory
Air Force Wright Aeronautical Laboratories
Wright-Patterson Air Force Base, Ohio

April 1983

Interim Report for Period 1 September 1981 - 31 March 1983

Approved for public release; distribution unlimited

MATERIALS LABORATORY
AIR FORCE WRIGHT AERONAUTICAL LABORATORIES
AIR FORCE SYSTEMS COMMAND
WRIGHT-PATTERSON AIR FORCE BASE, OHIO 45433

NOTICE

When Government drawings, specifications, or other data are used for any purpose other than in connection with a definitely related Government procurement operation, the United States Government thereby incurs no responsibility nor any obligation whatsoever; and the fact that the government may have formulated, furnished, or in any way supplied the said drawings, specifications, or other data, is not to be regarded by implication or otherwise as in any manner licensing the holder or any other person or corporation, or conveying any rights or permission to manufacture use, or sell any patented invention that may in any way be related thereto.

This report has been reviewed by the Office of Public Affairs (ASD/PA) and is releasable to the National Technical Information Service (NTIS). At NTIS, it will be available to the general public, including foreign nations.

This technical report has been reviewed and is approved for publication.

DAVID W. FISCHER
Project Monitor
Laser & Optical Materials Branch

G. EDWARD KUHL, Chief
Laser & Optical Materials Branch
Electromagnetic Materials Division

FOR THE COMMANDER

MERRILL L. MINGES, Chief
Electromagnetic Materials Division
Materials Laboratory
Air Force Wright Aeronautical Laboratories

"If your address has changed, if you wish to be removed from our mailing list, or if the addressee is no longer employed by your organization please notify AFWAL/MLPO, W-PAFB, OH 45433 to help us maintain a current mailing list".

Copies of this report should not be returned unless return is required by security considerations, contractual obligations, or notice on a specific document.

REPORT DOCUMENTATION PAGE		READ INSTRUCTIONS BEFORE COMPLETING FORM
1. REPORT NUMBER	2. GOVT ACCESSION NO.	3. RECIPIENT'S CATALOG NUMBER
4. TITLE (and Subtitle) MEASUREMENT AND THEORY OF THE HALL SCATTERING FACTOR AND THE CONDUCTIVITY MOBILITY IN ULTRA PURE p-TYPE SILICON AT LOW TEMPERATURES		5. TYPE OF REPORT & PERIOD COVERED Interim Report 6. PERFORMING ORG. REPORT NUMBER
7. AUTHOR(s) F. Szmulowicz, W. Mitchel, F. Madarasz, P. Hemenger		8. CONTRACT OR GRANT NUMBER(s) F33615-81-C-5095
9. PERFORMING ORGANIZATION NAME AND ADDRESS University of Dayton Research Institute 300 College Park Avenue Dayton, Ohio 45469		10. PROGRAM ELEMENT, PROJECT, TASK AREA & WORK UNIT NUMBERS 2306 Q1 06
11. CONTROLLING OFFICE NAME AND ADDRESS Materials Laboratory (AFWAL/MLP) AF Wright Aeronautical Laboratories, AFSC Wright-Patterson Air Force Base, Ohio 45433		12. REPORT DATE April 1983 13. NUMBER OF PAGES 98
14. MONITORING AGENCY NAME & ADDRESS(if different from Controlling Office)		15. SECURITY CLASS. (of this report) Unclassified 15a. DECLASSIFICATION/DOWNGRADING SCHEDULE

16. DISTRIBUTION STATEMENT (of this Report)

Approved for public release; distribution unlimited

17. DISTRIBUTION STATEMENT (of the abstract entered in Block 20, if different from Report)

18. SUPPLEMENTARY NOTES

19. KEY WORDS (Continue on reverse side if necessary and identify by block number)

Conductivity mobility, Hall mobility, Hall scattering factor, r-factor, acoustic phonon-limited mobilities, high purity p-type silicon, p-type germanium, Boltzmann equation, distribution functions cubic harmonics, deformation potential theory, high and low field Hall coefficient measurements, Hall bar, van der Pauw configuration

20. ABSTRACT (Continue on reverse side if necessary and identify by block number)

Acoustic phonon-limited conductivity and Hall mobilities for p-type silicon and germanium have been calculated from solutions of the full Boltzmann equation without the relaxation time approximation. These quantities have been measured as well for p-type silicon in the temperature range 20-50K. Using the deformation potential scattering theory of Tiersten we obtain the necessary hole-acoustic phonon transition rates, with no adjustable parameters, as a first-

20. Continued

principles input into the transport equations. Excellent agreement is found for both mobilities with our experimental data on silicon. Calculated results were compared with data from the open literature on germanium and similar agreement is found for the conductivity mobility. The success of this calculation is due to the inclusion of all three top valence bands, careful treatment of the scattering matrix elements, and the use of the full Boltzmann equation solutions to obtain the transport coefficients. Results of our calculation confirm the quantitative accuracy of the deformation potential theory.

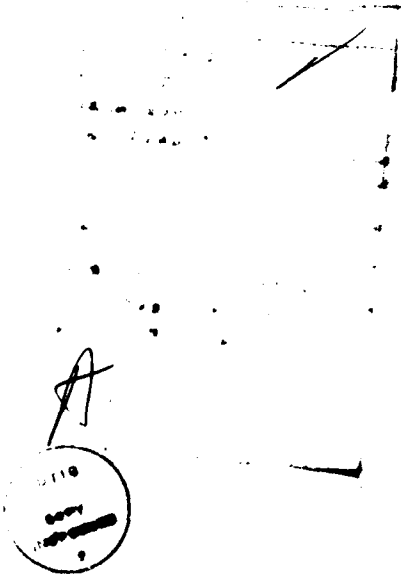

PREFACE

The electrical behavior of a semiconductor is critical to its usefulness in a broad spectrum of applications ranging from infrared sensitive detectors and microwave amplifiers to high density integrated circuits. This behavior is controlled by extremely low concentrations of impurities and defects in the semiconductors and by its temperature. The only method available for quantitatively measuring small impurity concentrations and determining their identities is based upon the Hall effect. The electrical transport properties, namely resistivity, Hall mobility, and carrier concentration are calculated as functions of temperature by combining resistivity and Hall effect measurements. The temperature dependent carrier concentration data is analyzed to obtain the concentrations and identities of the impurities. Concentrations of less than $5 \times 10^{11} cm^{-3}$ (1 part in 10^{11}) are measured routinely in silicon.

Interpretation of the Hall data is limited by our incomplete knowledge of the Hall scattering factor (or r-factor) which is the ratio of the Hall mobility to the conductivity mobility, $r = \mu_H / \mu_c$. The data analysis calls for the conductivity mobility while the Hall mobility is provided by the experiment. Uncertainties in dopant concentration as great as 50% can result when little or no information is available on the precise values and the temperature dependence of the r-factor. Unfortunately, no straightforward experimental method is available to measure r(T) over all temperatures and impurity concentrations of interest, due in the case of silicon to material and facilities limitations, mainly a sufficiently large magnetic field.

Theory of charge carrier scattering can in principle be used to calculate $\mu(T)$ over all physically realistic temperature and impurity ranges. By comparing theoretical functions with experimental results taken over a sufficiently broad region, parameter selection can be verified and the theoretical functions can be extended with confidence to temperature and impurity ranges unreachable experimentally.

Two primary developments prompted undertaking a new and more thorough solution to the r(T) problem, namely the increasing technological importance of more precise silicon analyses and the availability of ultra-high purity silicon that made new experimental measurements feasible. A coordinated experimental and theoretical program was planned and implemented to solve the low temperature region in p-type silicon where charge carrier transport is limited by acoustic phonon scattering. New results are presented for silicon and germanium and impurity analysis has been significantly improved as demonstrated for the silicon case. It is planned to extend the theoretical calculations to higher temperatures through the inclusion of optical phonon scattering which will build directly upon the acoustic phonon work. It is hoped to eventually complete the low temperature region for doped semiconductors by solving the ionized impurity scattering problem.

The theoretical work was performed under Air Force Contract Nos. F33615-78-C-5064 and F33615-81-C-5095 at the Materials Laboratory, Wright-Patterson Air Force Base, Ohio. We are indebted to Mr. John A. Detrio of the University of Dayton Research Institute for his long-standing support of this work. W. C. Mitchel gratefully acknowledges support by a National Research Council Fellowship. We would also like to acknowledge Drs. R. S. Allgaier, P. J. Price, M. Tiersten, J. C. Hensel, S. Zukotynski, C. Elbaum, J. E. Lang, and C. Searle, for many helpful discussions. A special note of thanks goes to Miss Niki Maxwell for a fine and meticulous job in typing the manuscript.

TABLE OF CONTENTS

LIST OF ILLUSTRATIONS

LIST OF ILLUSTRATIONS
(Continued)

LIST OF ILLUSTRATIONS
(Concluded)

LIST OF TABLES

SECTION I
INTRODUCTION

The Hall effect has long been one of the principal means of characterizing semiconductors. The hole concentration can be determined from the relation $p=r/eR_H$ where R_H is the Hall coefficient and r is a dimensionless parameter of order one called the Hall factor which depends on both the band structure and the scattering mechanisms of the material being studied as well as on the magnetic field. Measurement and curve fitting of the carrier concentration as a function of temperature yields information on the identities and concentrations of dopants and impurities in the material. In addition, the carrier concentration can be used with the conductivity, σ, to determine the mobility from the definition $\mu_c \equiv \sigma/pe = \sigma R_H/r$. Because the Hall factor is not known precisely, it is often set equal to one for convenience. Unfortunately, this assumption is strictly valid only for degenerate semiconductors or when the magnetic field is high enough that the magnetic motion dominates the scattering. This occurs when $\omega_c\tau >> 1$. Here $\omega_c = eH/m^*$ is the cyclotron frequency and $\tau = \sigma m^*/pe^2$ is the scattering time. H is the magnetic flux density and m^* is an effective mass. For many practical situations the condition, $\omega_c\tau >> 1$, is unattainable. For this reason a distinction is made between two mobility definitions. The conductivity mobility is defined as $\mu_c = \sigma/pe$ and the Hall mobility is defined as $\mu_H = \sigma R_H$. The ratio of the two mobilities, μ_H/μ_c is therefore the Hall factor. The conductivity mobility is the one most often calculated by theorists and the low field Hall mobility is the one most often experimentally determined. This unfortunate situation has developed over the years because, while the Hall mobility is the easiest to measure, the conductivity is the easiest to calculate since it contains only one component of the magnetoconductivity tensor, σ_{xx}, but the Hall mobility contains two, σ_{xx} and σ_{xy}. A similar situation exists when one attempts to use Hall effect data to determine the dopant or impurity concentration, but here no formal distinction is made between the actual

concentrations and those determined by assuming a simple form for r. Traditionally the form of r used to analyze the data is mentioned in the report so there is rarely any real confusion, but, unless the Hall effect measurements were made in the high field limit or the correct r used in the data analysis, the resultant dopant concentration can be off by as much as a factor or two when compared with the results of other techniques such as C-V[1] or neutron activation analysis[2].

We have measured the magnetic field dependence of the Hall coefficient as a function of temperature of ultra-pure, p-type silicon. We have determined both the high and low field limits, $\omega_c\tau>>1$, and $<<1$ respectively. We have determined the Hall factor from the relation $r=R_H(0)/R_H(\infty)$, and we have also determined the low field Hall and the conductivity mobilities, all in the temperature range 20-50K.

Theoretical modeling in support of the experimental effort was motivated by a general lack of theoretical calculations for p-type silicon carried from first-principles without adjustment of parameters to fit the data. Acoustic phonon-limited electronic transport in diamond[3-25] and zincblende[26-28] type structures has often been modeled within the framework of the deformation potential theory. Within the theory the strength of the carrier-phonon interaction is governed by an experimentally determined set of deformation potential parameters. These parameters are obtained from experiments which measure shifts and distortions of the bands upon application of selected strains to the crystal[29-39]. However, in some versions of the scattering theory it has been found necessary to regard these interaction parameters as adjustable in order to obtain a quantitative agreement with the transport data. This is particularly the case in the transport calculations for p-type materials[10-14,17,21-24] where either effective deformation potentials or the relaxation times were fitted to the transport data.

The need for adjustment of parameters arises as a result of approximations introduced in the theoretical treatment of the

full deformation potential scattering theory. It is a common simplification to use a relaxation time approximation for the solution of the Boltzmann equation. One of the most elaborate examples of such a model is provided in the work of Bir, Normantas, and Picus[6]. This model employs separate intra- and interband relaxation rates which depend on averaged deformation potential constants whose magnitudes are varied in the calculation. Other authors have considered separate relaxation times for each band, with a common effective deformation potential, but without any interband coupling[10,14,16,22,25].

Along with the relaxation time approximation, the degree to which the full nonspherical-nonparabolic nature of the valence bands has been taken into account, at various points in the calculation, has varied from one theoretical treatment to another. The simplest approach, as for example that taken by Bir et al.[6] and Costato et al.[14], is to consider just the two top valence bands - the heavy hole band and the light hole band. Both bands are treated as spherical-parabolic. A slightly more complex model treats the light hole band on the average as nonparabolic. This model was set by Ottaviani et al.[16] who also considered a single nonspherical but parabolic band model along with a Monte Carlo technique in order to study the effects of anisotropy[16]. Asche and von Borzeszkowski[22], on the other hand, studied the effect of band nonparabolicity on mobilities. In order to account for band nonparabolicities as accurately as possible they calculated the hole density of states factors in the relaxation rates by using a spherically averaged Kane[40] secular equation, which results in isotropic bands. Following Asche and von Borzeszkowski, Nakagawa and Zukotynski[10] performed a calculation in the same spirit but did not spherically average the bands. And, more recently, Takeda, Sakui and Sakata[25] repeated the work on Nakagawa and Zukotynski but in addition considered the spin-orbit split-off band's contribution to the mobility[25]. In view of the number of approximations introduced in previous treatments of the problem it appears worthwhile to approach the problem again from a first principles point of view, without the band shape or the relaxation time approximations.

Except for the treatments of Tiersten[3] and Lawaetz[4] for Ge, a complete implementation of the deformation potential theory has not been pursued from first principles. These two authors did not use the relaxation time approximation but instead each solved the Boltzmann equation directly. Tiersten used the deformation potential theory of Whitfield[41] and the vector mean free path theory of Price[42] to solve the Boltzmann equation. Lawaetz, on the other hand, used the transition rates of Bir and Picus[5] and solved the Boltzmann equation by expanding the distribution function in cubic harmonics. Both methods were found to agree with one another to within 2% for the conductivity mobility of Ge and were within a few percent of the experimental mobility. In addition, Lawaetz calculated the Hall mobility and other galvanomagnetic coefficients. Here he found that his results could not be reconciled with the independently measured set of deformation potential parameters. Partly, this discrepancy can be attributed to the incomplete knowledge of the parameters, or to the quality of data used for comparison with the theory. In our work, however, we will show that the results for the Hall mobility, at least, can be improved by treating the light hole band as nonparabolic, which was done by neither Tiersten nor Lawaetz.

No comparable treatment to that of Tiersten or Lawaetz has been tried for p-type silicon. Whereas germanium has a large 0.30 eV spin-orbit splitting, in silicon the corresponding splitting is only 0.044 eV. Therefore, its bands are decidedly more nonparabolic than is the case for germanium. Even in the case of germanium we will show that light holes dominate the Hall mobility, and the light hole band's nonparabolicity, however small, does influence the results. To this end we have calculated hole — acoustic-phonon transition rates for Si and Ge using experimentally determined deformation potential parameters. We pointed out in two previous papers[43,44], that inclusion of the full nonparabolic nature of the Si valence band system results in a strikingly energy dependent set of transition probabilities.

Parabolic bands, though, lead to energy independent transition probabilities.

The goal of the present work is to fully implement the deformation potential theory for the calculation of conductivity and Hall mobilities in Si and Ge, with emphasis on Si, in the acoustic phonon limited regime. By using the eigenfunctions obtained from the numerical solution of the full 6x6 $\vec{k}\cdot\vec{p}$ Hamiltonian we make no approximations concerning the nonspherical-nonparabolic nature of the Si valence band structure. Our transition probabilities are energy dependent and depend on both the incident and scattered hole wave vectors as well. We solve the Boltzmann equation directly, by a variant of the method used by Lawaetz[4], for the distribution function. Then, analogously to Lawaetz, we obtain the conductivity and Hall mobilities.

In Section II we formulate the transport theory to be used in the present work. Our formalism differs in a few details from that of Lawaetz who, in addition, has not provided the full derivation. Given the complexity of the formalism, we include in Section III details of the computational procedure and ways to simplify its various steps. Section IV is used as a test of the computational scheme. Here we use the parameters of Tiersten and Lawaetz for Ge and exhibit an overall agreement between our respective results. In the case of the Hall mobility we show an overall improvement in our results as compared with experiment. Section V is devoted to the presentation of experimental and theoretical results for Si. Conclusions are presented in Section VI.

SECTION II
THEORY

Our task is to solve the Boltzmann equation for the hole distribution functions for p-type Si when both the electric field $\vec{F}$ and magnetic field $\vec{B}$ are present. With the distribution functions we are to calculate both the conductivity mobility μ_c, the Hall mobility μ_H, and their ratio, $\mu_H/\mu_c=r$ -- the so-called Hall r-factor.

The Boltzmann equation is[2]

$$\left[\frac{e}{\hbar}\vec{F}\cdot\vec{\nabla}_{\vec{k}}-\frac{e}{\hbar^2}\vec{B}\cdot\left(\vec{\nabla}_{\vec{k}}E_N(\vec{k})\times\vec{\nabla}_{\vec{k}}\right)\right] f_N(\vec{k}) = S_{op}f_N(\vec{k}) \quad , \qquad (1)$$

where $f_N(\vec{k})$ is the steady-state distribution function for valence band N of energy $E_N(\vec{k})$ at wave vector $\vec{k}$ in the Brillouin zone of Si. S_{op} is the scattering operator given by

$$S_{op}f_N(\vec{k}) = \frac{V}{(2\pi)^3}\sum_{M=1}^{3}\int d\vec{k}'\,[f_M(\vec{k}')-f_N(\vec{k})]W_{NM}(\vec{k},\vec{k}'), \qquad (2)$$

V is the volume of the crystal, and the sum over M is carried over the three top valence bands of Si. The transition probabilities for hole scattering by acoustic phonons between bands N at $\vec{k}$ and M at $\vec{k}'$ were expressed in a previous paper as[44]

$$W_{NM}(\vec{k},\vec{k}') = \frac{\pi k_B T}{2V\hbar}\left[\sum_i\sum_{LL'}A^i_{NL,ML'}(E_N(\vec{k}))\left(\sum_{\mu=1}^{\ell_i}K_L^{i\mu}(\hat{k})K_{L'}^{i\mu}(\hat{k}')\right)\right] \times \delta\,E_N(\vec{k})-E_M(\vec{k}') \quad . \qquad (3)$$

Here k_B is the Boltzmann constant, T is the absolute temperature and $K_L^{i\mu}(\hat{k})$ is a normalized cubic harmonic in direction $\hat{k}$ with angular index L transforming like the μth row of the ith irreducible representation of O_h with dimension ℓ_i. The coefficients A were fitted to the transition rates in a previous paper on angular variations of the rates[44]. These rates were calculated in Ref. 43 using the deformation potential theory of Tiersten[3]. In that paper, the three top valence bands of silicon were used

taking into account both their nonparabolicity and anisotropy. Similar rate calculations were performed by Tiersten and Lawaetz in the parabolic band regime for Ge[3,4]. In the rather good elastic scattering approximation of holes by acoustic-phonons, the expansion coefficients A are only functions of one of the holes' energies[44]. The delta function in (3) reflects this energy conservation condition.

The Boltzmann equation, 1, can be written more concisely as[4]

$$[\vec{F}\cdot\vec{F}_{op} + \vec{B}\cdot\vec{B}_{op}]f_N(\vec{k}) = S_{op}f_N(\vec{k}) \quad , \tag{4}$$

where from (1)

$$\vec{F}_{op} = \frac{e}{\hbar}\vec{\nabla}_{\vec{k}} \tag{5}$$

$$\vec{B}_{op} = -\frac{e}{\hbar^2}\,(\vec{\nabla}_{\vec{k}}E_N(\vec{k})\times\vec{\nabla}_{\vec{k}}) \quad . \tag{6}$$

To first order in both the electric and magnetic fields, the steady-state distribution function can be written as[4]

$$f_N(\vec{k}) = f_N^o(\vec{k}) + F\psi_{10}^N(\vec{k}) + FB\psi_{11}^N(\vec{k}) \quad , \tag{7}$$

where ψ_{10}^N reflects the deviation of the distribution function from its thermal equilibrium value

$$f_N^o(\vec{k}) = e^{-(E_N(\vec{k})-\mu)/k_BT} = f_N^o(E_N(\vec{k})) \quad , \tag{8}$$

where μ is the chemical potential, upon application of the electric field. ψ_{11}^N, similarly, is the added deviation from $f_N^o(\vec{k})$ when additionally a low magnetic field $\vec{B}$ is turned on. Inserting Eq. (7) for $f_N(\vec{k})$ into Eq. (4), and equating the same powers of $\vec{F}$ and $\vec{B}$ on both sides of (4), one obtains

$$(\hat{F}\cdot\vec{F}_{op})f_N^o(\vec{k}) = S_{op}\psi_{10}^N(\vec{k}) \quad , \tag{9a}$$

and

$$(\hat{B}\cdot\vec{B}_{op})\psi_{10}^N(\vec{k}) = S_{op}\psi_{11}^N(\vec{k}) \quad , \tag{9b}$$

where $\hat{F}$ and $\hat{B}$ are unit vectors in the directions of $\vec{F}$ and $\vec{B}$, respectively. Equations (9a) and (9b) reflect the ascending hierarchy of equations needed to evaluate high order F^nB^m

perturbations of the distribution function. Equations for general order n,m in the series have been exhibited by Lawaetz[4]. For calculations of conductivity and Hall mobilities we need go no further than the first two equations 9a and 9b. This is consistent with typically low magnitudes of the electric and magnetic fields used in the Hall experiments. Incidentally, the hot-electron effects, in the non-Ohmic regime, necessitate higher order F powers in the $f_N(\vec{k})$ expansion, Eq. (7).

We solve the Boltzmann equation using the method developed by Lawaetz. For this we expand ψ^N_{10} and ψ^N_{11} in a cubic harmonic series

$$\psi^N_{10}(\vec{k}) = f^\circ_N(\vec{k}) \sum_{k\eta\lambda'} \phi^{k\eta}_{N\lambda'}(E_N(\vec{k})) K^{k\eta}_{\lambda'}(\hat{k}) \quad , \tag{10a}$$

$$\psi^N_{11}(\vec{k}) = f^\circ_N(\vec{k}) \sum_{k\eta\lambda'} \chi^{k\eta}_{N\lambda'}(E_N(\vec{k})) K^{k\eta}_{\lambda'}(\hat{k}) \quad , \tag{10b}$$

with expansion coefficients ϕ and χ, respectively. Note that the most rapid energy variations of ψ^N_{10} and ψ^N_{11} have been factored out in

$$f^\circ_N(\vec{k}) = f^\circ_N(E_N(\vec{k})) \quad , \tag{11}$$

leaving relatively smooth functions ϕ and χ.

1. SOLUTION OF THE BOLTZMANN EQUATION

Our method for solving Eqs. (9) is sufficiently different from that of Lawaetz to merit its own development in this subsection. Whereas Lawaetz[2] multiplies both sides of Eqs. (9) on the left by a cubic harmonic $K^{j\nu}_{\lambda''}(k)$ and integrates over the angle $\hat{k}$, we in addition multiply these equations by $\delta(E_N(\vec{k})-E)$ and integrate over the whole Brillouin zone. The field term in Eq. (9a) becomes then

$$\frac{e}{\hbar}\hat{F}\cdot\int d\vec{k}\; K^{j\nu}_{\lambda''}(\hat{k})\,\delta(E_N(\vec{k})-E)\,\vec{\nabla}_{\vec{k}} f^\circ_N(\vec{k}) \quad . \tag{12}$$

In order to carry out the Brillouin zone integral in Eq. (12), we define for each band, N = S, L, and H (spin-orbit, light, and heavy valence bands, respectively), functions γ_N, where

$$k_N^2 \equiv \frac{2m_o}{\hbar^2}\ \gamma_N(E_N(\vec{k}),\hat{k}) \quad , \tag{13}$$

and m_o is the free-electron mass. Most conveniently

$$\frac{\hbar^2}{2m_o} = 1\ \text{Ry(a.u.)}^2, \tag{14}$$

where Ry = Rydberg = 13.6058 eV, and 1 a.u. = atomic unit of length = 1 Bohr radius = 0.5292×10^{-8} cm. As we will show, the atomic units are a more natural set of units to carry out the calculation than the units employed in two previous publications[43,44].

Eq. 13 suggests the change of the integration element to

$$k^2dk = \frac{1}{2}\left(\frac{2m_o}{\hbar^2}\right)^{\frac{3}{2}}\frac{1}{2}\gamma_N^{\frac{1}{2}}(E_N(\vec{k}),\hat{k})\frac{d\gamma_N(E_N(\vec{k}),\hat{k})}{dE_N(\vec{k})}dE_N(\vec{k}) \quad . \tag{15}$$

Altogether, with Eqs. (8) and (15), Eq. (12) assumes the form

$$-\frac{ef_N^o(E)}{2\hbar k_B T}\ \hat{F}\cdot\vec{g}_{N\lambda'}^{j\nu}(E) \quad , \tag{16}$$

where

$$\vec{g}_{N\lambda''}^{j\nu}(E) = \left(\frac{2m_o}{\hbar^2}\right)^{\frac{3}{2}}\int d\hat{k}\ K_{\lambda''}^{j\nu}(\hat{k})\gamma_N^{\frac{1}{2}}(E,\hat{k})\frac{d\gamma_N(E,\hat{k})}{dE}(\vec{\nabla}_{\vec{k}}E_N(\vec{k}))_E^{-1}, \tag{17}$$

and the energy gradient is evaluated on the constant energy E surface. Since γ is in Rydbergs, g is in $(\text{a.u.})^{-2}$.

The collision term, on the right hand side of Eq. (9a), can be similarly simplified. But first we note that the expansion coefficients A in Eq. (3) for W_{NM} were given in Refs. 41 and 42 in units of $(\text{eV})^2\text{cm}^3/\text{erg}$. This prefactor can also be written in atomic units as 7.9537×10^{11} Ry(a.u.)^3. In the old units the A's were on the order of 10^{-11} so that in the new units the A's are on the order of unity. We will keep the atomic units until comparison is made with the mobility data. Multiplying Eq. (9a) by $K_{\lambda''}^{j\nu}(\hat{k})\delta(E_N(\vec{k})-E)$ and integrating over $\vec{k}$ and $\vec{k}'$, with ψ_{10}^N given by Eq. (10a), S_{op}

defined by Eq. (2), and W_{NM} by Eq. (3), and the change of variables Eq. (15), we obtain

$$\text{R.H.S.} = \frac{1}{4}\frac{k_B T}{(4\pi)^2\hbar} f_N^{\circ}(E) \sum_{kM\eta\lambda'} S^{jk}_{N\nu\lambda'',M\eta\lambda'}(E)\phi^{k\eta}_{M\lambda'}(E) \quad . \tag{18}$$

Here, we define the scattering matrix S as

$$S^{jk}_{N\nu\lambda'',M\eta\lambda'}(E) = \sum_{i\mu LL'} \Bigg(\langle j\nu\lambda''|\Gamma_N|i\mu L\rangle A^{i}_{NL,ML'} \langle i\mu L'|\Gamma_M|k\eta\lambda'\rangle - \delta_{NM} \sum_{P=1}^{3} \langle j\nu\lambda'',k\eta\lambda'|\Gamma_N|i\mu L\rangle A^{i}_{NL,PL'} \langle i\mu L'|\Gamma_P|1\rangle \Bigg) . \tag{19}$$

The bra-kets denote angular Brillouin zone integrals between normalized cubic harmonics

$$\langle \hat{k}|j\nu\lambda\rangle = K^{j\nu}_{\lambda}(\hat{k}) \quad , \tag{20}$$

and the local operator Γ_N is defined as

$$\Gamma_N(E,\hat{k}) = \langle \hat{k}|\Gamma_N(E)|\hat{k}\rangle = \left(\frac{2m_o}{\hbar^2}\right)^{\frac{3}{2}} \gamma_N^{\frac{1}{2}}(E,\hat{k}) \frac{d\gamma_N(E,\hat{k})}{dE} \quad . \tag{21}$$

It is very important to the rest of the analysis that

$$\Gamma_N(E,R\hat{k}) = \Gamma_N(E,\hat{k}) \quad , \tag{22}$$

for all rotations $R\epsilon O_h$, the cubic point group, so that $\Gamma_N(E,\hat{k})$ transforms like the identity representation. The property (22) follows trivially from the defining Eq. (21) for Γ_N and (13) for γ_N, where one has

$$E_N(R\vec{k}) = E_N(\vec{k}) \tag{23}$$

from the invariance of the electron Hamiltonian with respect to space-group operations of the crystal. It is easy to show that the collision matrix S, Eq. (19), has units of $(\text{Ry a.u.}^3)^{-1}$. The advantage of the form Eq. (19) over the one used by Lawaetz is that our matrix S is symmetric in indices ($Nj\nu\lambda$, $Mk\eta\lambda'$).

Since Γ_N belongs to the identity representation we may employ orthogonality of the cubic harmonics with respect to the representation and partner indices; i.e., in Eq. (19)

$$j=k \qquad \text{and} \qquad \nu=\eta$$

so that

$$S^{jk}_{N\nu\lambda'',M\eta\lambda'}(E) \equiv S^{j\nu}_{N\lambda'',M\lambda'}(E)\delta_{jk}\delta_{\nu\lambda} =$$

$$= \sum_{LL'}\Bigg(\langle j\nu\lambda''|\Gamma_N|j\nu L\rangle A^{j}_{NL,ML'}\langle j\nu L'|\Gamma_M|j\nu\lambda' - \delta_{NM}\sum_{P=1}^{3}\langle j\nu\lambda'',j\nu\lambda'|\Gamma_N|\alpha L\rangle A^{\alpha}_{NL,PL'}\langle\alpha L'|\Gamma_P|1\rangle\Bigg) \quad . \tag{24}$$

We use α in Eq. (24) to denote the one dimensional identity representation.

Combining results of Eqs. (16), (18), and (24) the following system of linear equations results:

$$-2e\left(\frac{4\pi}{k_B T}\right)^2 \hat{F}\cdot\vec{g}^{j\nu}_{N\lambda'} = \sum_{M\lambda'} S^{j\nu}_{N\lambda'',M\lambda'}\ \phi^{j\nu}_{M\lambda'} \quad . \tag{25}$$

Eq. (25) is to be solved for the expansion coefficients ϕ. As can be seen, the system of linear equations factors out into separate problems for different irreducible representation j and partner indices ν. If we go one step further we can show that solutions ϕ have a simple dependence on the partner index ν. From the matrix element theorems we can write the integrals in Eq. (24) as follows[45]

$$\langle j\nu\lambda''|\Gamma_N|j\nu\lambda\rangle = \frac{1}{\ell_j}\sum_{\mu=1}^{\ell_j}\langle j\mu\lambda''|\Gamma_N|j\mu\lambda\rangle \quad , \tag{26}$$

for all $1\leq\nu\leq\ell_j$, where ℓ_j is the dimensionality of the jth irreducible representation of O_h, since Γ_N transform like the identity representation. Similarly, the "Gaunt-like" integral of three cubic harmonics in Eq. (24)

$$\langle j\nu\lambda'',j\nu\lambda'|\Gamma_N|\alpha L\rangle = \frac{1}{\ell_j}\sum_{\mu=1}^{\ell_j}\langle j\mu\lambda'',j\mu\lambda'|\Gamma_N|\alpha L\rangle \ ,$$

where $\Gamma_N|\alpha L\rangle$ transforms like the identity representation since $\langle\hat{k}|\alpha L\rangle$ is a cubic harmonic for the identity representation. Eqs. (26) and (27) show then that the index ν on S in Eqs. (24) and (25) is redundant.

Examining the $\vec{g}$ vector, Eq. (17), shows that j must belong to the vector representation, Γ_{15}, since $\vec{\nabla}_{\vec{k}} E_N(\vec{k})$ transforms like Γ_{15} (or δ in the notation of Von der Lage and Bethe - VdLB[46]). For all other j the L.H.S. of Eq. (25) is zero so that $\phi=0$ for $j\neq\delta$. Rows of the δ representation, ν, can be labelled by the Cartesian coordinates x, y, and z. The matrix element theorem expressed by Eq. (26) can be used for g as well, with the result that for fixed ν

$$\vec{g}^{j\nu}_{N\lambda''}(E) = \left[\frac{1}{\ell_j}\sum_{\mu=1}^{\ell_j}\int d\hat{k}\; K^{j\mu}_{\lambda''}(\hat{k})\,\Gamma_N(E,\hat{k})\left(\frac{\partial E_N(\vec{k})}{\partial k_\mu}\right)_E\right]\hat{e}_\nu$$

$$\equiv \left[-(G^j_{N\lambda''}(E)/2)\right]\hat{e}_\nu \quad , \tag{27}$$

where $\hat{e}_\nu$ is a unit vector in the νth direction. Using the above developments, Eq. (25) becomes

$$e\left(\frac{4\pi}{k_B T}\right)^2(\hat{F}\cdot\hat{e}_\nu)G^j_{N\lambda''}(E) = \sum_{M\lambda'} S^j_{N\lambda'',M\lambda'}(E)\phi^j_{M\lambda'}(E) \quad , \tag{28}$$

which has the solution

$$\phi^{j\nu}_{N\lambda'} = e\left(\frac{4\pi}{k_B T}\right)^2(\hat{F}\cdot\hat{e}_\nu)\left[\sum_{M\lambda''}\left(S^j_{N\lambda',M\lambda''}(E)\right)^{-1}G^j_{N\lambda''}(E)\right]$$

$$\equiv e\left(\frac{4\pi}{k_B T}\right)^2(\hat{F}\cdot\hat{e}_\nu)\left[\theta^j_{N\lambda'}(E)\right] \quad , \tag{29}$$

where the directional dependence is contained in $\hat{F}\cdot\hat{e}_\nu$. If we def define

$$\vec{\Phi}_N(E,\hat{k}) \equiv \sum_\lambda e\left(\frac{4\pi}{k_B T}\right)^2 \begin{pmatrix} K^{\delta x}_\lambda(\hat{k})\hat{e}_x \\ K^{\delta y}_\lambda(\hat{k})\hat{e}_y \\ K^{\delta z}_\lambda(\hat{k})\hat{e}_z \end{pmatrix} \theta^\delta_{N\lambda}(E) \quad , \tag{30}$$

then to first order in the electric field Eq. (7) can be written in the familiar form

$$f_N(\vec{k}) = f^o_N(\vec{k})\,[1+\vec{F}\cdot\vec{\Phi}_N(E,\hat{k})] \quad . \tag{31}$$

Clearly, the units of $\vec{\Phi}$ and ϕ are those of the (electric field)$^{-1}$, while those of θ are (Ry a.u.).

Eq. (29) provides the solution for that part of the distribution function which is perturbed by the application of the electric field only. The second part of the problem is the solution of Eq. (9b) for the part of the distribution function which is perturbed by the simultaneous application of the magnetic field. As for the R.H.S., we use the expansion (10b) for ψ_{11}, multiply the R.H.S. by $K^{j\nu}_{\lambda''}(\hat{k})\delta(E_N(\vec{k})-E)$ and integrate over $\vec{k}$. This part of the calculation is identical to the calculation above with χ replacing ϕ, so that

$$\text{R.H.S.} = \frac{1}{4}\frac{k_B T}{(4\pi)^2\hbar} f^o_N(E) \sum_{M\lambda'} S^{j}_{N\lambda'',M\lambda'}(E)\chi^{j\nu}_{M\lambda'}(E) \quad , \qquad (32)$$

where χ are the expansion coefficients for ψ^N_{11} in Eq. (10b). On the L.H.S., Eq. (9b), ψ^N_{10} is the solution obtained earlier in Eq. (30), and the $\vec{B}_{op}$ is given by Eq. (6). $\vec{B}_{op}$, due to the presence of the cross-product, commutes with any function of energy, such as $f^o_N(E_N(\vec{k}))$, matrices S and G, and expansion coefficients ϕ. Multiplying the field term, Eq. (9b), by

$$K^{j\nu}_{\lambda''}(\hat{k})\delta(E_N(\vec{k})-E) \quad ,$$

and integrating over $\vec{k}$, we obtain

$$\text{L.H.S.} = -\frac{e}{2\hbar^2} f^o_N(E) \sum_{\mu\lambda'''} \phi^{i\mu}_{N\lambda'''}(E)\left(\hat{B}\cdot\vec{H}^{i\mu,j\nu}_{N\lambda''',N\lambda''}(E)\right) \quad , \qquad (33)$$

where the magnetic field matrix is given by

$$\vec{H}^{i\mu,j\nu}_{N\lambda''',N\lambda''}(E) = \int d\hat{k}\; K^{j\nu}_{\lambda''}(\hat{k})\Gamma_N(E,\hat{k})\left[\vec{\nabla}_{\vec{k}}E_N(\vec{k})\times\vec{\nabla}_{\vec{k}}\right]_E K^{i\mu}_{\lambda'''}(\hat{k}) \quad , \qquad (34)$$

evaluated on the constant energy E surface. The sum over $\mu\lambda'''$ in Eq. (33) comes about because of the cubic harmonic expansion of ψ^N_{10}. Clearly, index $i=\delta$ and $\mu=x,y$, or z. H is in $(\text{a.u.})^{-1}$.

As we shall show later, Eq. (52b) for the Hall mobility calculation we need only the part of ψ^N_{11} which transforms like the vector representation $\Gamma_{15}=\delta$, so that $j=\delta$ as well. We shall not calculate the part of ψ^N_{11} transforming like the $\Gamma_{25}=\varepsilon'$ representation since it is irrelevant for our goals. We note that

$$\left(\vec{\nabla}_{\vec{k}} E_N(\vec{k}) \times \vec{\nabla}_{\vec{k}}\right)_E \equiv \vec{h}_N(E,\hat{k}) \tag{35}$$

transforms like a pseudovector according to the $\Gamma'_{15}=\delta'$ representation. The magnetic field matrix, Eq. (34), can be shown to be nonvanishing for the choice i=j=δ since the direct product

$$\Gamma_{15} \otimes \Gamma'_{15} = \Gamma_{15}+\Gamma_{25}+\Gamma'_1+\Gamma'_{12} \tag{36}$$

contains Γ_{15} in its decomposition. The pseudovector operator h transforms under coordinate rotations according to

$$P(R)h_p P(R^{-1}) = \sum_{q=1}^{3} \Gamma^m_{qp}(R) h_q \quad , \tag{37}$$

where P(R) are the scalar rotation operators which operate on functions, as opposed to rotation matrices R which operate on vectors. $\Gamma^m(R)$ is the matrix for the pseudovector Γ'_{15} irreducible representation of O_h

With these preliminaries, we can show that

$$\vec{H}^{\delta\mu,\delta\nu}_{N\lambda''',N\lambda''}(E) = \langle \delta\nu\lambda'' | \Gamma_N \vec{h}(E) | \delta\mu\lambda''' \rangle \tag{38}$$

$$= \frac{1}{48} \sum_{R\epsilon O_h} \sum_p \hat{e}_p \langle P(R)\delta\nu\lambda'' | \Gamma_N(E) P(R) h_p(E) P(R^{-1}) | P(R) | \delta\mu'\lambda''' \rangle .$$

$$= \frac{1}{48} \sum_{R\epsilon O_h} \sum_{p,q,\nu',\mu'} \hat{e}_p \Gamma^{\delta}_{\nu',\nu}(R) \Gamma^m_{qp}(R) \Gamma^{\delta}_{\mu',\mu}(R) \langle \delta\nu'\lambda'' | \Gamma_N(E) h_q(E) | \delta\mu'\lambda''' \rangle .$$

Summing over the 48 rotations of O_h, we obtain the following result

$$\vec{H}^{\delta\mu,\delta\nu}_{N\lambda''',N\lambda''}(E) = \tag{39}$$

$$= \frac{1}{6} \sum_p \hat{e}_p \epsilon_{\nu p\mu} \left[\sum_{\nu',p',\mu'} \epsilon_{\nu' p' \mu'} \langle \delta\nu'\lambda'' | \Gamma_N(E) h_{p'}(E) | \delta\mu'\lambda''' \rangle \right]$$

$$\equiv \frac{1}{6} \sum_p \hat{e}_p \epsilon_{\nu p\mu} \left[H^{\delta}_{N\lambda''',N\lambda''}(E) \right] \quad ,$$

where $\epsilon_{\nu p\mu}$ is the Levi-Cevita symbol.

Therefore, the L.H.S. in Eq. (33) becomes

$$\text{L.H.S.} = -\frac{e}{12\hbar^2} f_N^\circ(E) \sum_{\mu\lambda'''} \phi^{\delta\mu}_{N\lambda'''}(E) \sum_p (\hat{e}_p \cdot \hat{B}) \epsilon_{\nu p\mu} H^\delta_{N\lambda''',N\lambda''}(E) \quad , \tag{40}$$

and substituting Eq. (29) for ϕ gives

$$\text{L.H.S.} = -\left(\frac{4\pi e}{\hbar k_B T}\right)^2 \frac{f_N^\circ(E)}{12} \sum_{\mu\lambda'''} \theta^\delta_{N\lambda'''}(E) (\hat{F}\cdot\hat{e}_\mu) \sum_p (\hat{e}_p \cdot \hat{B}) \epsilon_{\nu p\mu} H^\delta_{N\lambda''',N\lambda''}(E) . \tag{41}$$

Summing over μ and p, we finally obtain

$$\text{L.H.S.} = +\left(\frac{4\pi e}{\hbar k_B T}\right)^2 \frac{f_N^\circ(E)}{12} \sum_{\lambda'''} \theta^\delta_{N\lambda'''}(E) H^\delta_{N\lambda''',N\lambda''}(E) [(\hat{F}x\hat{B})\cdot\hat{e}_\nu] \quad . \tag{42}$$

In combination with the R.H.S., Eq. (32), the linear system of equations has the solution

$$\chi^{\delta\nu}_{P\lambda} = \left[\left(\frac{4\pi}{k_B T}\right)^3 \frac{4\pi e^2}{\hbar}\right] \left[\frac{1}{3} \sum_{N\lambda''\lambda'''} \left(S^\delta_{P\lambda,N\lambda''}\right)^{-1} \theta^\delta_{N\lambda'''}(E) H^\delta_{N\lambda''',N\lambda''}(E)\right] \tag{43}$$

$$x\ [(\hat{F}x\hat{B})\cdot\hat{e}_\nu] \equiv \left[\left(\frac{4\pi}{k_B T}\right)^3 \frac{4\pi e^2}{\hbar}\right] [\hat{F}x\hat{B}\cdot\hat{e}_\nu]\ \xi^\delta_{P\lambda}(E) \quad .$$

Defining

$$\vec{X}_N(E,\hat{k}) \equiv \sum_\lambda \left[\left(\frac{4\pi}{k_B T}\right)^3 \frac{4\pi e^2}{\hbar}\right] \xi^\delta_{N\lambda}(E) \begin{pmatrix} K^{\delta x}_\lambda(\hat{k})\hat{e}_x \\ K^{\delta y}_\lambda(\hat{k})\hat{e}_y \\ K^{\delta z}_\lambda(\hat{k})\hat{e}_z \end{pmatrix} , \tag{44}$$

the distribution function to first order in the magnetic field becomes

$$f_N(\vec{k}) = f_N^\circ(\vec{k}) [1 + \vec{F}\cdot\vec{\Phi}_N(E,\hat{k}) + (\vec{F}x\vec{B})\cdot\vec{X}_N(E,\hat{k})] \quad . \tag{45}$$

2. TRANSPORT COEFFICIENTS

The average thermal velocity in a material is given by

$$\langle \vec{V} \rangle = \frac{\sum_{\vec{k}} \sum_{N} \vec{V}_N(\vec{k}) f_N(\vec{k})}{\sum_{\vec{k}} \sum_{N} f_N(\vec{k})} \tag{46}$$

where

$$\vec{V}_N(\vec{k}) = \frac{1}{\hbar} \vec{\nabla}_{\vec{k}} E_N(\vec{k}) \quad .$$

In Appendix A we derive, for completeness sake, the relationship between the current density $\vec{J}$ and the fields to be[47]

$$\vec{J} = pe\langle \vec{V} \rangle = \sigma_o \vec{F} + \sigma_o \mu_H (\vec{F} \times \vec{B}) + \ldots \quad , \tag{47}$$

where p is the carrier density, σ_o is the conductivity

$$\sigma_o = pe\mu_c \quad , \tag{48}$$

μ_c is the conductivity mobility, and μ_H is the Hall mobility. Hall experiments measure μ_H, although the data analysis for carrier densities requires μ_c. These are related by the so-called r-factor

$$r = \mu_H / \mu_c \quad . \tag{49}$$

We shall develop the necessary theoretical framework for evaluating μ_H and μ_c.

Since the distribution function contains terms proportional to F and FB, we can write Eq. (46) in the following form

$$\langle \vec{V} \rangle = \langle \vec{V}_{10} \rangle F + \langle \vec{V}_{11} \rangle FB \quad , \tag{50}$$

which through Eqs. (47) and (48) provide us with the means of calculating mobilities. These equations are

$$\mu_c = \hat{F} \cdot \langle \vec{V}_{10} \rangle \tag{51a}$$

$$r\mu_c^2 = (\hat{F} \times \hat{B}) \cdot \langle \vec{V}_{11} \rangle / |\hat{F} \times \hat{B}|^2 \quad . \tag{51b}$$

Performing the fields of expansion, Eq. (50), we obtain

$$\mu_c = \frac{\sum_{\vec{k}N} \cdot \sum_{\mu\lambda} \left(\hat{F}\cdot\vec{V}_N(\vec{k})\right) \; f_N^o(\hat{k})\,\phi_{N\lambda}^{\delta\mu}\left(E_N(\vec{k})\right) \; K_\lambda^{\delta\mu}(\hat{k})}{\sum_{\vec{k}N} \; f^o{}_N(\vec{k})} \tag{52a}$$

$$r\mu_c{}^2 = \frac{\sum_{\vec{k}N} \cdot \sum_{\mu\lambda} \left((\hat{F}x\hat{B})\cdot\vec{V}_N(\vec{k})\right) \; f_N^o(\vec{k})\,\chi_{N\lambda}^{\delta\mu}\left(E_N(\vec{k})\right) K_\lambda^{\delta\mu}(\hat{k})}{|\hat{F}x\hat{B}|^2 \sum_{\vec{k}N} \; f_N^o(\vec{k})} \tag{52b}$$

It is clear now that due to the vectorial nature of $\vec{V}_N(\vec{k})$ only the δ parts of f_N contribute to the mobilities. Denominators in Eqs. (46), (52a) and (52b) are the total number of carriers in the crystal.

The integrals occurring in Eqs. (52a and b) can be written in terms of integrals evaluated earlier. The forms we adopt are

$$\mu_c = \frac{1}{\hbar}\,\hat{F}\cdot\frac{\sum_{N\mu\lambda}\int_o^\infty dE\; e^{-\beta E}\phi_{N\lambda}^{\delta\mu}(E)\;\vec{g}_{N\lambda}^{\delta\mu}(E)}{4\pi\sum_N\int_o^\infty dE\; e^{-\beta E}\langle\alpha_o|\Gamma_N|\alpha_o\rangle} \tag{53a}$$

where $\beta = (k_B T)^{-1}$, and

$$r\mu_c{}^2 = \frac{\hat{F}x\hat{B}}{|\hat{F}x\hat{B}|^2}\cdot\frac{\sum_{N\mu\lambda}\int_o^\infty dE\; e^{-\beta E}\chi_{N\lambda}^{\delta\mu}(E)\vec{g}_{N\lambda}^{\delta\mu}(E)}{4\pi\sum_N\int_o^\infty dE\; e^{-\beta E}\langle\alpha_o|\Gamma_N|\alpha_o\rangle} \tag{53b}$$

Since $\phi^{\delta\mu}\sim(\hat{F}\cdot\hat{e}_\mu)$ and $\vec{g}^{\delta\mu}\sim\hat{e}_\mu$, Eqs. (29) and (28), respectively,

$$\mu_c \sim \sum_\mu (\hat{F}\cdot\hat{e}_\mu)(\hat{F}\cdot\hat{e}_\mu) = |\hat{F}|^2 = 1 \quad ,$$

so that μ_c is independent of the magnitude and direction of the electric field, as it should for ohmic mobility of cubic materials. Similarly, from Eq. (43)

$$\chi^{\delta\mu} \sim (\hat{F}x\hat{B}) \cdot \hat{e}_\mu$$

so that

$$r\mu_c^2 = \mu_H \mu_c \sum_\mu \frac{\left[(\hat{F}x\hat{B}) \cdot \hat{e}_\mu\right]\left[(\hat{F}x\hat{B}) \cdot \hat{e}_\mu\right]}{|\hat{F}x\hat{B}|^2} = 1 \quad ,$$

and μ_H is independent of the directions and magnitudes of $\vec{F}$ and $\vec{B}$, as long as they are not parallel.

The symmetry analysis presented in this section, with some modifications, can be carried over to noncubic materials. A main difference will arise due to the fact that the three Cartesian coordinates will no longer be equivalent, and as a result mobilities will be anisotropic.

In the next section we will show how to implement the above developed formalism.

SECTION III
COMPUTATIONAL APPROACH

In order to implement the theory outlined in Section II we need to evaluate a number of Brillouin zone integrals. In all cases the weighting factor is

$$\Gamma_N(E,\hat{k}) = \left(\frac{2m_o}{\hbar^2}\right)^{\frac{3}{2}} \gamma_N^{\frac{1}{2}}(E,\hat{k}) \frac{d\gamma_N(E,\hat{k})}{dE} \tag{54}$$

where

$$k_N^2 = \left(\frac{2m_o}{\hbar^2}\right) \gamma_N(E,\hat{k})$$

defines $\gamma_N(E,k)$. The γ_N for all three bands are obtained from the solution of the cubic equation as given by Madarasz, Lang, and Hemenger[48]

$$H_3\gamma^3+H_2\gamma^2+H_1\gamma+H_o = 0 \quad , \tag{55}$$

where the coefficients H_i are functions of energy and the angle $\hat{k}$. Band parameters A, B, and C for Si are taken to be dimensionless so that γ's come out in Rydbergs. It is a simple matter, given a general solution of Eq. (55), to take its energy derivative to form the Γ_N for all three top valence bands.

One type of angular integrals which may be performed with relative ease are those contained in the definition of the scattering matrix. The simplest of these is

$$\langle \alpha L | \Gamma_N | 1 \rangle = \int d\hat{k}\ K_L^{\alpha}(\hat{k}) \left(\frac{2m_o}{\hbar^2}\right)^{\frac{3}{2}} \gamma_N^{\frac{1}{2}}(E,\hat{k}) \frac{d\gamma_N(E,\hat{k})}{dE} \cdot 1 \ . \tag{56}$$

All the functions in the integrand transform like the identity representation, so that the integral can be performed over one irreducible wedge of the Brillouin zone and the result multiplied by 48 - the number of such wedges in the Brillouin zone. The numerical technique we employ is that of 12 x 12 point Gaussian integration; i.e., 12 points for the azimuthal angle and 12 points for the polar angle in Eq. (56)[10,48]. As a check, one may note that in the parabolic limit

$$E(\vec{k}) = \frac{\hbar^2 k^2}{2m^*} \quad , \tag{57a}$$

$$\gamma(E,\hat{k}) = \frac{\hbar^2 k^2}{2m_o} = E\,\frac{m^*}{m_o} \quad , \tag{57b}$$

where m^* is the effective mass for the band and $m_o = 1/2$ is the free electron mass. If we use $(m^*/m_o) = 0.58$ for the heavy-hole band and $(m^*/m_o) = 0.16$ for the light-hole band[21], we can calculate

$$\langle \alpha_o | \Gamma | \alpha_o \rangle = \left(\frac{m^*}{m_o}\right)^{\frac{3}{2}} E^{\frac{1}{2}} \left(\frac{2m_o}{\hbar^2}\right)^{\frac{3}{2}} \tag{58}$$

at $E = 0.00450$ eV to be $8.03\text{x}10^{-3}(\text{Ry}^{-1}\text{a.u.}^{-3})$ for the H-band and $1.16\text{x}10^{-3}(\text{Ry}^{-1}\text{a.u.}^{-3})$ for the L band. By comparison, using the nonparabolic-nonspherical solutions for γ from Eq. (55), the computer calculates at this very low energy $8.08\text{x}10^{-3}(\text{Ry}^{-1}\text{a.u.}^{-3})$ and $1.17\text{x}10^{-3}(\text{Ry}^{-1}\text{a.u.}^{-3})$ for the H and L bands, respectively. The small difference between these numbers gives us confidence in our ability to perform these integrals, and points to the fact that the parabolic approximation at very lowest energies is a fair approximation to the true bands. All angular integrals calculated here were also calculated using a 7x7 Gaussian mesh with little difference from results of the larger 12x12 mesh.

Another type of integrals encountered in the evaluation of the scattering matrix S, Eq. (26), involves cubic harmonics for the δ representation.

$$\langle \delta\nu\lambda'' | \Gamma_N | \delta\nu\lambda \rangle = \frac{1}{3} \sum_{\mu=1}^{3} \langle \delta\mu\lambda'' | \Gamma_N | \delta\mu\lambda \rangle \tag{59}$$

which in fact are independent of the partner index ν. In order to reduce Eq. (59) to an integral over one irreducible wedge we derive the following identity:

$$\frac{1}{\ell_j}\sum_{\mu=1}^{\ell_j} \langle j\mu L|\Gamma_N|j\mu L'\rangle =$$

$$\frac{1}{\ell_j}\sum_{\mu=1}^{\ell_j}\sum_{R\in O_h}\int_W d\hat{k}\; K_L^{j\mu}(R\hat{k})\,\Gamma_N(E,R\hat{k})\,K_{L'}^{j\mu}(R\hat{k}) \quad ,$$

where W denotes one irreducible wedge, and

$$\Gamma_N(E,R\hat{k}) = \Gamma_N(E,\hat{k})$$

$$K_L^{j\mu}(R\hat{k}) = P(R^{-1})K_L^{j\mu}(\hat{k}) = \sum_\nu \Gamma^j(R)_{\mu\nu}K_L^{j\nu}(\hat{k}) \quad ,$$

so that from the greater orthogonality theorem[45]

$$\frac{1}{\ell_j}\sum_{\mu=1}^{\ell_j} \langle j\mu L|\Gamma_N|j\mu L'\rangle = \frac{48}{\ell_j}\sum_{\mu=1}^{\ell_j}\int_W d\hat{k}\; K_L^{j\mu}(\hat{k})\,\Gamma_N(E,\hat{k})\,K_{L'}^{j\mu}(\hat{k}) \quad . \quad (60)$$

For the identity representation $\ell_j=1$, which explains the factor of 48 in connection with Eq. (56). For the $\Gamma_{15}=\delta$ representation the premultiplier is 16 since $\ell_\delta=3$.

The third type of angular integrals encountered in the calculations is that for $\vec{g}$ in the field term of the Boltzmann equation, Eq. (17),

$$\vec{g}_{N\lambda}^{j\nu} = \langle j\nu\lambda|\Gamma_N|(\vec{\nabla}_{\vec{k}}E_N(\vec{k}))_E\rangle \quad . \quad (61)$$

Since the energy gradient transforms accordingly to the vector representation, $j=\delta$, Eq. (61) can be reduced to the form of Eq. (60) with $\ell_j=3$. *In order to obtain the energy gradient* we differentiate the secular equation, Eq. (55), with respect to Cartesian components of $\vec{k}$. After some tedious algebra, one can show that

$$\left(\frac{\partial E_N}{\partial k_z}\right)_E = 2\gamma_N^{-\frac{1}{2}}\left[z\Pi_1(E,\hat{k})+z^3\Pi_2(E,\hat{k})+\frac{1}{z}\Pi_3(E,\hat{k})\right] \quad , \quad (62a)$$

or

$$2\gamma_N^{-\frac{1}{2}} \left[z\Pi_4(E,\hat{k})+z^3\Pi_5(E,\hat{k})+z^5\Pi_6(E,\hat{k})\right] , \tag{62b}$$

where expansion coefficients Π_i, $1\leq i\leq 6$, are too lengthy to reproduce on these pages. The important point is that the Π's were constructed so that they transform according to the identity representation, therefore, $\frac{\partial E_N}{\partial k_z}\sim z$, $z^3, \frac{1}{z}$ has three factors transforming like the vector representation, $\Gamma_{15}=\delta$. As a check on this part of our computational procedure we note that in the parabolic limit

$$\left(\frac{2m_o}{\hbar^2}\right)^{\frac{3}{2}} \int \delta_{1z}(\hat{k}) \left(\frac{\partial E}{\partial k_z}\right)_E \gamma^{\frac{1}{2}} \frac{d\gamma}{dE} d\hat{k} = \langle \delta z1 | \Gamma_N | \left(\frac{\partial E}{\partial k_z}\right)_E \rangle =$$

$$\left(\frac{2m_o}{\hbar^2}\right)\left(\frac{m^*}{m_o}\right) \frac{8\pi}{3} E \sqrt{\frac{3}{4\pi}} , \tag{63}$$

which for the H band at E=0.00450 eV is 7.85×10^{-4}a.u.$^{-2}$ and 2.17×10^{-4}a.u.$^{-2}$ for the L band. Computer generated numbers for these two cases are 7.45×10^{-4} and 2.14×10^{-4}a.u.$^{-2}$, respectively.

The fourth type of integrals is the most involved. It arises in the evaluation of the magnetic field term vector, H, Eq. (34). The H matrix is given by

$$H^{\delta\mu,\delta\nu}_{N\lambda'',N\lambda''}(E) \equiv \int d\hat{k}\ K^{\delta\nu}_{\lambda''}(\hat{k})\Gamma_N(E,\hat{k}) \left[\vec{\nabla}_{\vec{k}}E_N(\vec{k})\times\vec{\nabla}_{\vec{k}}\right]_E K^{\delta\mu}_{\lambda''}(\hat{k})$$

$$\equiv \int d\hat{k}\ K^{\delta\nu}_{\lambda''}(\hat{k})\Gamma_N(E,\hat{k})\vec{h}^N(E,\hat{k})\ K^{\delta\mu}_{\lambda'''}(\hat{k}) , \tag{64}$$

where $\vec{h}_N$ operator was defined in Eq. (35). The angular integral can be reduced to a one wedge integral from the known transformation properties of the factors in the integrand

$$\vec{H}^{\delta\mu,\delta\nu}_{N\lambda'',N\lambda''}(E) = \sum_q \hat{e}_q \sum_{R\epsilon O_h} \sum_{\nu',p,\mu'} \Gamma^{\delta}_{\nu',\nu}(R)\Gamma^{m}_{qp}(R)\Gamma^{\delta}_{\mu',\mu}(R)$$

$$\times \int_W d\hat{k}\ K^{\delta\nu'}_{\lambda''}(\hat{k})\Gamma_N(E,\hat{k})h^N_q(E,\hat{k})K^{\delta\mu'}_{\lambda'''}(\hat{k}) . \tag{65}$$

Summing over the 48 rotations in O_h yields

$$\vec{H}^{\delta\mu,\delta\nu}_{N\lambda'',N\lambda'} = 8 \sum_p \hat{e}_p \epsilon_{p\mu\nu} \left\{ \sum_{p'\mu'\nu'} \epsilon_{p'\mu'\nu'} \int_W d\hat{k}\, K^{\delta\nu'}_{\lambda''}(\hat{k})\, \Gamma_N(E,\hat{k}) \right.$$

$$\left. h^N_{p'}(E,\hat{k}) K^{\delta\mu'}_{\lambda'''}(\hat{k}) \right\} \quad . \tag{66}$$

In practice, we choose the direction of the electric field along the x-direction so that $\mu=1$, the magnetic field in the y-direction so that $p=2$, then we only require the $\nu=3$ part of χ in order to calculate the Hall mobility.

We still have to calculate the bracketed term in Eq. (66). We find it most effective to write out the magnetic field operator $\vec{h}$ in the form of Eq. (35).

$$\vec{h}^N(E,\hat{k}) = (\vec{\nabla}_{\vec{k}} E_N(\vec{k}) \times \vec{\nabla}_{\vec{k}})_E \quad ,$$

with the energy gradient expanded in the form of Eq. (62). We then form all the necessary gradients of the cubic harmonics in order to evaluate the bracketed term in Eq. (66). The resulting expressions are tedious to derive, are lengthy, and inelegant. Therefore, we will not repeat them. Another method for evaluating the bracketed term in Eq. (66) is suggested in Appendix B.

It should be said at this stage, for benefit of other workers wishing to perform similar calculations, that in spite of our emphasis on employing the cubic harmonics the entire calculation can be performed without them. The lengthy expressions in evaluating the derivatives of cubic harmonics are partly the result of their orthonormality. One can form symmetry adapted cubic functions which have correct transformation properties yet need not be orthogonal to one another. As an example, for the δ representation we could have used simple functions like x,y,z; x^3,y^3,z^3; x^5,y^5,z^5; etc., rather than the orthogonal set

$$x$$
$$x^3 - \frac{3}{5}x$$
$$x^3 - \frac{10}{9}(x-\frac{3}{5}x) - \frac{3}{7}x \quad .$$

This would simplify the gradient expressions considerably. That the use of cubic harmonics is not essential is due to the form of the angular integrals we are evaluating. All of them contain a weighting factor between two cubic harmonics. Therefore, we never have a chance to use the orthonormality of cubic harmonics with respect to their angular momentum indices. The same was true in our discrete least-squares fitting of the transition probabilities[44].

As always, we tested this part of the calculation in the parabolic limit. For example, in the parabolic-isotropic limit

$$\int d\hat{k}\,\delta_{1z}(\hat{k})\,\Gamma(\hat{k},E)\,h_y(\hat{k},E)\,\delta_{1x}(\hat{k}) = 2\hbar\left(\frac{2m_o}{\hbar^2}\right)^{\frac{3}{2}}\left(\frac{m^*}{m_o}\right)^{\frac{1}{2}} E^{\frac{1}{2}} \quad , \qquad (67)$$

which for the L-band at $E=0.0045$ eV yields 0.0145 a.u.$^{-1}$ and for the H band 0.0277 a.u.$^{-1}$. The corresponding results for the actual silicon valence bands are 0.0144 and 0.0268 a.u.$^{-1}$, respectively.

With all the angular integrals calculated we proceed as follows. Using the expansion coefficients A for the transition rates we form the S matrix in Eq. (24). The λ', λ'' indices ranged through angular momenta 1,3,5, and 5′ (for the δ_5' harmonic). The angular momenta for the α_L cubic harmonics were L=0,4,6, and 8. The S matrix inversion was performed using the Gauss-Jordan method[49]. As noted earlier, our form of the scattering matrix S is symmetric in the combined $N\lambda$ indices. The symmetry of S also serves as a check of our computational procedure. In the next step we multiply the $\vec{G}$ vector by the S^{-1} matrix and calculate ϕ in Eq. (29). Similarly, we calculate the χ coefficients from ϕ and H on L.H.S., Eq. (33), and the S matrix, as indicated in Eq. (43).

The last sensitive procedure is the evaluation of the energy integrals (53a and b) containing the Boltzmann factor. Here, we use the Gauss-Laguarre integration method with 25-points along the energy scale[50]. We perform a change of variables so that the coordinate of the 25th point occurs at

$$E_{25} = -(k_B T)\ln 0.001 \qquad (68)$$

We also tried $E_{25}=-(k_B T)\ln 0.01$ with little change in the results. This, of course, required us to interpolate the integrand at the adjustable Gauss-Laguerre mesh. The interpolation was done via the Lagrange interpolation using 16 first principles points as input[51].

All the energy dependent quantities were evaluated at two separate energy meshes. The "rough" energy mesh had the energy interval of 0.0045 eV and 16 energies from 0.0045 eV to 0.072 eV. The same quantities were also calculated on a finer mesh near E=0 eV with the mesh size of 0.0135/17 eV; again, 16 energies with that mesh size were used. Using the finer mesh we fitted the energy dependence of the numerators and denominators in Eqs. (53a and b) in a convenient form for the interpolation purposes. It was our observation that for energies less than the first mesh point the Lagrange interpolation was ineffective, so the fitting was indicated. From presence of the Boltzmann factor it is clear that the integrals derive much of their magnitudes at these low energies.

The energy dependence for the integrands can be obtained from a simple analysis. At low energies the expansion coefficients A for W_{MN} in Eq. (3) are essentially energy independent, as if to a first approximation the bands were parabolic. This makes the scattering matrix proportional to Γ_N^2, so that

$$S \sim \Gamma^2 \sim \left(\gamma^{\frac{1}{2}} \frac{d\gamma}{dE}\right)^2 \sim E \quad . \tag{69}$$

From (63), we also see that $g \sim E$, so that

$$\phi \sim S^{-1} g \sim \frac{1}{E} E \sim \text{const.} \quad , \tag{70}$$

which implies that the numerator in Eq. (53a) behaves like E at low energies. Even though this is a polynomial form, the necessity for fitting the energy dependence of the numerator arises from the general weakness of the Lagrange interpolation near the endpoints of the supplied mesh.

Next, we observe that, Eq. 43,

$$\chi \sim S^{-1} \phi H \quad . \tag{71}$$

Eq. (67) shows that $H \sim E^{\frac{1}{2}}$, so that

$$\chi \sim E^{-\frac{1}{2}} \quad , \tag{72}$$

and

$$\chi g \sim E^{\frac{1}{2}} \quad . \tag{73}$$

Therefore, the numerator in Eq. (53a) goes as $E^{\frac{1}{2}}$ and has to be fitted to that form for low energies. Similarly, from Eq. (58), we see that the denominators in Eqs. (53a and b) go as $E^{\frac{1}{2}}$. The square root dependence explains why the Lagrange interpolation is ineffective for energies less than the first mesh point. The Lagrange interpolation is a polynomial interpolation scheme and would have a difficult time fitting a function like $E^{\frac{1}{2}}$ near end-points of the energy mesh.

In Sections IV and V we shall display both the numerators and denominators of Eqs. (53a and b) for both germanium and silicon. We consider the calculation for germanium using Tiersten's and Lawaetz's parameters as a test of the overall theory developed in Section II and the computational procedure developed in this section. The test is provided in the next section.

SECTION IV

TEST OF THE THEORY AND COMPUTATIONAL PROCEDURE - CALCULATION FOR GERMANIUM

The only two calculations similar in spirit to the present one were performed in the 60's by Tiersten[3] and Lawaetz[4] for germanium. In order to assure ourselves of the validity of our theory and computational procedure, we performed the calculation for germanium using the same set of input parameters for Ge as did Tiersten and Lawaetz. In practice, this entails a change of about 10 lines in our code for silicon.

Table 1 provides the parameters which serve as an experimental input into this part of the calculation. We have to emphasize that there is a large spread in experimentally measured values of the deformation potential parameters for Ge. From tabulations of various measured values for a, b, and d for Ge it is apparent that there is a large uncertainty in their magnitudes and, at times, in their signs as well[4,28,35,52]. Since this part of the calculation serves mainly as a check of our computational procedure we adopt the Tiersten's set of parameters. This way we assure ourselves of a one-to-one comparison with the earlier works in the field. Moreover, Tiersten and Lawaetz did motivate their selection of the deformation potential parameters from physical considerations. We then expect that these values are reasonable representations of the experimental state of affairs in measurements for Ge.

TABLE 1

EXPERIMENTAL INPUT PARAMETERS USED IN THE MOBILITY CALCULATION FOR GERMANIUM

Valence Band Parameters[a] (dimensionless)		Deformation Potentials[a] (eV)		Phonon Parameters[a] ρc_s^2 (dyne/cm^2)	
A	-13.27	a	2.0	s=transverse	5.75×10^{11}
B	- 8.63	b	-2.1	s=longitudinal	1.53×10^{12}
C	12.4	d	-7.0		

[a] Ref. 3, ρ=mass density, c_s=phonon speed for branch s

With the set of parameters in Table 1 we have calculated the transition probabilities for Ge in the manner described in our first paper on the subject[43]. These were then fitted to a double cubic harmonic series using the method treated in detail for Si in our second paper[44]. The expansion coefficients A, Eq. (3), that we calculated for Ge are in closest agreement with those reported by Tiersten for transitions involving the more parabolic H band. In turn, Lawaetz[4] reports that the coefficients he calculated also agree with those of Tiersten[3].

Before presenting the final mobility results for Ge, it would be worthwhile to exhibit some of the intermediate results for eventual comparison with Si. These intermediate results relate to the solution of the Boltzmann equation and have not been displayed by either Tiersten or Lawaetz. But first, we should keep in mind a few differences between our respective calculations. We use the three top valence bands by solving the cubic equation, Eq. (55), for the valence band dispersions. As a result, our bands are slightly nonparabolic, whereas Tiersten and Lawaetz use only the two top valence bands which, as a result, are parabolic. We adopt an isotropic phonon spectrum with spherically averaged phonon velocities for the three polarization branches. Tiersten and Lawaetz do use full solutions of the dynamical matrix for the phonon spectra and polarization vectors. Lawaetz shows, however, the results he obtained are insensitive to this detail[4].

In Figs. 1 and 2 we show the solution for that part of the distribution function affected by the application of electric field only, θ, for the L and H bands of Ge. It is convenient to display θ, Eq. (29), where

$$\theta^{\delta}_{N\lambda}(E) \equiv \sum_{M\lambda'} \left[S^{\delta}_{N\lambda,M\lambda'}(E)\right]^{-1} G^{\delta}_{M\lambda'}(E) \quad , \tag{74}$$

and has the units of (Ry a.u.). In practical units Eq. (30) is

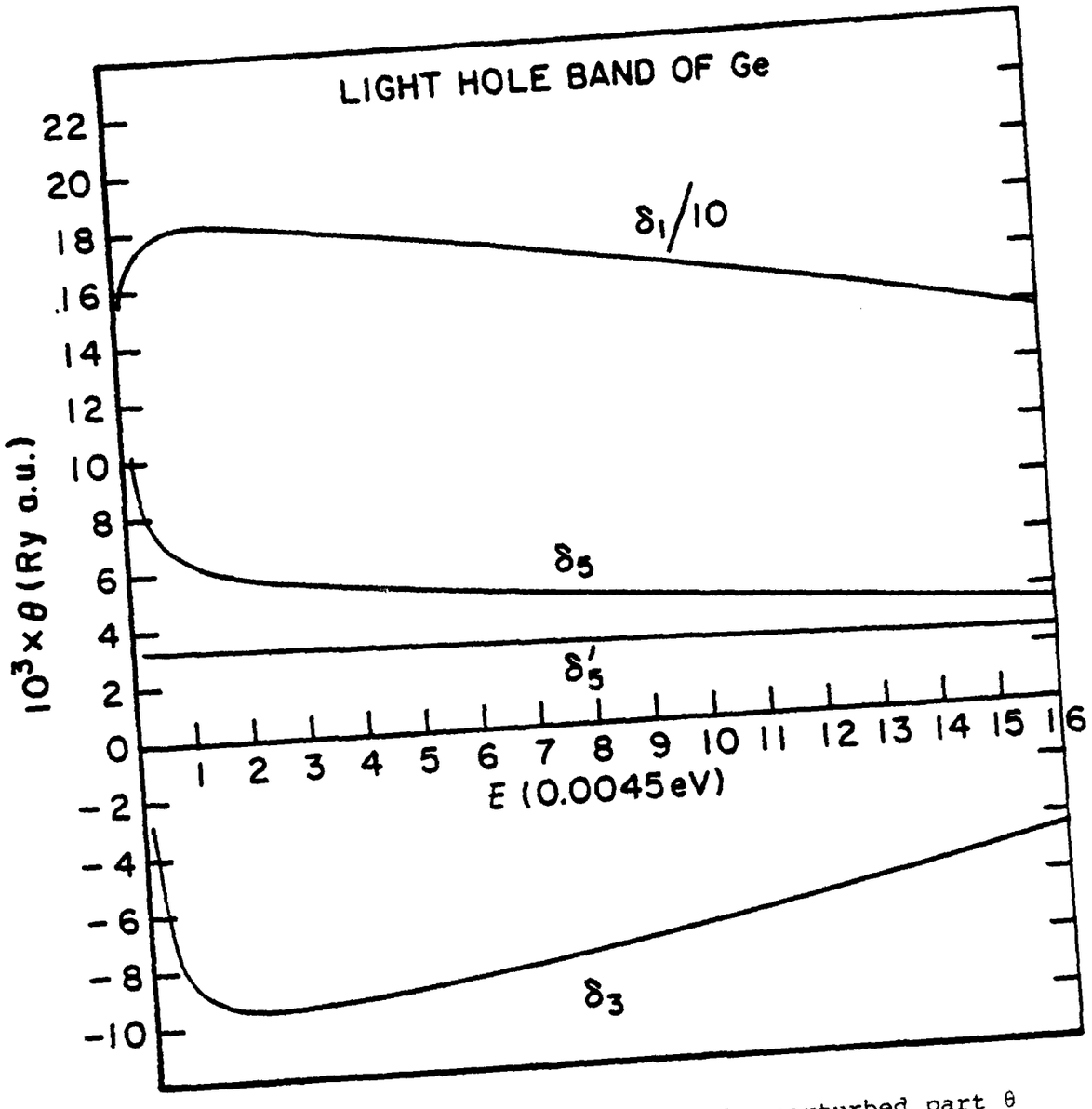

Fig. 1. Cubic harmonic decomposition of the perturbed part θ of the distribution function, Eq. (74), as a function of hole energy, for the light hole band of germanium.

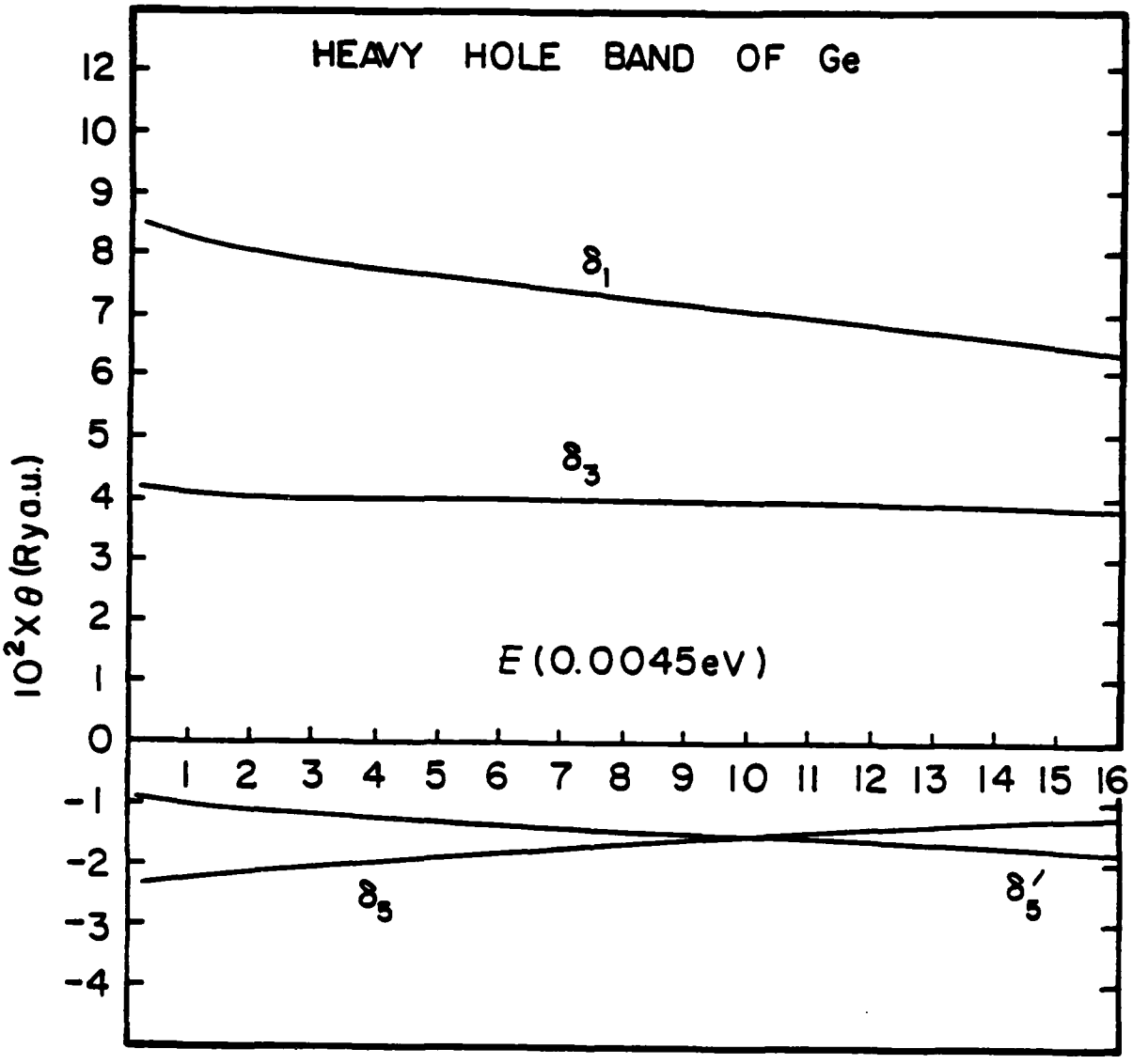

Fig. 2. Cubic harmonic decomposition of the perturbed part θ of the distribution function, Eq. (74), as a function of hole energy, for the heavy hole band of germanium.

$$\vec{\phi}_N(E,\hat{k}) = \frac{1.5312\times10^3}{t^2}\left(\frac{V}{cm}\right)^{-1}\sum_\lambda \begin{pmatrix} K_\lambda^{\delta x}(\hat{k})\hat{e}_x \\ \vdots \end{pmatrix} \bar{\theta}_{N\lambda}^{\delta}(E) \quad , \tag{75}$$

where t is the numerical value of the absolute temperature

$$T = (t)(°K) \quad , \tag{76a}$$

and $\bar{\theta}$ is the numerical value of θ,

$$\theta = \bar{\theta}\ (\text{Ry a.u.}) \quad . \tag{76b}$$

Since $f_N(\vec{k})$ is dimensionless, $\vec{\phi}$ has the units of inverse electric field.

From Figs. 1 and 2 we see that $\vec{\phi}$ is fairly well converged by the time the last, δ_5', cubic harmonic is taken into account. θ for the heavy hole band is remarkably constant over the entire energy range, whereas θ for the light hole band has an appreciable energy dependence at very low energies. This appears to be due to the closer proximity of the L band to the S band resulting in a greater nonparabolicity for the L band than for the H band. In practice, the H band, being more flat than the L band, contains more holes at any given temperature so that the transport properties of Ge (and Si) are greatly influenced by the less mobile holes in the H band. Yet, Fig. 1 does indicate that even in Ge one cannot treat the L band as being parabolic. In fact, one can consult Fig. 1 of Kane's paper[40] to ascertain that the H band is accurately parabolic, while the L band is not. From the dimensional analysis, Eq. (70), we expect for parabolic bands that $\phi\sim$constant. In fact, this is closely reflected in Fig. 2 for the H band, except at the very lowest of energies where there may be difficulties due to the neglect of the phonon energy in the argument of the delta function, Eq. (3). Since $\chi\sim\phi E^{-\frac{1}{2}}$ (72), any strong energy dependence in ϕ, or S and H, will reflect itself in the χ vs. E curves, which we show next.

In Figs. 3 and 4 we show the solution for the part of the distribution function affected by the application of the magnetic field, χ, for the L and H bands of Ge. From Eq. (43) we define an auxiliary quantity, ξ, through

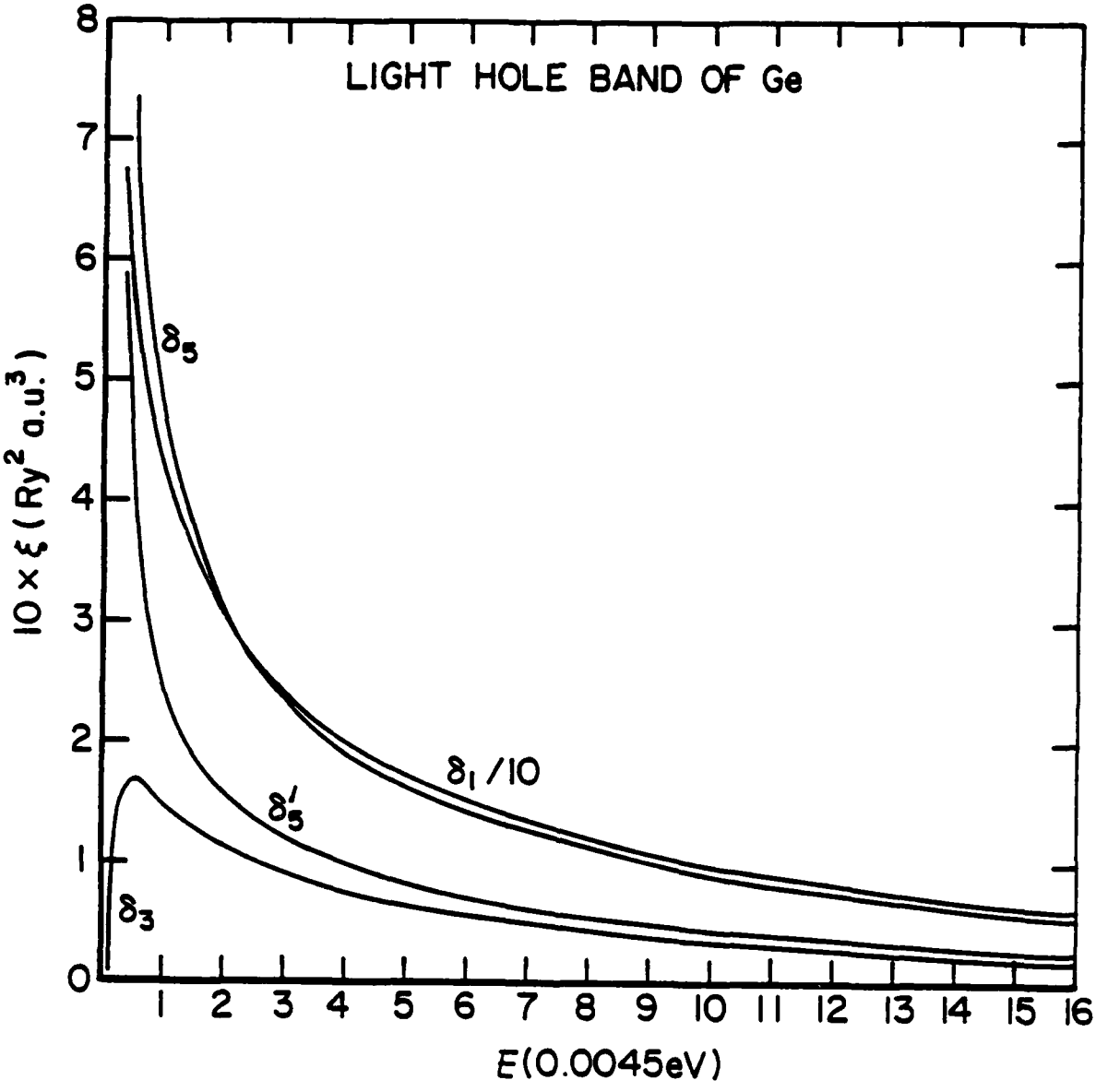

Fig. 3. Cubic harmonic decomposition of the perturbed part ξ of the distribution function, Eq. (77), as a function of hole energy, for the light hole band of germanium.

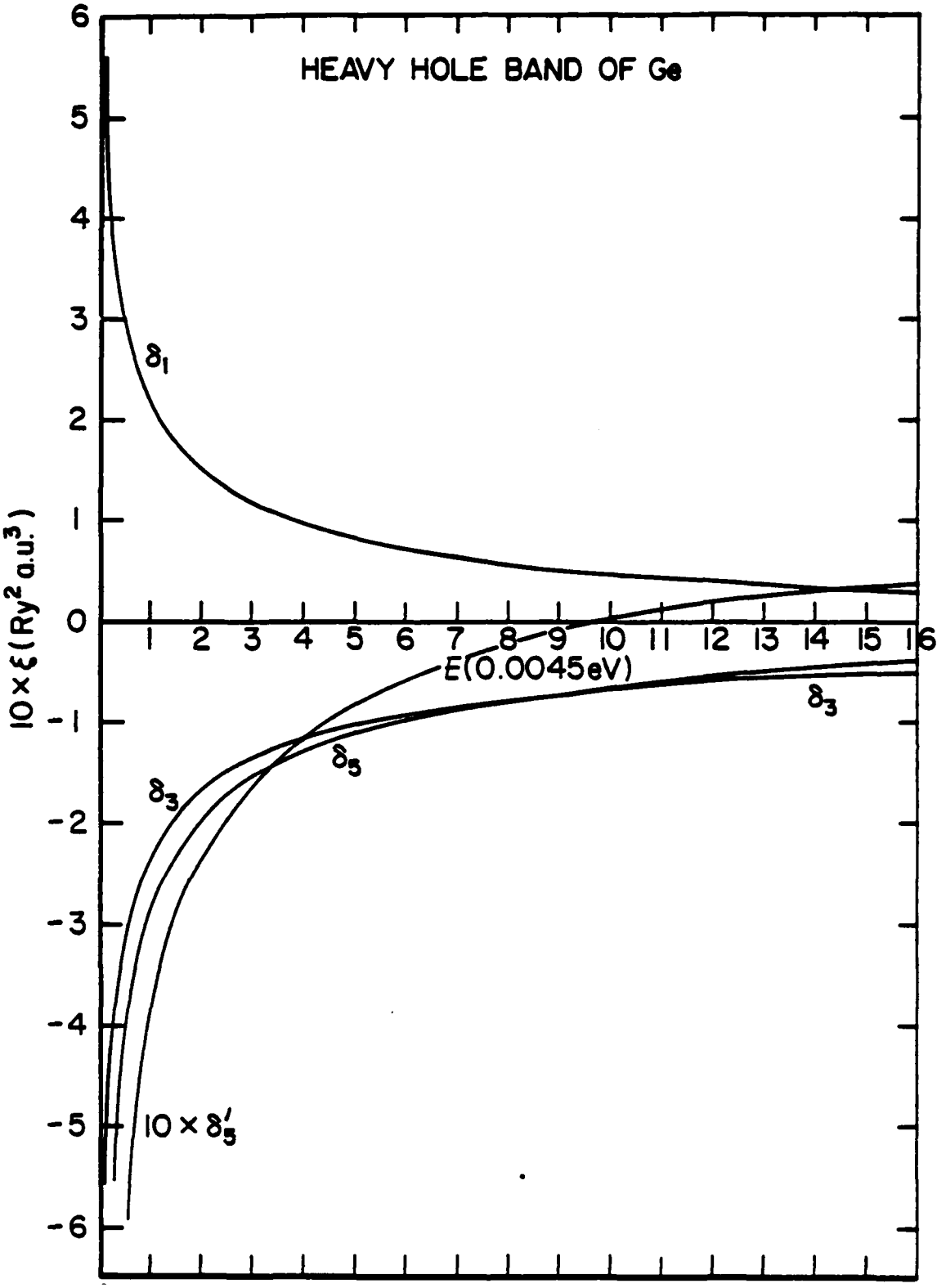

Fig. 4. Cubic harmonic decomposition of the perturbed part ξ of the distribution function, Eq. (77), as a function of hole energy, for the heavy hole band of germanium.

$$\chi^{\delta\nu}_{N\lambda}(E) \equiv \left(\frac{4\pi}{k_B T}\right)^3 \frac{4\pi e^2}{\hbar} \xi^{\delta}_{N\lambda}(E) \left[(\hat{F}x\hat{B})\cdot\hat{e}_\nu\right] , \qquad (77)$$

where $\xi_{N\lambda}(E)$ is in $(Ry^2 a.u.^3)$. In practical units

$$\chi^{\delta\nu}_{N\lambda}(E) = \frac{1.624 \times 10^9}{t^3} \frac{cm^3}{V^2 sec} \bar{\xi}^{\delta}_{N\lambda}(E) \left[(\hat{F}x\hat{B})\cdot\hat{e}_\nu\right] , \qquad (78)$$

where t is defined in (76a), and $\xi \approx \bar{\xi}$ $(Ry^2 a.u.^3)$. Since the B field is in $\frac{Vsec}{cm^2}$ and $F \sim \frac{V}{cm}$, χ has the units of $(FB)^{-1}$ to make f_N dimensionless

Figs. 3 and 4 mostly meet our expectations of displaying the $E^{-\frac{1}{2}}$ behavior, Eq. (72). The δ_3 part of ξ for the L band displays a rather violent downturn near the origin. This phenomenon can be traced to inflections in the corresponding θ curve, Fig. 1. We would like to point out that this behavior occurs over a very limited range of energies near the origin and should not affect our results for but the lowest temperatures, T<10K or so. In part, we can attribute the behavior to the known shortcomings of the theory for the lowest of energies where some assumptions of the theory break down. Of these, the most important one is the assumption of the elastic scattering between holes and phonons, Eq. (3), for low hole energies.

To further assure ourselves of the validity of our calculation, and to gain a further insight into its results, we present another intermediate result before displaying mobility curves for Ge. The integrands, apart from the Boltzmann factor, in Eqs. (53a and b) are known functions of energy in the parabolic limit. We define

$$U_N(E) \equiv \sum_\lambda \theta^{\delta}_{N\lambda}(E) g^{\delta\mu}_N(E) \quad \text{in } (Ry\ a.u.^{-1}) \qquad (79)$$

$$D_N(E) \equiv 4\pi \langle \alpha_o | \Gamma_N | \alpha_o \rangle \quad \text{in } (Ry^{-1} a.u.^{-3}) , \qquad (80)$$

and

$$W_N(E) \equiv \sum_\lambda \xi^{\delta}_{N\lambda}(E) g^{\delta\mu}_{N\lambda}(E) \quad \text{in } (\text{Ry}^2 \text{ a.u.}). \tag{81}$$

$D_N(E)$ is related to the density of states and for parabolic bands

$$D \sim \Gamma \sim \gamma^{1/2} \frac{d\gamma}{dE} \sim E^{1/2} , \tag{82}$$

whereas

$$U \sim \theta g \sim (\text{const.}) \times E \sim E , \tag{83}$$

$$W \sim \xi g \sim E^{-1/2} E \sim E^{1/2} . \tag{84}$$

Figs. 5, 6, and 7 display U, D, and W, respectively, for the light and heavy hole bands of germanium. In spite of the complicated θ dependence, displayed in Fig. 1, the U curve for the L band is close to being linear in E except for a small inflection for $E<0.0045$ eV. The plot for the H band is almost indistinguishable from a straight line. As expected $U_H > U_L$, by about a factor of four, since the heavy hole band has a greater density of states than the L band. Since $U_H/U_L \sim 4$, the conductivity mobility will be influenced by the H band more than by the L band. It turns out that the effect of the λ sum and the multiplication by g in Eq. (79) is to smooth out the small imperfections in the calculation of ϕ, Figs. 1 and 2, at small energies.

Fig. 6 displays the density-of-states like curves, D_N, for the L and H bands of Ge. As expected these do behave as $\sqrt{E}$. The densities of states are in the approximate ratio $D_H/D_L \sim 20$, so that there are many more H holes than L holes at any given temperature. Fig. 7 for W_N, which enters the Hall mobility calculation, again displays the expected $\sqrt{E}$ behavior and $W_L/W_H \sim 2$, therefore, the Hall mobility will be dominated by the L band. In all the cases, Figs. 5-7, the small energy dependence was verified and holds true to good accuracy. This is in spite of rather complicated behavior of θ and ξ in Figs. 1-4. In part, this is due to the averaging effect in summing over λ in Eqs. (79) and (81), and to the strong band effects contained in $g(E)$. This does not mean, of course, that any part of the treatment can or should be simplified since every step leading up to the final result has a

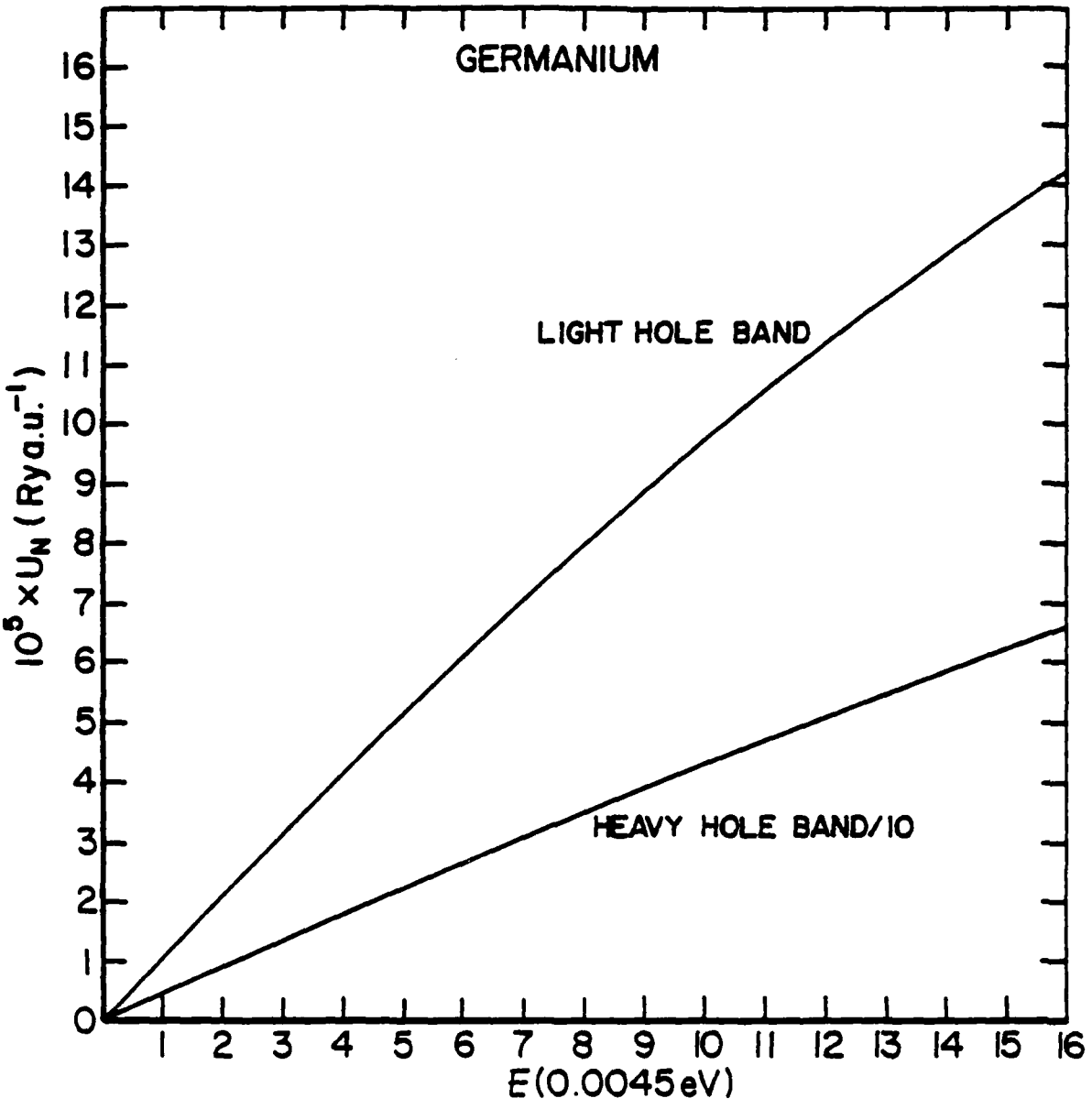

Fig. 5. Temperature independent part of the integrand in the numerator of Eq. (53a) for μ_c, defined by Eq. (79).

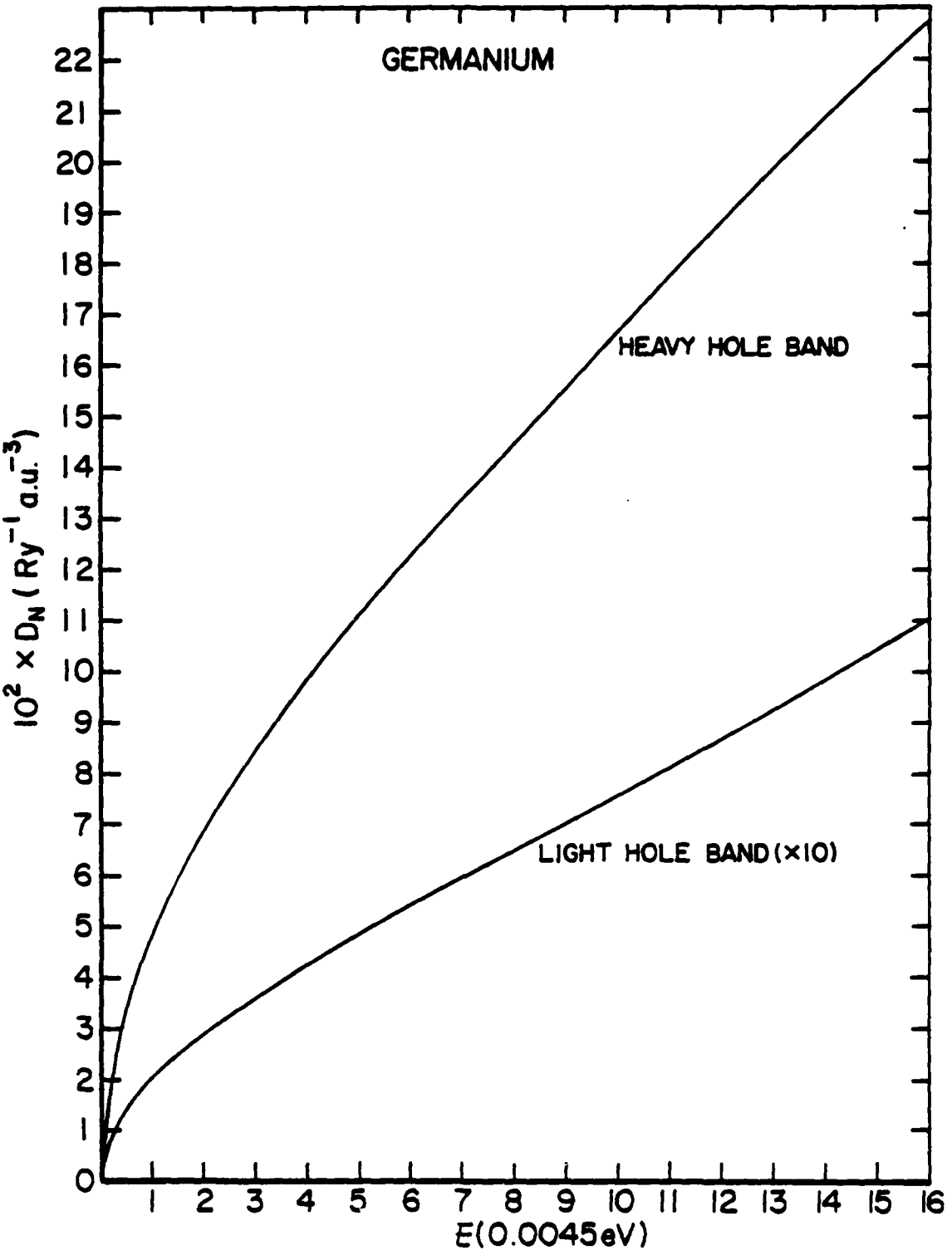

Fig. 6. Temperature independent part of the integrand in the denominators of Eqs. (53a and b) for μ_C and μ_H, defined by Eq. (80).

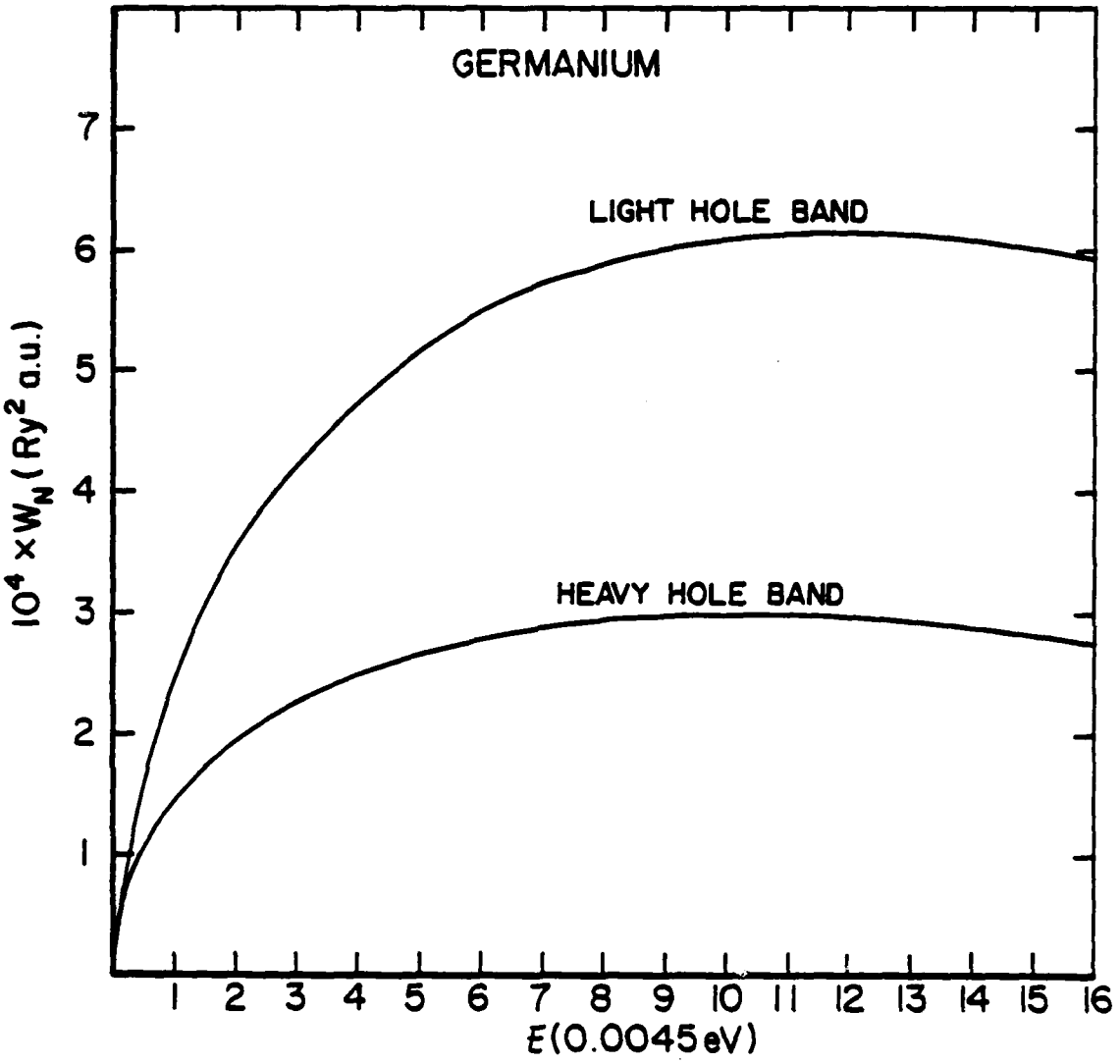

Fig. 7. Temperature independent part of the integrand in the numerator of Eq. (53b) for μ_H, defined by Eq. (81).

quantitative bearing on its accuracy. Finally, Figs. 5-7 validate our low energy interpolation procedure discussed in Eqs. (69)-(73).

Figs. 8 and 9 show the total and partial conductivity and Hall mobilities, respectively, as a function of absolute temperature for Ge. The partial mobilities are defined by the following equation

$$\mu_{c,H} = \frac{\sum_N p_N \mu^N_{c,H}}{\sum_N p_N} \tag{85}$$

where $\mu^N_{c,H}$ are the partial mobilities. Eq. (85) is motivated by a model where the bands conduct current as a parallel resistor network. In this model, therefore, the band conductivities are additive as though the bands were noninteracting. Since we have shown that the interband scattering is as important as the intraband scattering, the motivation for the model does not hold any longer. Yet, we can still define the partial band mobilities through Eq. (85) and draw some conclusions from the results. In the case of both mobilities the light hole band mobility is the larger of the two, Figs. 8 and 9, with $\mu^L_c/\mu^H_c \sim 5$ and $\mu^L_H/\mu^H_H \sim 40$. Physically, the larger light hole band mobilities are the consequences of its having a smaller effective mass[21], $M_H/M_L \sim 8$. In the case of the Hall mobility the L band becomes the dominant band in spite of the fact that it contains twenty times fewer holes than the H band.

Let us now compare the results of our theoretical formulation of the problem and calculational formalism with the results of calculations by Tiersten and Lawaetz. Tiersten calculated the conductivity mobility for Ge in the parabolic band approximation using the H and L bands only. As we have shown, the L band's nonparabolicity has its strongest effect on the Hall mobility. Using the parameters listed in Table 1 Tiersten obtained the expected $T^{-1.5}$ temperature dependence for the conductivity mobility, as did Lawaetz, with

$$\mu_c(100K) = 3.13 \times 10^4 \text{ cm}^2/\text{Vsec}.$$

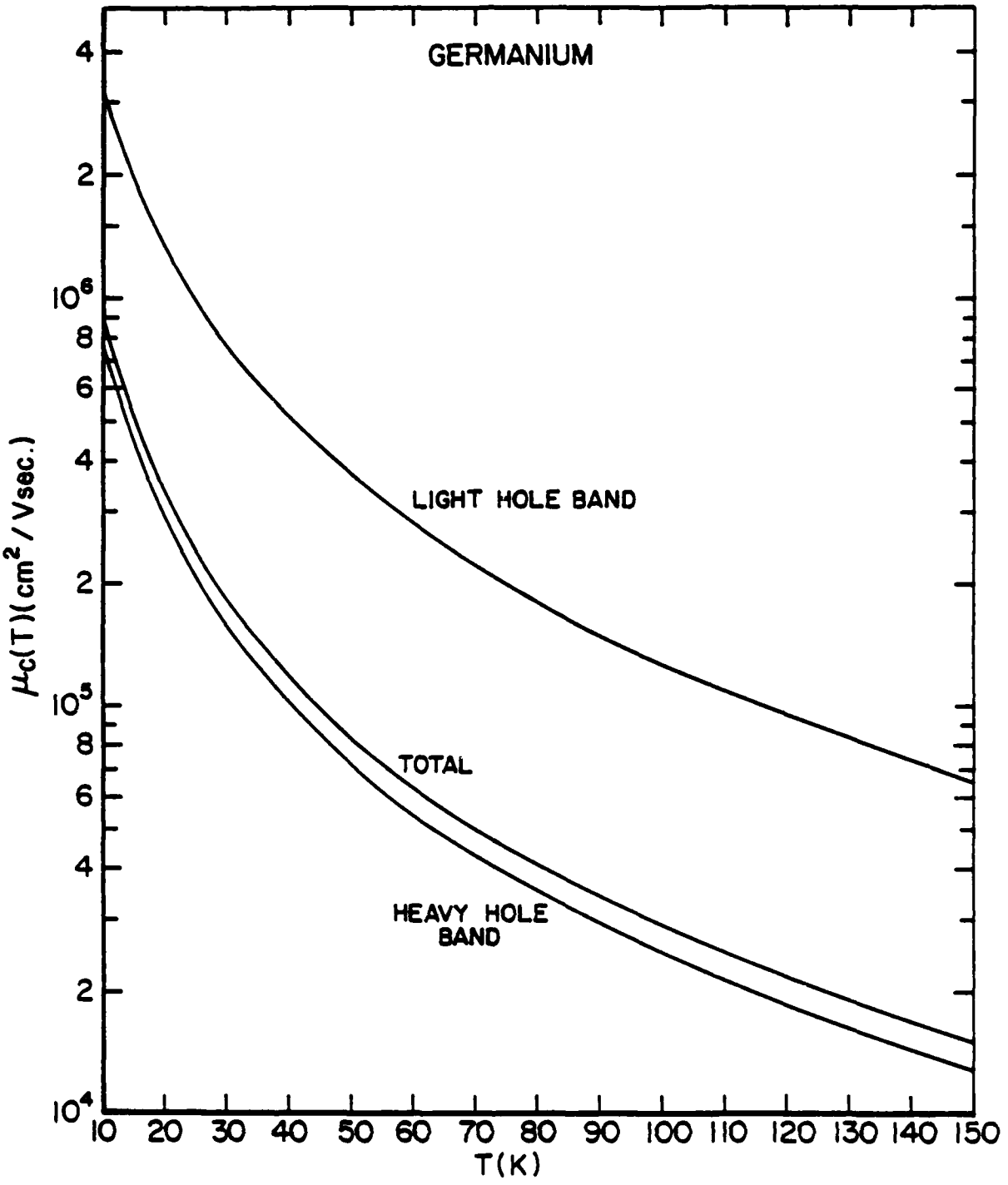

Fig. 8. Calculated total and partial conductivity mobilities, in the acoustic phonon limited regime, as a function of temperature.

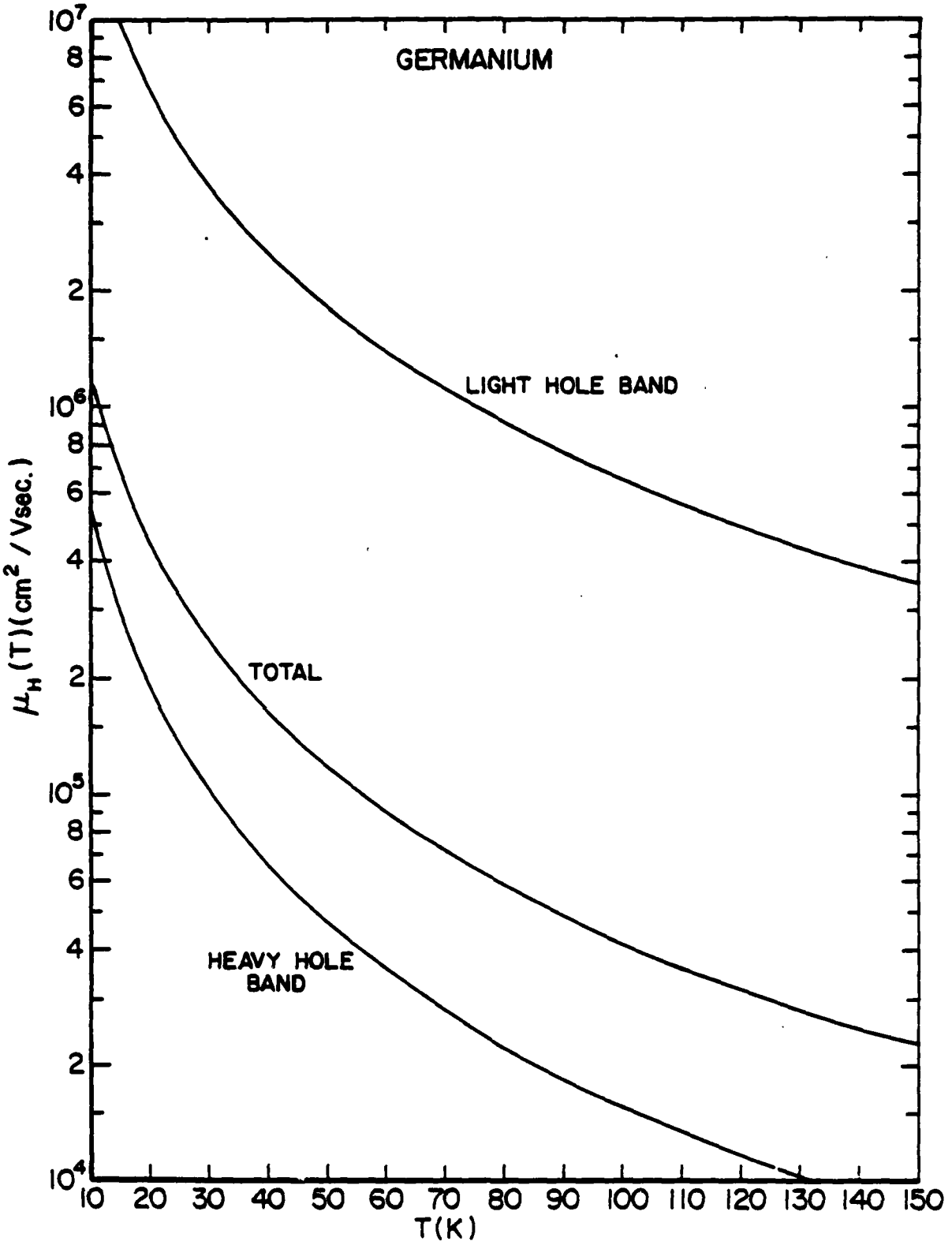

Fig. 9. Calculated total and partial Hall mobilities, in the acoustic phonon limited regime, as a function of temperature.

Lawaetz using essentially the same formalism as ours, but with two parabolic bands, states that his 100K value for μ_c differs from Tiersten's value by about 2%. Our value for the acoustic phonon iimited conductivity mobility at this temperature is

$$\mu_c(100K) = 2.89 \times 10^4 \text{ cm}^2/\text{Vsec} \quad ,$$

which differs from Tiersten's result by about 7.7%.

This small difference can be accounted for by several factors which distinguish our respective calculations. One of these might be the precision with which the transition probabilities were fitted to the double cubic harmonic series. We use a far larger sampling of $(\hat{k},\hat{k}')$ scattering directions than Tiersten and a larger number of cubic harmonic pairs for the fit[44]. In addition, we do not treat the L band as parabolic which is a progressively worse approximation as higher galvanomagnetic coefficients are calculated. On the other hand, Tiersten's more rigorous treatment of the phonon spectrum is an improvement over our isotropic phonon spectrum approximation. However, we believe that it is the parabolic L band approximation which accounts for the bulk of the difference.

Fig. 10 displays both the calculated r-factor for germanium, data to be discussed later, and exponents α_c,α_H in

$$\mu_c = AT^{-\alpha_c} \tag{86}$$

$$\mu_H = BT^{-\alpha_H} \quad . \tag{87}$$

The temperature exponent of the conductivity mobility, α_c, starts out at 10K with $\alpha_c = 1.498$ and rises monotonically to $\alpha_c = 1.575$ at 120K. The temperature exponent for the Hall mobility, α_H, rises steadily from $\alpha_H = 1.420$ at 10K to $\alpha_H = 1.545$ at 120K. This represents a rather small temperature variation about the value $\alpha_{c,H} = 1.5$ for strictly parabolic bands.

It is more difficult to compare our results for μ_H and r with those of Lawaetz (Tiersten did not calculate these quantities). Lawaetz does obtain $\alpha_H = 1.5$ which is the correct

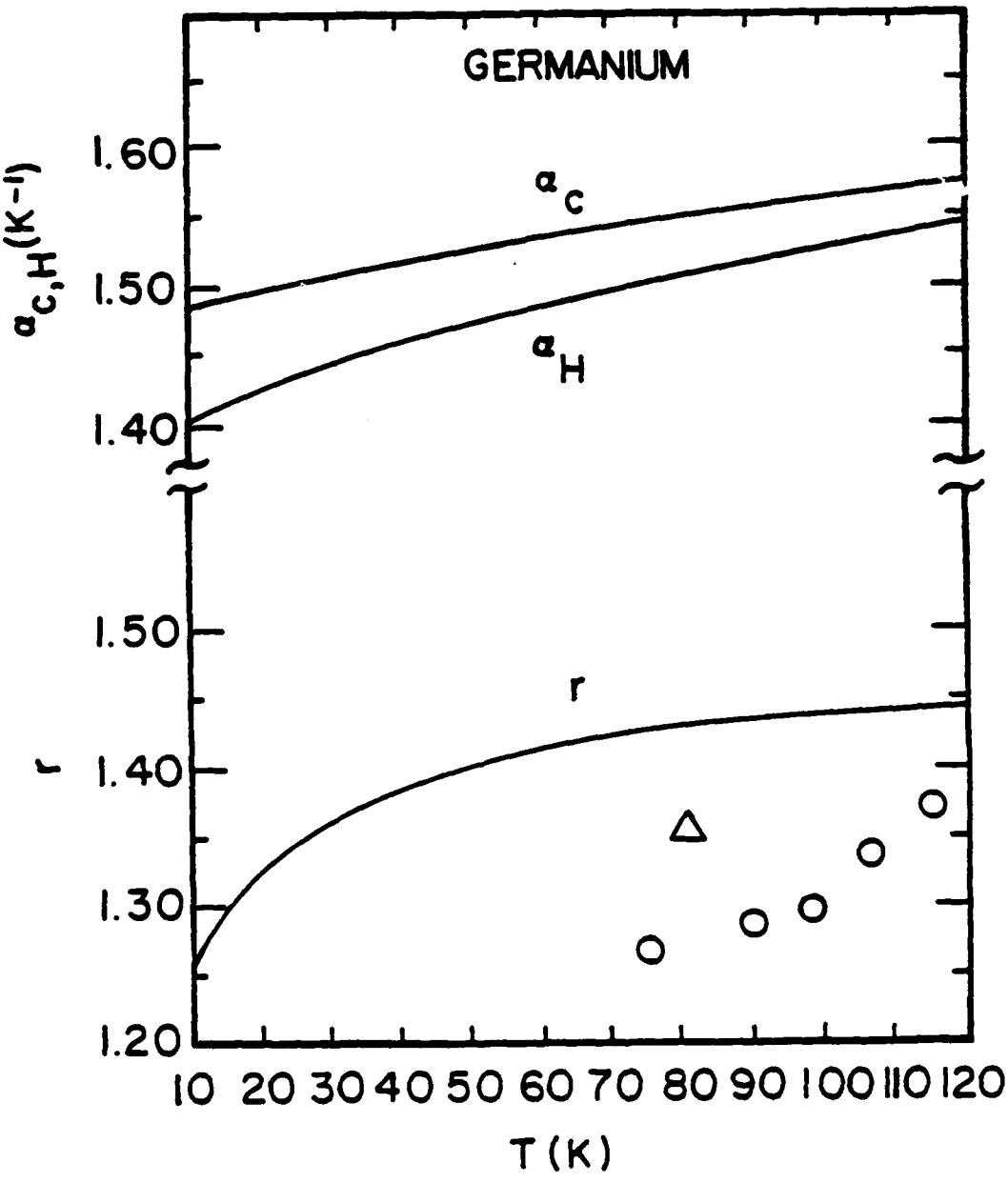

Fig. 10. Top scale: Calculated temperature exponents α_c for the conductivity mobility, and α_H for the Hall mobility (solid line).

Lower scale: The calculated r-factor (solid line) and experimental data of Beer and Willardson-triangles (Ref 53, impurity content $1x10^{13}cm^{-3}$), Goldberg, et al.-circles (Ref. 54, sample D, impurity content $2.4x10^{13}cm^{-3}$).

exponent for both mobilities in the parabolic band regime. Our α_H is lower than 1.5 for T<70K thus reflecting the dominant influence of the light hole band to μ_H. Lawaetz provides the value of r = 1.60 for the choice of the deformation potential parameters b = -2eV, d = -7eV, and a value of the dilatational deformation potential a>0 which will yield the lowest value for r for acoustic mode scattering only. The value of r = 1.60, therefore, represents the lowest value Lawaetz calculated for acoustic phonon limited mobility with fixed b and d, and a positive value for a. From Fig. 3 of Ref. 2 we estimate that for the parameters in Table 1 Lawaetz obtained r$\sim$1.6-1.7.

The experimental value for r that Lawaetz used for comparison with the theory is the value of r = 1.36 $\pm$ 0.07 at 81K obtained by Beer and Willardson[53] (sample impurity content $1x10^{13}cm^{-3}$). This is far below Lawaetz's r$\sim$1.6-1.7. On the other hand, our result at 81K is r = 1.43, Fig. 10, which is very close to the r of Beer and Willardson, with the parameters used by Lawaetz.

We can suggest primarily two reasons for the different results of the two theoretical calculations. As we have shown, the light hole band is quite nonparabolic and dominates the Hall mobility. The L band, therefore, alters μ_H and r from the values calculated in the parabolic approximation. We also have one misgiving about Lawaetz's chosen form for his scattering matrix K (S in our notation). His K matrix, Eq. 3.15 of Ref. 4, uses the completeness relation for cubic harmonics in the second term of K involving the sum over $\mu\nu$. Formally, this is correct, but computationally one has to achieve convergence in the sum over an additional angular momentum index. The sum over μ can be eliminated by using the completeness relation so there will be only one sum over ν to carry to convergence. We feel this would be a safer procedure considering that in order to calculate μ_H one must use S^{-1} twice, Eqs. (29) and (43).

Fig. 10 also displays the data for sample D of Goldberg, et al.[54] with the impurity concentration of $2.4 \times 10^{13} cm^{-3}$ (their sample G was less pure than sample D). Older data of Morin[55] for r is not shown, since the impurity content is unknown, but it generally falls below the data of Goldberg, et al. Thus, by comparison with the data of Goldberg, et al. the calculated r factor is about 12% too high. It appears that the data of Beer and Willardson coming from a purer sample may be more representative of a high purity sample with less of ionized impurity scattering. By contrast, Nagakawa and Zukotynski[10] calculate $r \sim 2.0$ in this temperature range, far above the measured values. Ref. 10 also shows that ionized impurity scattering has the effect of dramatically lowering the value of r.

Although it has not been our aim to provide a critical comparison between experiment and theory for Ge, we can offer several suggestions concerning the results. First of all, the data used for comparison in Fig. 10 is in the temperature range where the optical phonon scattering should come in for germanium. Therefore, the data may not be representative of the temperature regime for the acoustic phonon limited mobility T<80K. Second, we would have liked to use for comparison data obtained from higher purity samples, on the order of $10^{11} cm^{-3}$, for low temperatures, T<80K. No such data for the same sample seems to exist for Ge where both the high and low magnetic field limits were explored to obtain the conductivity and Hall mobilities, respectively. Third, the values of the deformation potential parameters for Ge are still in doubt. In particular, the compilation of these parameters by Wiley[28] suggests that our value for d is probably too high. We, however, do not feel that the experimental situation here has been resolved enough to warrant another calculation for Ge at this time.

Fig. 11 presents the comparison between our calculated conductivity mobility and results of measurements by Ottaviani, et al.[56] and Brown and Bray[57]. A rather close agreement is found for T<80°K, while for T>80K one can see already the influence of the optical phonon scattering in the data of Brown and Bray. Also, the 20°K μ_c point of Ottaviani et al.[54] may

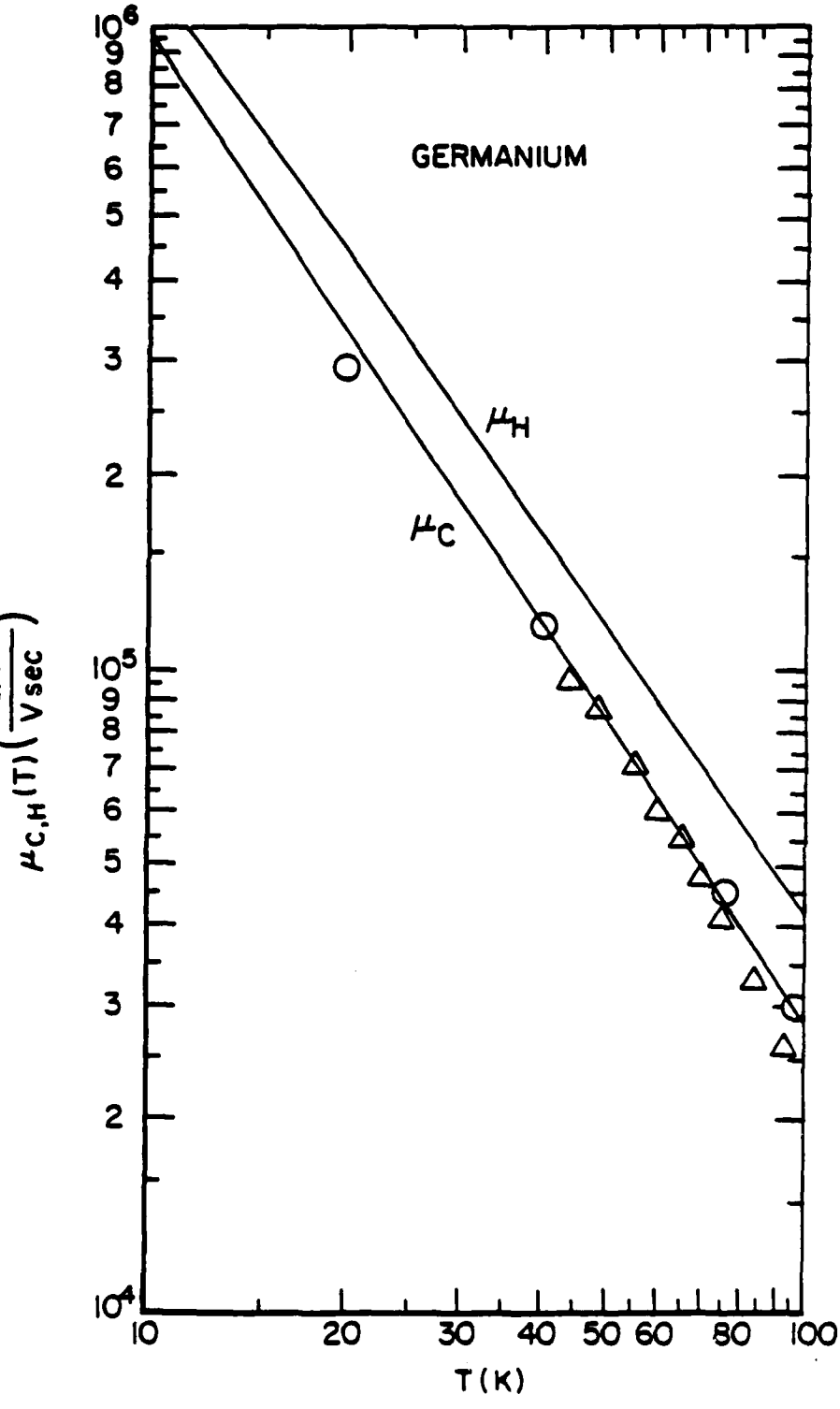

Fig. 11. Calculated conductivity and Hall mobilities (solid lines) and the data for μ_c of Ottaviani, et al.-circles (Ref. 56, time-of-flight method, impurity content $<1x10^{11}cm^{-3}$), and Brown and Bray-triangles (Ref. 57, impurity content $1.25x10^{13}cm^{-3}$).

be indicating the presence of ionized impurity scattering. Owing to the lack of the μ_H and μ_C data on the same high purity sample for low temperatures, we cannot present a comparison with theory for μ_H. For this purpose it is best to consult Fig. 10 for the r-factor.

The calculation for germanium has achieved its purpose as a testing ground for the theoretical and computational procedures. We have reproduced the results of earlier μ_c calculations of Tiersten and Lawaetz and improved considerably the results for μ_H by including the nonparabolicity for the L band. The degree of quantitatitive agreement this calculation has achieved with experiments does indicate that a first-principles approach can be quantitatively successful and confirms the fundamental correctness of the deformation potential theory. This viewpoint will be reinforced in the next section on Si where a more reliable set of deformation potential parameters will be used and comparison made with our experimental results.

SECTION V
RESULTS FOR SILICON

1. EXPERIMENT

The material used for this experiment was all ultra-high purity, vacuum float zoned, p-type silicon. The residual acceptor in this material is boron, which was found by conventional Hall analysis to be present in concentrations in the range of $10^{12}cm^{-3}$ or less. The total residual donor concentration was in the low $10^{11}cm^{-3}$ range for all but one of the samples studied. The donors are most likely phosphorus but were not identified. Both Hall bars and van der Pauw cloverleaf samples were cut from wafers of several boules. The Hall coefficients of these samples were measured over the magnetic field range of 0.003 to 2.0 T at several temperatures between 20 and 50K. The typical range of $\omega_c\tau$ at 20K, determined by assuming $\omega_c\tau \approx \mu_c H$, was between 0.05 and 30, so we were clearly able to reach both the high and the low field limits with our magnet. Accurate measurements of $R_H(\infty)$ were prevented for temperatures above 50K by the decrease in the mobility, which forced the high field values of $\omega_c\tau$ considerably below 10. Because of some lack of certainty, even at the lowest temperatures, as to the precise value of $R_H(\infty)$, the high field data at each temperature were fitted to a simple form to yield the saturation value. It is well known that the Hall coefficient must be an even function of H, which means that $R_H(\infty)$ must be approached as H^{-2}. We therefore fitted our high field data to the form

$$R_H(H) = R_H(\infty) + AH^{-2} \qquad (88)$$

with $R_H(\infty)$ and A as adjustable parameters. Only values of R_H for $\omega_c\tau>4$ were used at any temperature for this fitting. The low temperature limit for the measurements was determined by the input impedance of our Hall effect system which is about $10^{14}\Omega$. This limits the sample resistance to $10^{12}\Omega$ and the sample resistivity to about $10^{10}\Omega$-cm. This system is described elsewhere[58].

Because most Hall effect measurements are made in the low field limit, $\omega_c\tau<<1$, where R_H also approaches a constant value[59],

we will define a magnetic field independent r for the purposes of this report as the ratio of R_H in the two limits or

$$r = \frac{R_H(0)}{R_H(\infty)} = R_H(0)ne \qquad (89)$$

where $R_H(0)$ and $R_H(\infty)$ are respectively the low and high field limits of the Hall coefficient. In a similar manner, the Hall mobility will be considered as the low field Hall mobility.

Fig. 12 shows one of our cleaner field sweeps plotted as $R_H(\omega_c\tau)/R_H(\infty)$ versus $\omega_c\tau$. In this form the low field plateau represents r. The solid line is drawn to show the trend in the data and does not represent any attempt to fit the data to a functional form throughout the entire field range. Fig. 13, which is a collection of all such lines for the sample shown in Fig. 12, clearly shows a temperature dependence in r. This temperature variation was seen in all the samples we studied. Fig. 14 shows the temperature variation of r for our four samples. The open symbols are Hall bars and the solid ones are van der Pauw cloverleaves. All four samples came from different boules but were all of similar purity. Table 2 gives the results of conventional (r=1) Hall analysis of these samples.

TABLE 2

HALL ANALYSES OF SAMPLES

Sample	Shape	$N_B(cm^{-3})$	$N_D(cm^{-3})$	N_B/N_D
1300-V	v.d.P.	9.14×10^{11}	3.33×10^{11}	2.74
1202-H	Hall	6.57×10^{11}	3.96×10^{11}	1.66
2001-V	v.d.P.	2.62×10^{12}	2.08×10^{12}	1.26
4802-H	Hall	5.93×10^{11}	2.36×10^{11}	2.54

Although the scatter in Fig. 14 is considerable, the difference between the Hall bars and the van der Pauw samples could be real. The Hall bar is a more satisfactory configuration for high magnetic field measurements than the cloverleaf shape because the current path is less tortuous and therefore less likely to be

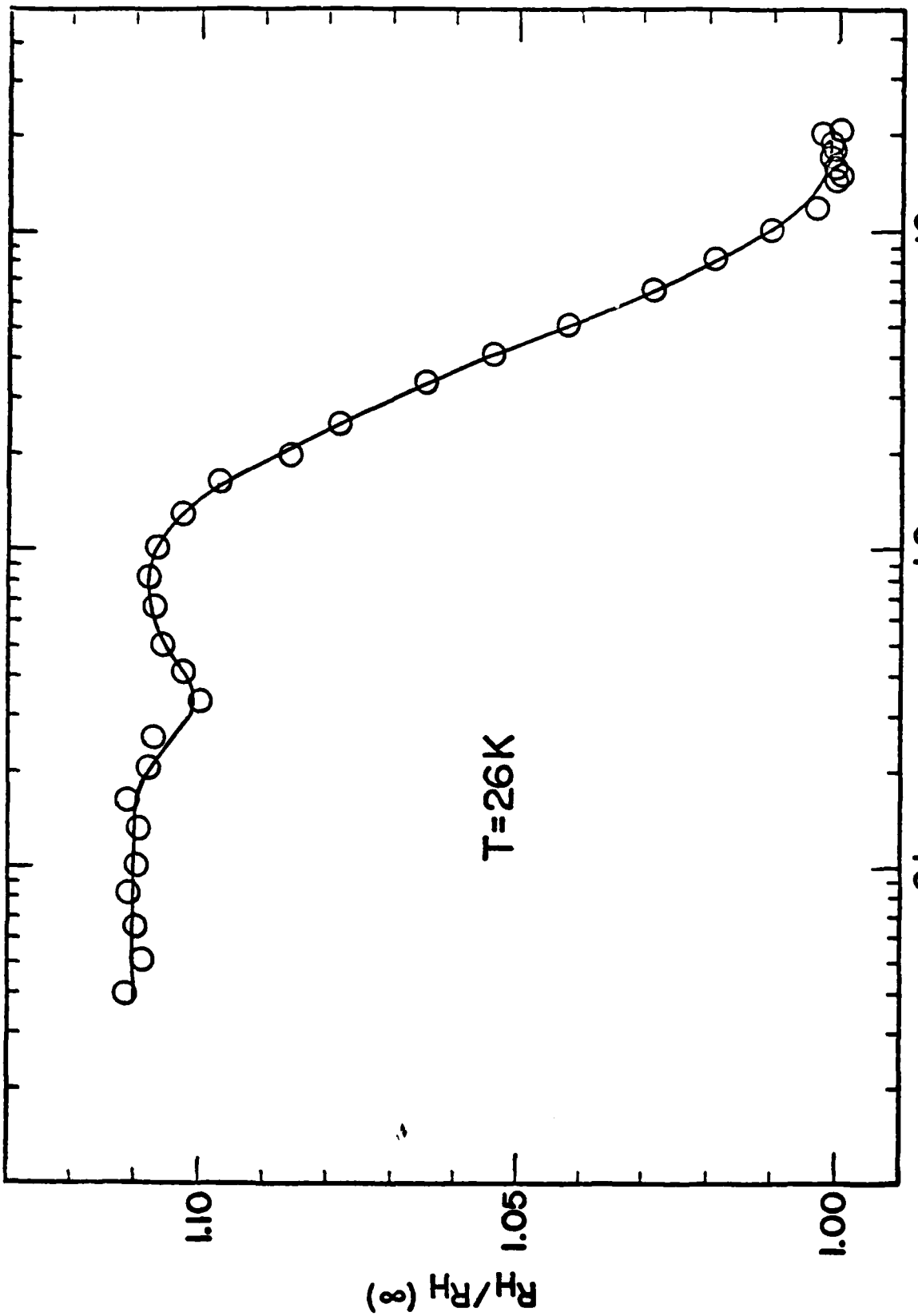

Fig. 12. Reduced Hall coefficient versus $\omega_c\tau$ for sample 1002-H at 26K.

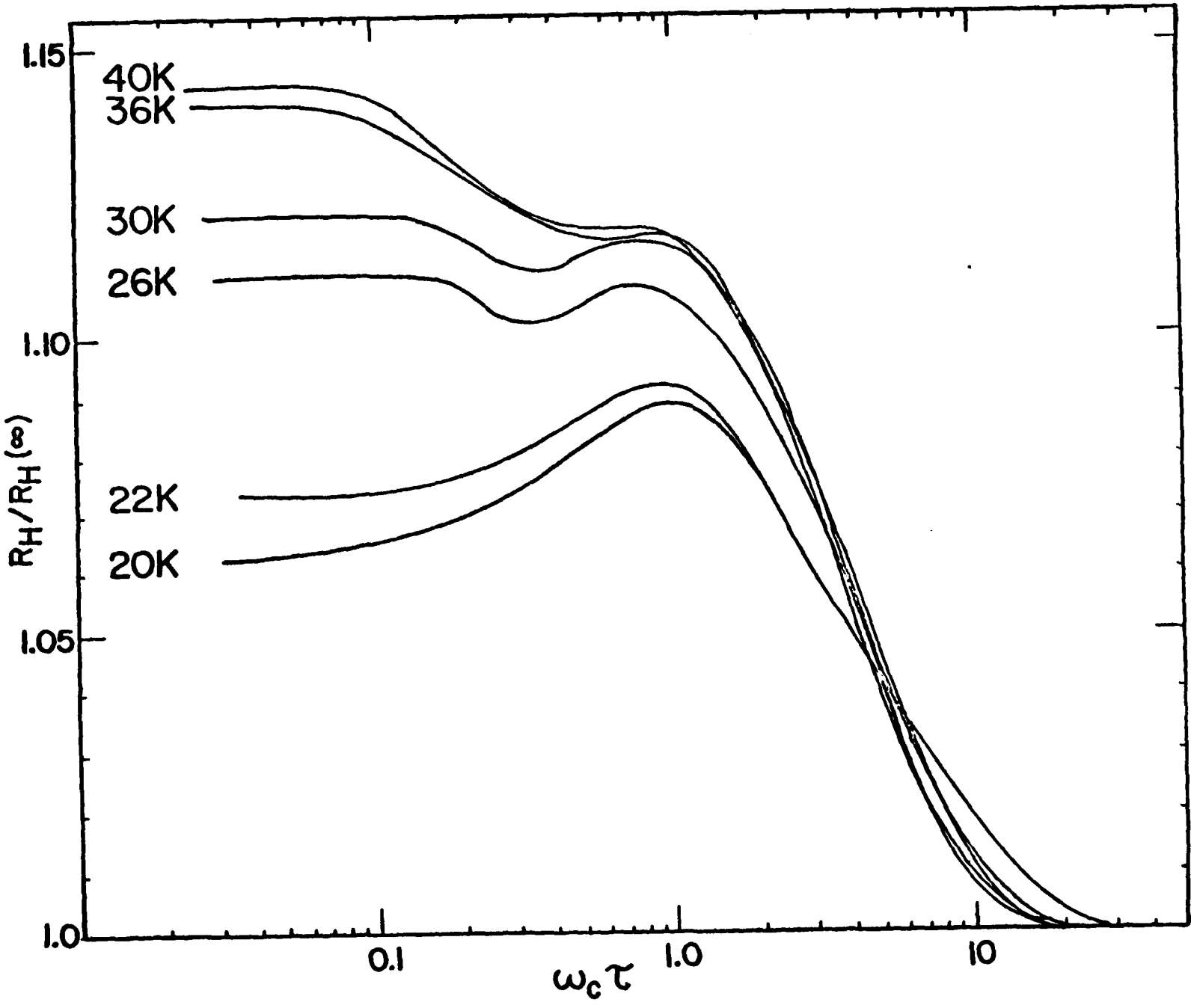

Fig. 13. Field dependence of the reduced Hall coefficient of sample 1202-H showing the variation with temperature.

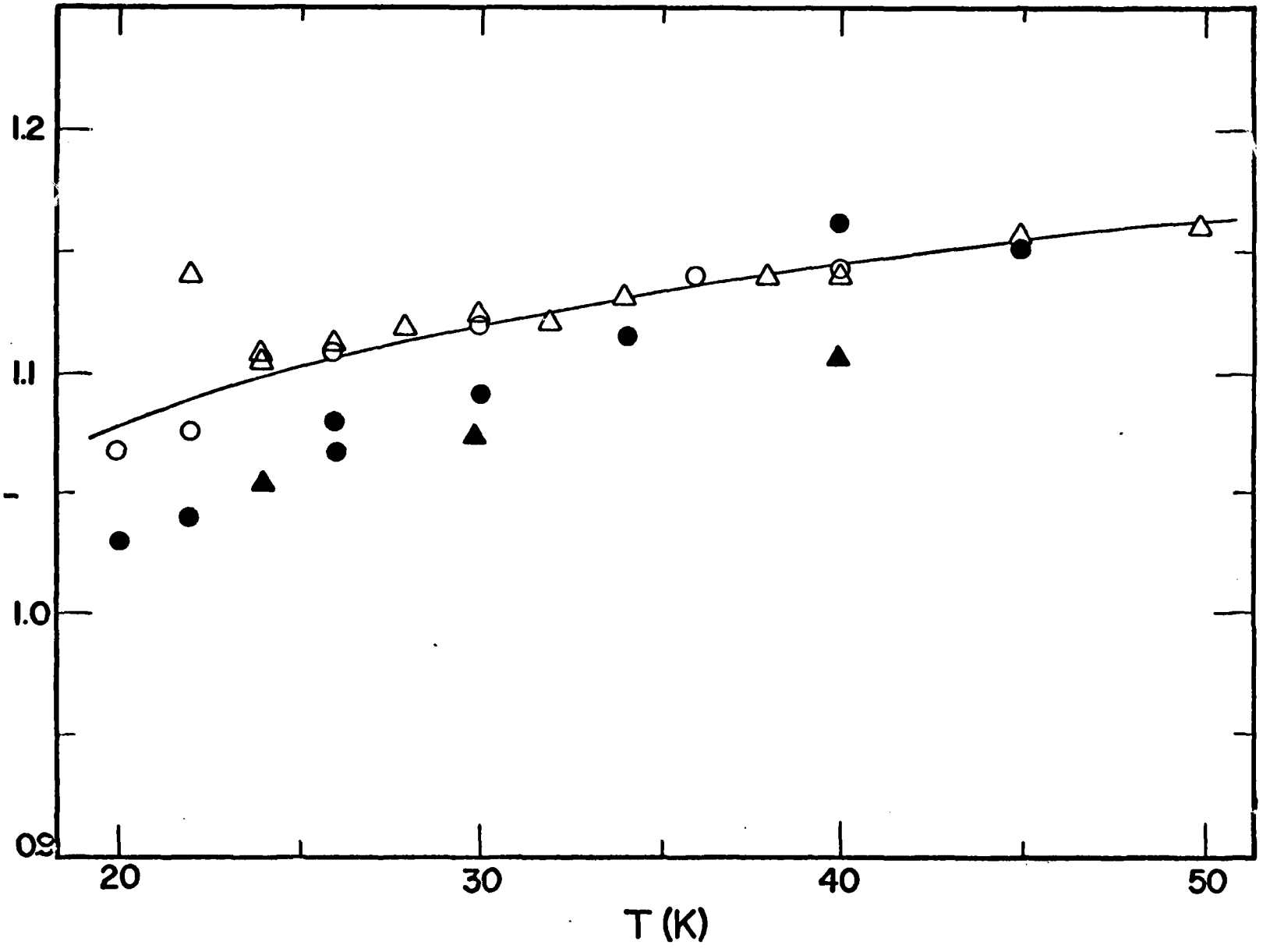

Fig. 14. Hall factor as a function of temperature. 0: 1202-H; Δ: 4802-H; ●: 1300-V; ▲: 2001-V. The solid line is the best fit to the Hall bar data.

distorted in large fields. Some aspects of probe effects and sample shape are discussed by Frederikse and Hosler[60].

The dominant feature in the curves in Fig. 13 is the hump near $\omega_c\tau=1$. The position of the hump shows little variation with temperature or between samples but the height does tend to vary between samples, those with the larger r at a given temperature show a slightly higher hump. This feature somewhat resembles the structure in the curves of r versus H for germanium calculated by Beer and Willardson[61] which is a result of the multiple nature of the valence bands. Since silicon and germanium have similar multiple valence bands, we feel that this is the likely source of this feature. Unfortunately, the scatter in our data is too large to make any quantitative statements about this interesting structure.

During the conventional Hall effect versus temperature measurements made on these samples for analysis, we also measured the Hall mobility from 20 to 380K at 0.1T which is shown in Fig. 15 for one sample. At the low temperature end the mobility appears to obey a simple power law, $\mu_H \propto T^{-\alpha_H}$, where α_H is a positive number. This dependence holds up to about 100K where there is a transition to a steeper negative slope in the log μ_H versus log T plots. This break is usually attributed to the onset of optical phonon scattering while the shallower slope is characteristic of acoustic phonon scattering. There is no indication of a turnover toward a positive slope at the low end which would indicate ionized impurity scattering. This is consistent with the fact that there are only $10^{12}cm^{-3}$ ionized centers in this material. The concentrations of neutral scattering centers are in the 10^{15}-$10^{16}cm^{-3}$ range and are primarily non-active oxygen and carbon impurities that were measured in similar material by optical absorption. The scattering in the temperature range of this experiment is therefore exclusively due to acoustic phonons.

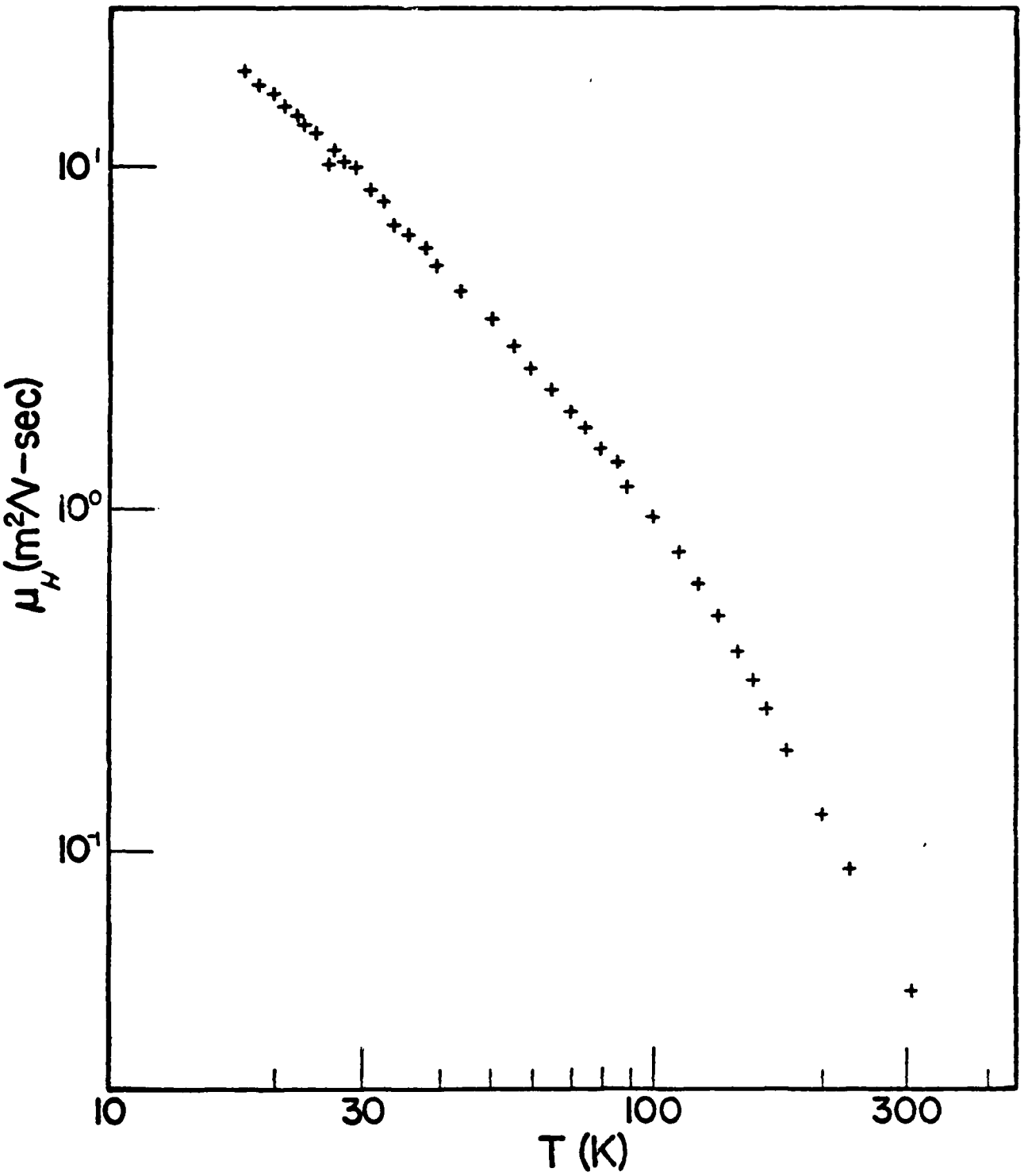

Fig. 15. 0.1T Hall mobility for sample 1202-H.

2. COMPARISON WITH PREVIOUS THEORETICAL RESULTS

Many attempts have been made over the years to calculate the Hall factor and the conductivity mobility for acoustic phonon scattering. The simplest calculation is a Drude-type approach which assumes a constant, isotropic scattering time and free electrons, that is, a single, spherical, parabolic band. This approach yields the simple result that r=1 for all magnetic fields. This, of course, implies that the conductivity and Hall mobilities are identical. The temperature dependence of the mobility in this model is due to the statistics of the phonons and electrical carriers. It is only when the scattering time is a function of energy or velocity that r deviates from unity. The standard textbook value of $3\pi/8$ for acoustic phonon scattering is obtained by assuming the scattering time, τ, is proportional to $E^{-\frac{1}{2}}$, again with a spherical and a parabolic band[62]. Lax and Mavroides[63,64] included the warpage of the valence band; i.e., nonspherical energy surfaces, but did not include nonparabolicity, which is important for the valence bands in this material. They used a relaxation time of the form $\tau=\ell E^{-\lambda}$. The value of r they obtained was again independent of temperature. More recently, Nakagawa and Zukotynski[10], using a relaxation time approximation, calculated the conductivity mobility of p-type silicon for acoustic phonon scattering. They included both the warpage and the nonparabolicity of the two major valence bands. In addition, they used a more realistic scattering time.

We used $R_H(\infty)$ and the zero field conductivity to determine the conductivity mobility, and in a similar manner determined the true low field Hall mobility using $R_H(0)$. Fig. 16 shows these two mobilities for the sample presented in Figs. 12 and 13. The temperature dependences are also given assuming a simple exponential. The exponent of T in the Hall mobility for all samples studied varied between 1.6 and 1.7 while that for the conductivity mobilities varied between 1.7 and 1.8. For a given sample the exponent for the Hall mobility was always the smaller positive number of the two.

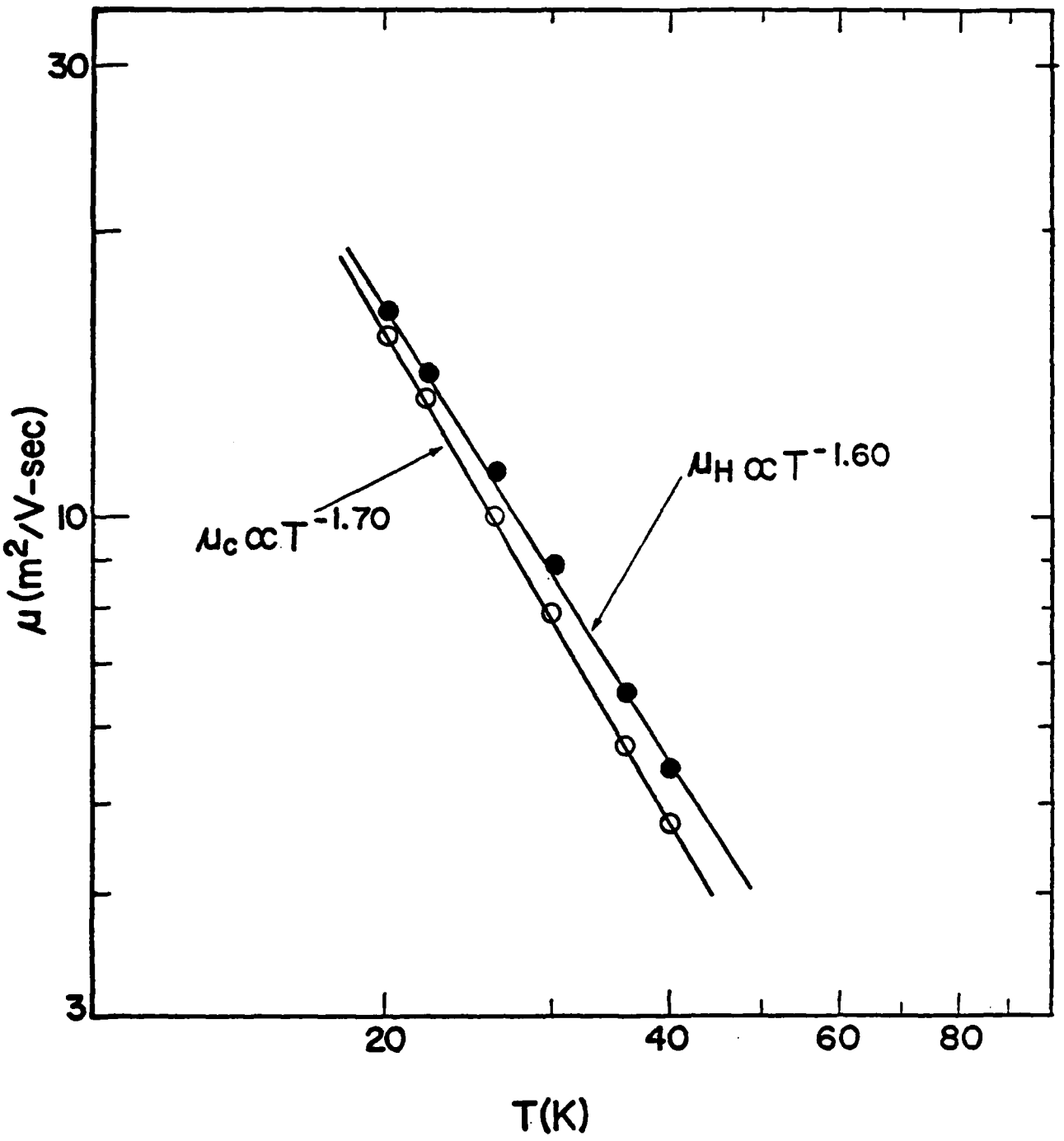

Fig. 16. Mobilities of sample 1202-H. Open circles: conductivity mobilities; solid circles: Hall mobilities.

From the simple physical arguments the temperature dependence of the Hall factor can be due to at least one of two possible effects. Firstly, the nonparabolicity of the valence bands combined with the warpage will produce a temperature variation and this can be seen quite simply. As shown by Lax and Mavroides, warpage alone produces a deviation from one in the Hall factor but if the bands are parabolic, there will be no change with temperature because the shape remains constant as the energy increases. If, however, there is a deviation from simple parabolicity, the shape of the constant energy surfaces will vary with increasing energy. As the temperature increases, more and more carriers will populate progressively deeper energy states and as they do they will see differently shaped energy surfaces, thus changing the overall Hall factor. The other possible source of the temperature variation could be a change in the fractional density of carriers in the three valence bands. The light and heavy hole and the split-off bands each have different warpages and nonparabolicities so each taken individually will have a different r. If the distribution of carriers amongst these bands varies with temperature, the total r will therefore also have to vary.

Assuming the simple form $r=aT^b$, we obtained a fit to the measured r's for the two Hall bar samples. The result of this fit is the solid line in Fig. 14. Our best fit gave a=0.85 and b=0.082. We used this simple fit to correct an anomaly that has been reported in the p vs. 1000/T data for ultra pure, p-type silicon and tentatively attributed to the effect of neglecting the Hall factor in the data analysis. Baron, et al.[65] reported that the saturation region in this material does not behave as expected. Instead of remaining flat after saturation is achieved, the hole concentration sometimes decreases slightly just before the steep rise due to band gap excitation and residual deep centers sets in. This occurs roughly between 60 and 100K for samples with boron concentrations below $10^{12}cm^{-3}$. This temperature range is outside that covered by our measurements but is still mostly in the region dominated by acoustic phonon scattering so it is logical to assume that the functional dependence of r(T) should not change

drastically from that which we measured at the lower temperatures. Following this assumption, we took the p vs. 1000/T data from the conventional Hall effect run on sample 1202-H and corrected the p's with our empirical r at each temperature. The results are shown in Fig. 17, which is a greatly expanded plot of the region of interest. The inclusion of the Hall factor has removed the anomaly. In addition to this, we corrected all the data for this run and then refitted the data to determine the boron concentration (the effective mass of Ref. 48 was used with the charge balance equation to fit this data). The inclusion of the Hall factor changed the boron concentration and energy from $6.57 \times 10^{11} cm^{-3}$ and .0448eV to $7.09 \times 10^{11} cm^{-3}$ and .0449 respectively. The calculated donor concentration remained unchanged at $3.96 \times 10^{11} cm^{-3}$. The largest change is in the boron concentration which has increased by about 10 percent.

3. PRESENT THEORETICAL RESULTS FOR SILICON

The mobility calculation for silicon has been performed using the parameters listed in Table 3. The deformation potential parameters given in Table 3 are not the ones used in the two previous publications[43,45]. The two sets of numbers come from two different compilations by Wiley[28,52]. The set used here is the more recent one[28] and, moreover, is in good agreement with the latest piezospectroscopic measurements on Si[30,38].

TABLE 3

EXPERIMENTAL INPUT PARAMETERS USED IN THE MOBILITY CALCULATION FOR SILICON

Valence Band Parameters[a] (dimensionless)		Deformation Potentials[b] (eV)		Phonon Parameters ρc_s^2 (dyne/cm^2)[b]	
A	-4.27	a	2.1	s=transverse	6.80×10^{11}
B	-0.63	b	-2.2	s=longitudinal	18.852×10^{-12}
C	4.93	d	-5.3		

[a] Ref. 10

[b] Ref. 28, ρ=mass density, c_s=phonon speed for branch s

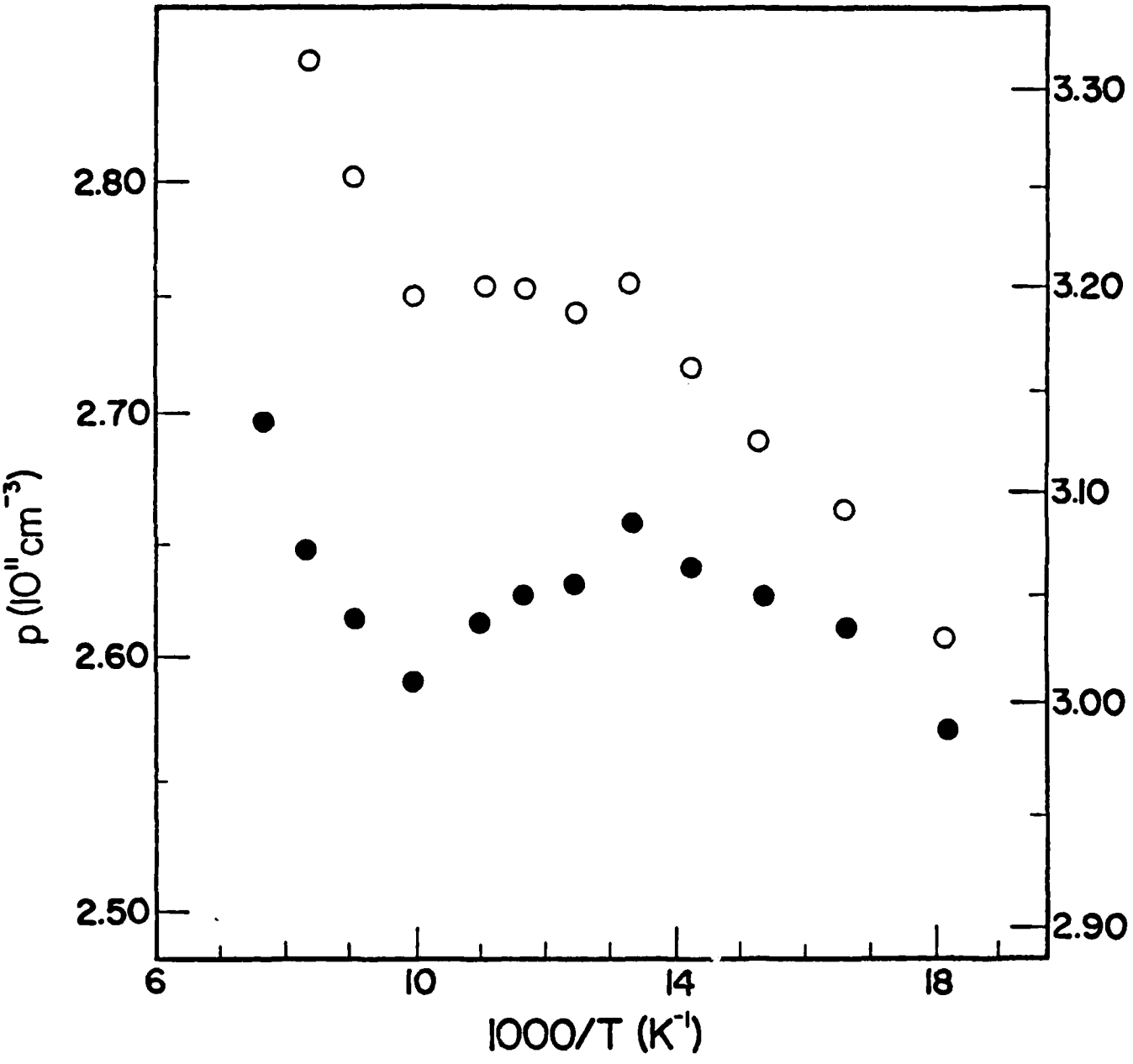

Fig. 17. Hole concentration vs. 1000/T for sample 1202-H. Solid circles: uncorrected data (left axis); open circles: same data corrected for Hall factor (right axis).

Fig. 18 provides functions θ, Eq. (74) for the L and H bands of silicon. As was the case in germanium, the δ_1 components of θ are the largest and the δ_5 and δ_5' components the smallest. Since the signs of the δ_1 contributions are positive the distribution functions for both bands are displaced in $\vec{k}$ space in the direction of the $\vec{F}$ field. θ's for the H band are somewhat smoother than the θ's for the L band indicating that the H band is the more parabolic of the two. The departure of the θ curves from a $\theta\sim$constant behavior can be attributed, in large part, to the fact that the expansion coefficients A, Eq. (3) are energy dependent themselves. Clearly, the closer proximity of the L band to the S band is the cause of the greater nonparabolicity of the L band.

Figs. 19 and 20 display the energy dependence of the ξ parts of the distribution functions for the L and H bands, respectively. Overall, the ξ contributions do behave in the approximate $E^{-\frac{1}{2}}$ manner. The δ_5' part of ξ for the H band starts out at first like $-(E)^{-\frac{1}{2}}$ and then reverts to the $(E)^{-\frac{1}{2}}$ behavior. The same trend was seen in the δ_3 part of ξ for the L band of Ge. We see that the ξ functions are not as well converged as in germanium. As far as mobility calculations are concerned the ξ convergence in λ is not the important question. What must be converged is the sum of products

$$\sum_{\lambda} g_{N\lambda}^{\delta\mu}(E)\,\theta_{N\lambda}^{\delta}(E) \quad , \tag{90}$$

for the conductivity mobility, Eq. (53a), and

$$\sum_{\lambda} g_{N\lambda}^{\delta\mu}(E)\,\xi_{N\lambda}^{\delta}(E) \quad , \tag{91}$$

for the Hall mobility, Eq. (53b), as a function of λ for all E of interest. For low energies, Eqs. (92) and (93) are better converged as a function of λ than the θ and ξ curves indicate, due to the convergence of $g_{N\lambda}$ itself as a function of λ. The total distribution functions for both bands are displaced overall in the $\vec{F}x\vec{B}$ direction; i.e., in the direction of the Hall field. This was ascertained by integrating Eq. (10b) for ψ_{11}^{N} over the hemisphere in the direction of the Hall field.

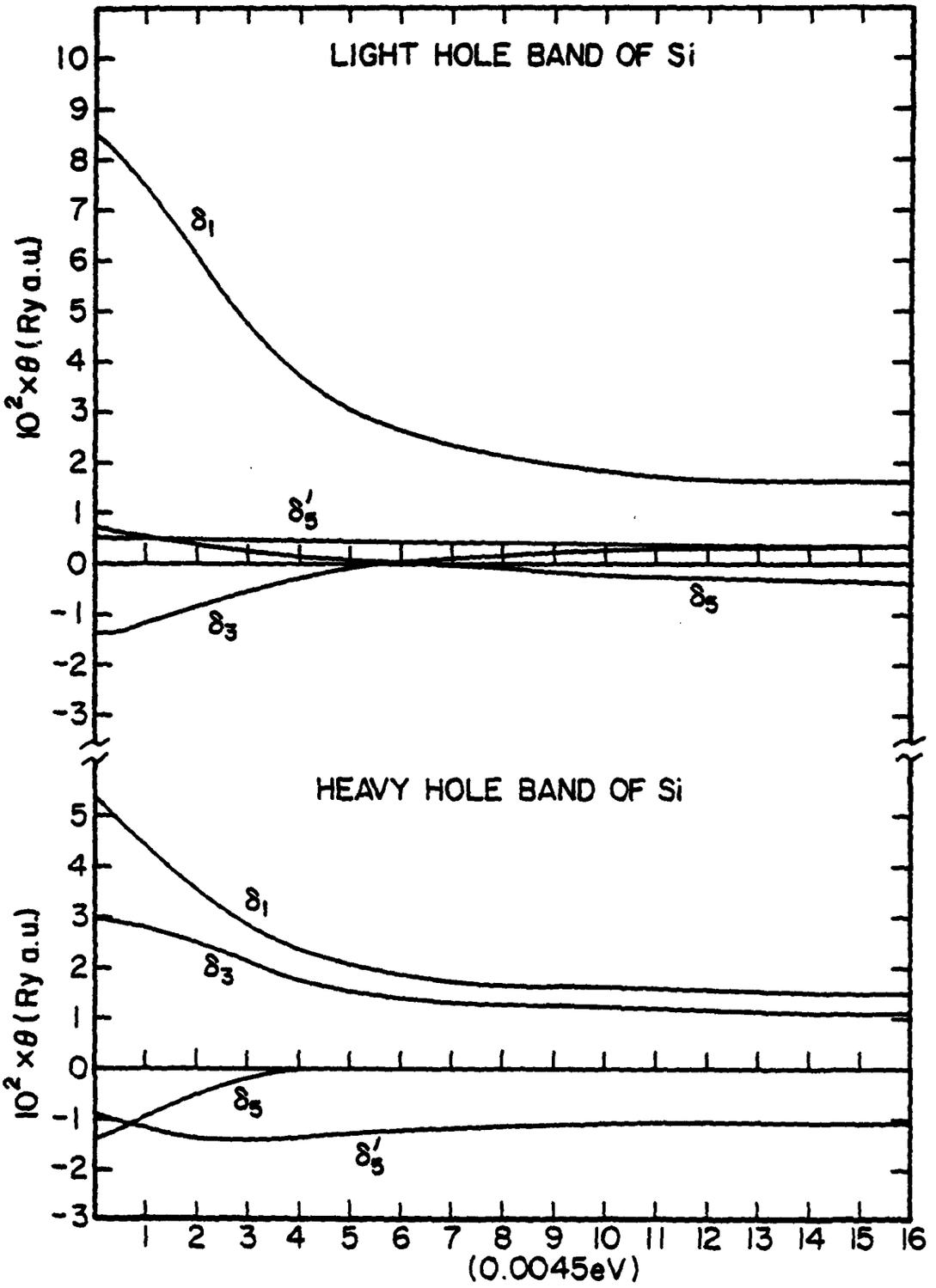

Fig. 18. Cubic harmonic decomposition of the perturbed part θ of the distribution function, Eq. (74) as a function of hole energy, for the light and heavy hole bands of silicon.

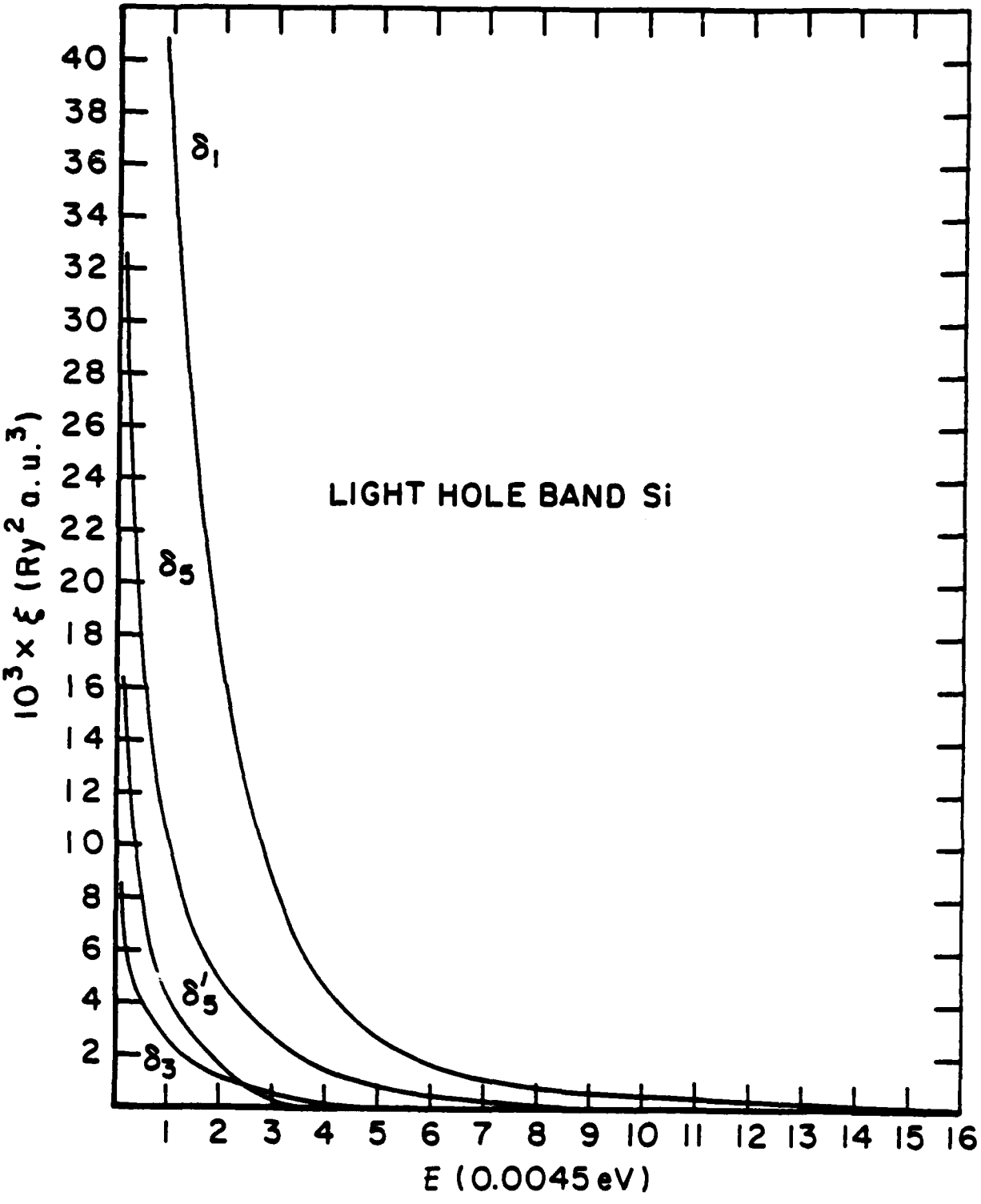

Fig. 19. Cubic harmonic decomposition of the perturbed part ξ of the distribution function, Eq. (77), as a function of hole energy, for the light hole band of silicon.

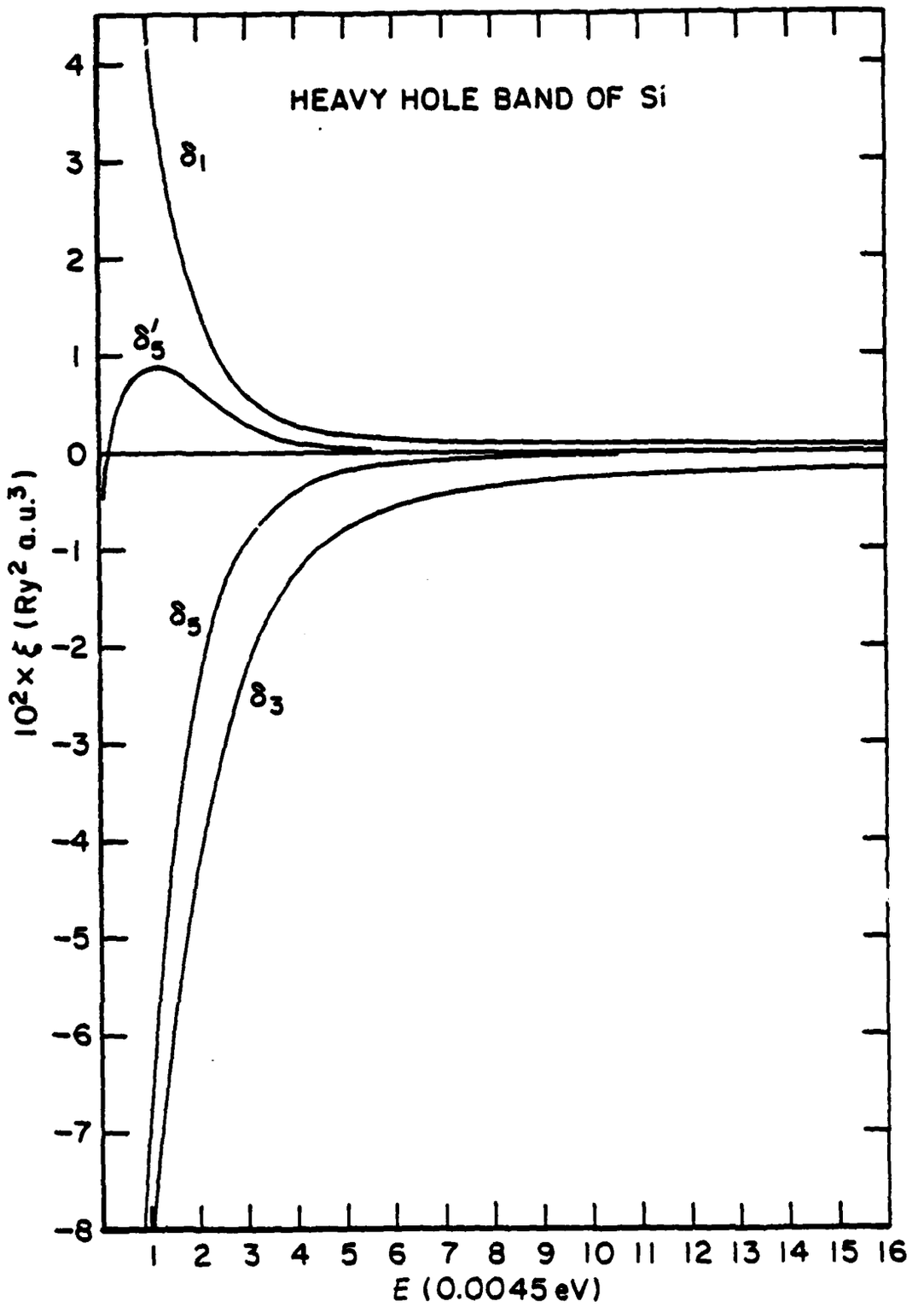

Fig. 20. Cubic harmonic decomposition of the perturbed part ξ of the distribution function, Eq. (77), as a function of hole energy, for the heavy hole band of silicon.

Figs. 21-23 exhibit functions U_N, D_N, and W_N which were defined in Eqs. (79), (80), and (81), respectively. The plots for U_N, Fig. 21, display marked deviations from the E behavior expected for parabolic bands. The ordering $U_H > U_L > U_S$ indicates that overall the H band will dominate the total conductivity mobility although its partial mobility μ_c^H is lower than μ_c^L. The spin-orbit band will have a small effect on the mobility at low temperatures. The density of states factors D_N, Fig. 22, start out approximately like $E^{\frac{1}{2}}$ but then depart considerably from that behavior. The ordering $D_H > D_L > D_S$ is expected from the band curvatures. A most complicated behavior for W_N is encountered for silicon in Fig. 23. The $E^{\frac{1}{2}}$ dependence is seen mostly at the very lowest of energies examined. Apparently, the approximate energy dependences of various factors in the parabolic limit, derived in Eqs. (69-73) and (82-84), break down completely when compounded to produce the W_N curves for silicon. A stronger or weaker energy dependence in either S, G, ϕ, H, or χ, from that expected in the parabolic limit, would produce the non-$E^{\frac{1}{2}}$ behavior of W_N. This is, of course, expected to be the case for silicon with its nonparabolic bands. Fig. 23 indicates that the light holes in the L band, in spite of their lower density at any given temperature, will contribute the most to the total Hall mobility.

Figs. 24 and 25 display the calculated partial and total conductivity and Hall mobilities, respectively. As expected, the L band has the more mobile holes and dominates the overall Hall mobility. The spin-orbit band makes a negligible contribution to either calculated mobility. Fig. 26 presents the calculated temperature exponents for both mobilities and the r-factor for silicon. The α_c coefficient starts out at 10K with $\alpha_c \sim 1.57$ and after a rapid rise saturates in value at about 2.10 for T>90K. The rise of α_H from 1.55 at 10K is monotonic in the temperature range examined. Therefore, it is only at the lowest temperatures that the mobilities come close to the parabolic band $\mu \sim T^{-1.5}$ behavior. Also shown in Fig. 26 are temperature exponents $\alpha_c \sim 1.75 \pm 0.05$ and $\alpha_H \sim 1.65 \pm 0.05$ measured by us in the 20-40K range.

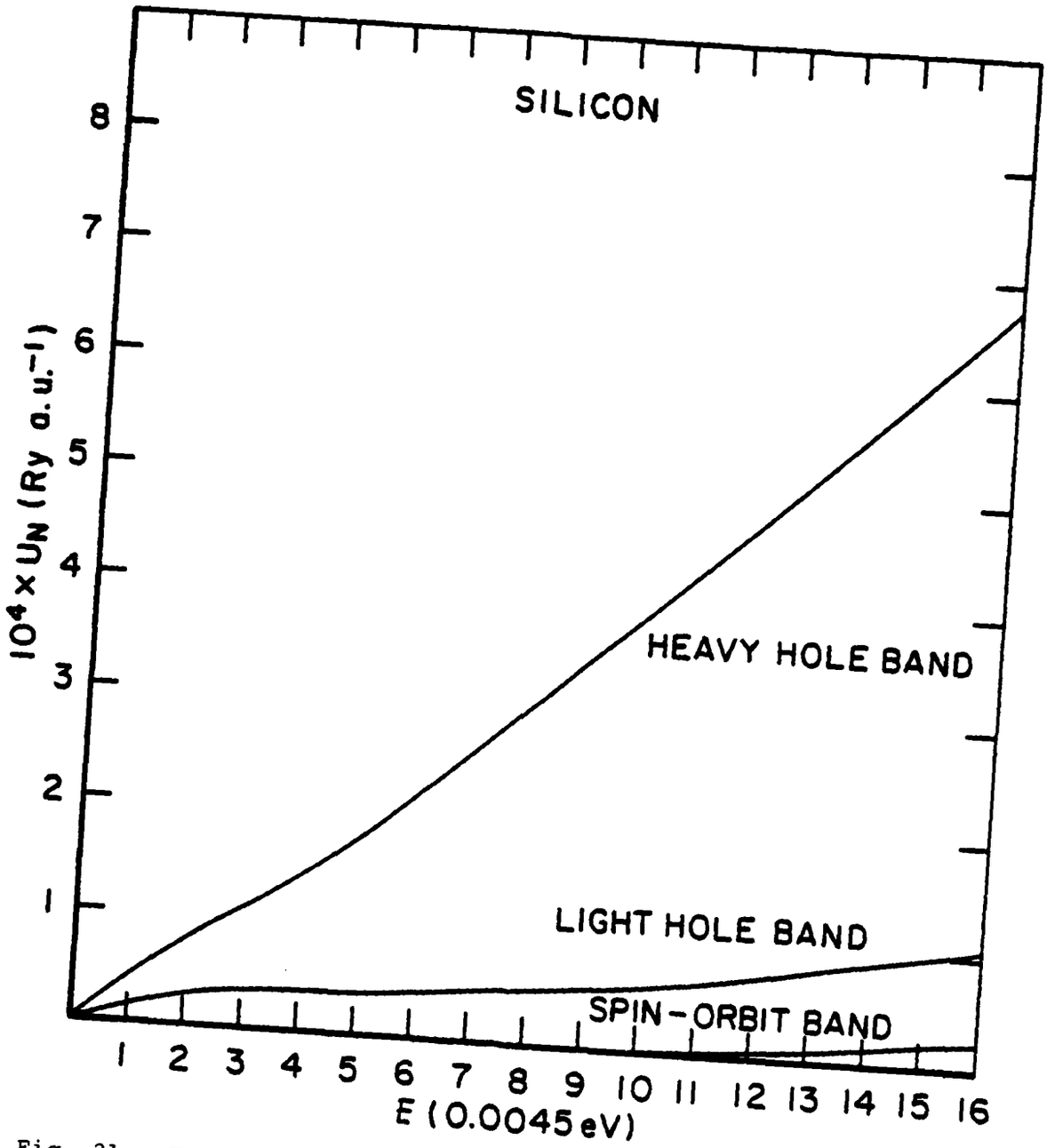

Fig. 21. Temperature independent part of the integrand in the numerator of Eq. (53a) for μ_c, defined by Eq. (79).

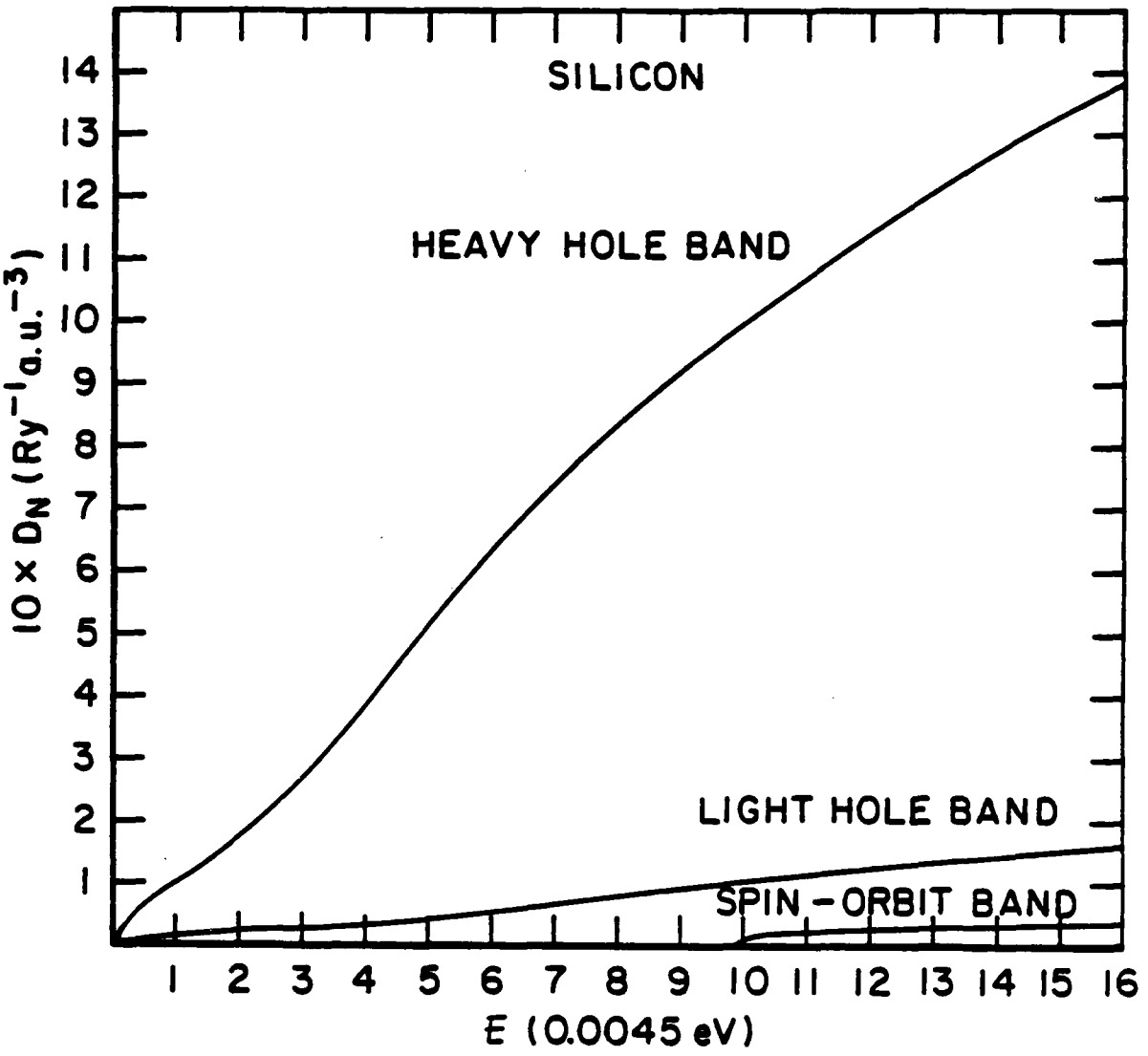

Fig. 22. Temperature independent part of the integrand in the denominators of Eqs. (53a and b) for μ_c and μ_H, defined by Eq. (80).

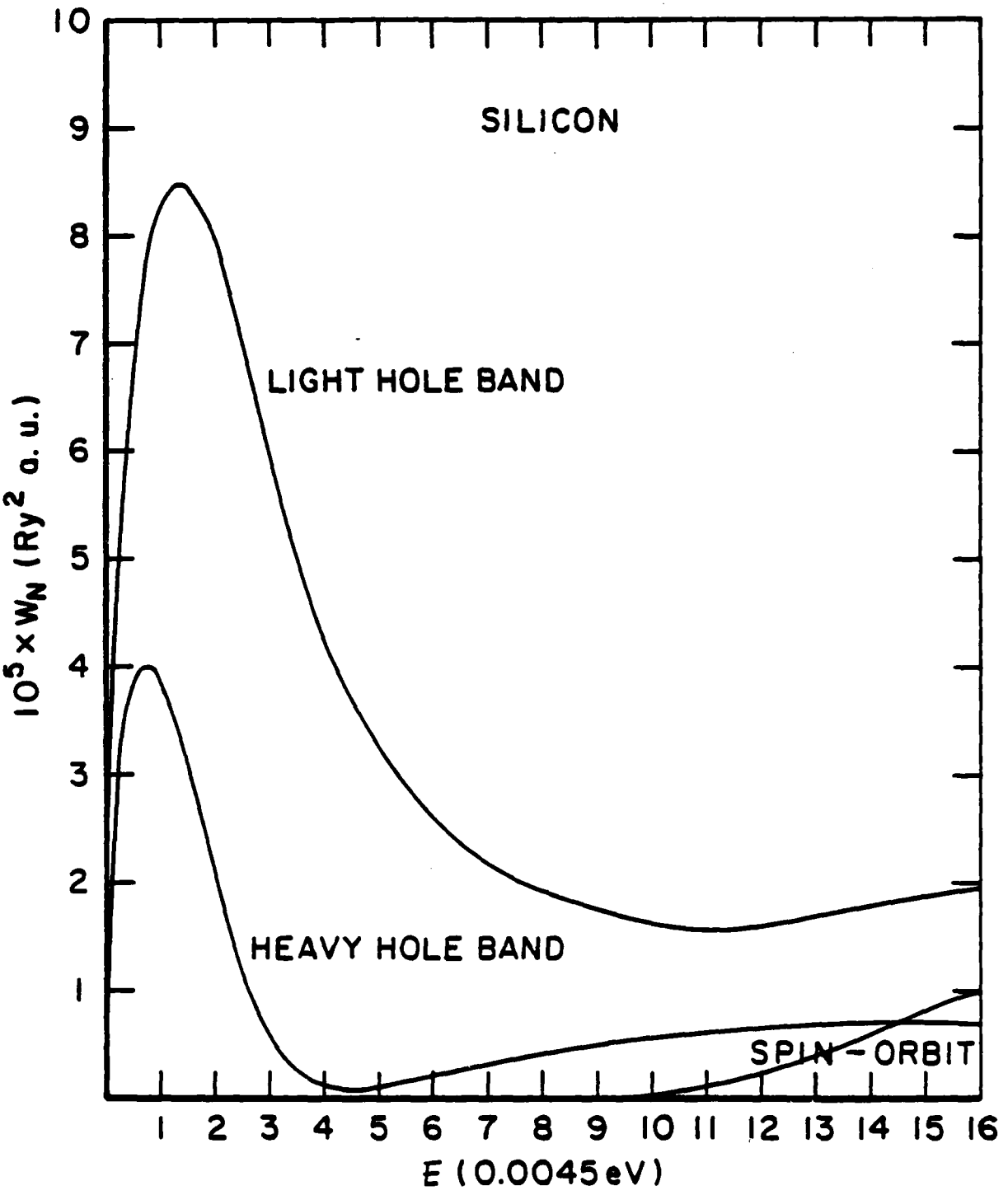

Fig. 23. Temperature independent part of the integrand in the numerator of Eq. (53b) for u_H, defined by Eq. (81).

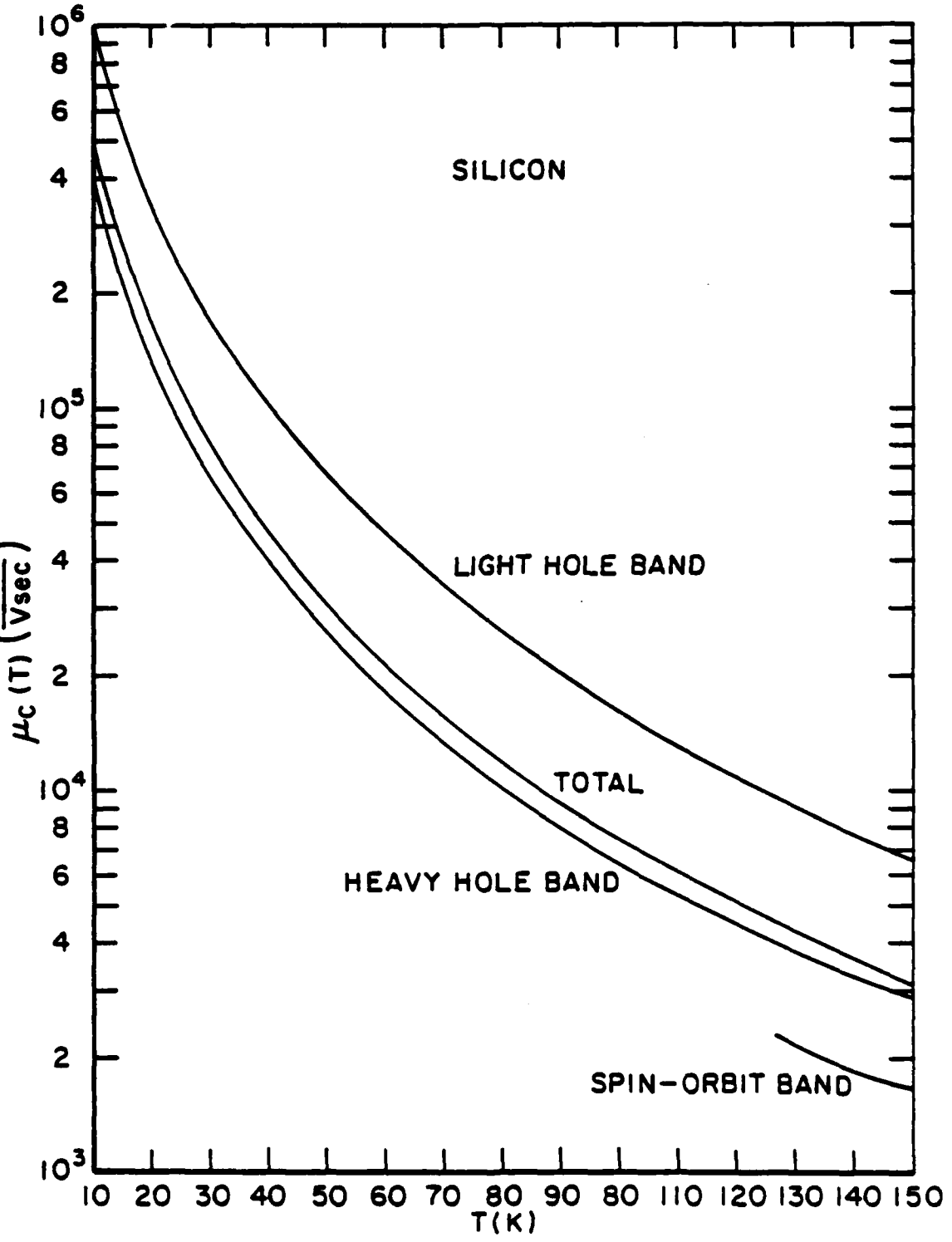

Fig. 24. Calculated total and partial conductivity mobilities, in the acoustic phonon limited regime, as a function of temperature.

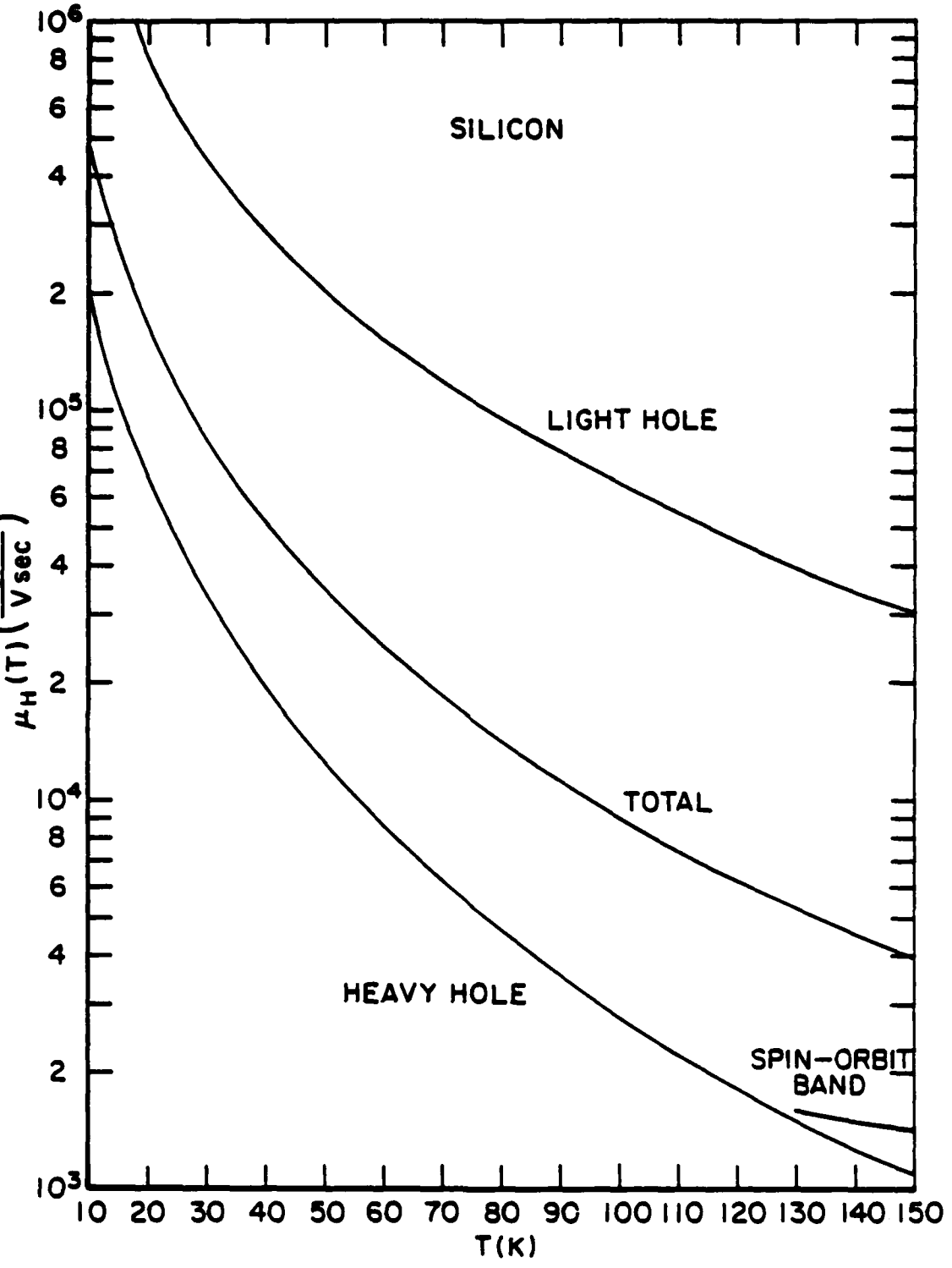

Fig. 25. Calculated total and partial Hall mobilities, in the acoustic phonon limited regime, as a function of temperature.

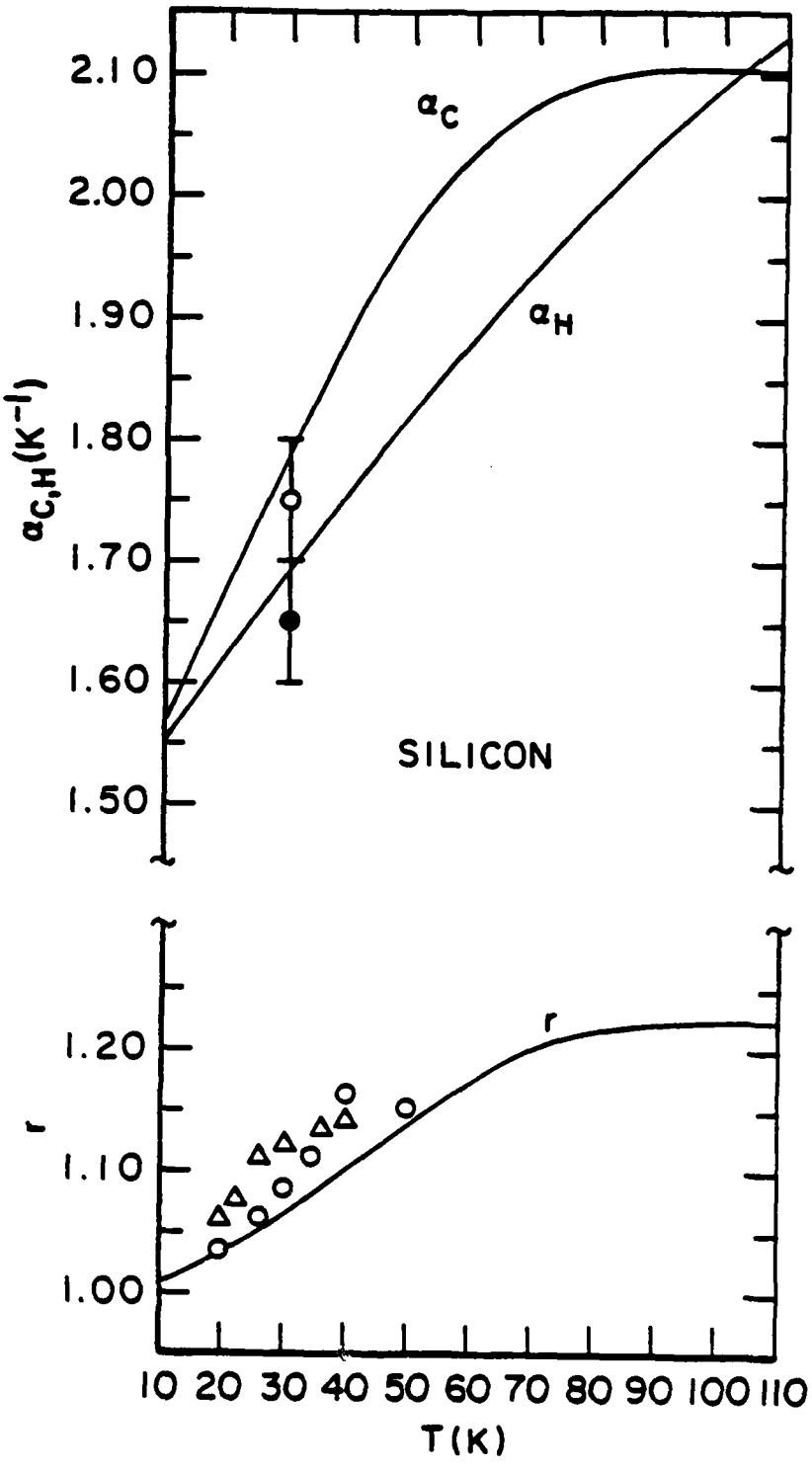

Fig. 26. Same as Fig. 10 for silicon. Experimental data for α_C (open circle) and α_H (filled circle). r-factor data from sample 1202-H, triangles (Hall bar acceptors $6.57 \times 10^{11} cm^{-3}$, donors $3.96 \times 10^{11} cm^{-3}$) and sample 1300-V, circles (van der Pauw configuration, acceptors $9.14 \times 10^{11} cm^{-3}$, donors $3.33 \times 10^{11} cm^{-3}$).

Fig. 26 shows a generally close agreement between experiment and theory for the exponents. Since only one exponent was fitted to the experimental data it is difficult to say whether the exponents have an appreciable temperature dependence themselves. Measurements encounter difficulties at lower temperatures, T<20K, due to the lack of signal connected with a low thermal hole population in high purity samples. Using lower purity samples complicates matters due to the presence of ionized impurity scattering. At higher temperatures, T>40K, the problem is the attainability of high enough magnetic fields to saturate the Hall coefficient. One must remember that this saturation is more difficult to achieve for heavy holes due to their lower mobility. On the other hand, the large light hole mobilities impose more stringent requirements on the electric fields in order to stay within the ohmic regime.

The calculated and measured r-factors are also displayed in Fig. 26. The two sets of data correspond to sample 1202-H (Hall bar configuration, $N_A=6.57\times10^{11}cm^{-3}$, $N_D=3.96\times10^{11}cm^{-3}$) and sample 1300-V (van der Pauw configuration, $N_A=9.14\times10^{11}cm^{-3}$, $N_D=3.33\times10^{11}cm^{-3}$). Considering the spread of experimental data the agreement between experiment and theory is very good and is on the order of 4%.

Fig. 27 shows the comparison between the calculated and measured conductivity mobility (sample 1202-H). The agreement is seen to be very good. There is a hint at lower temperatures of the influence of ionized impurity scattering in the data since the first two points fall slightly below the calculated curve. If this conjecture were to be true it would change the exponent α_c in Fig. 26 and make it more positive, in better agreement with the calculated α_c.

The low field limit of the Hall mobility as measured by us and Elstner[66], together with the calculated Hall mobility are shown in Fig. 28. Again, the agreement found here is very good. It is expected that at about 100K the influence of the optical phonon scattering will be felt. The theory presented in this paper can be extended to include that scattering mechanism as well,

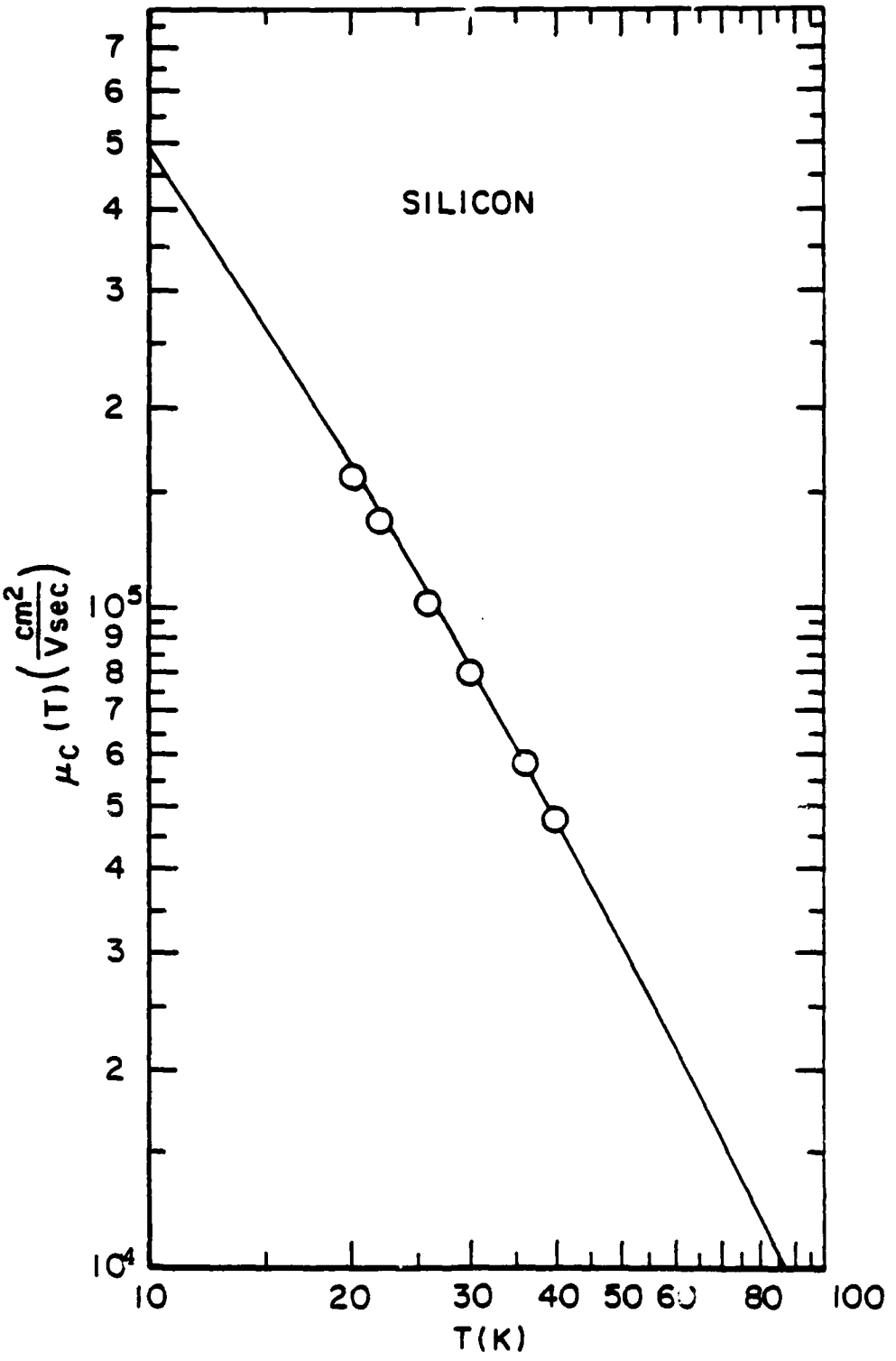

Fig. 27. Calculated conductivity mobility for silicon (solid line) and the experimental data for sample 1202-H.

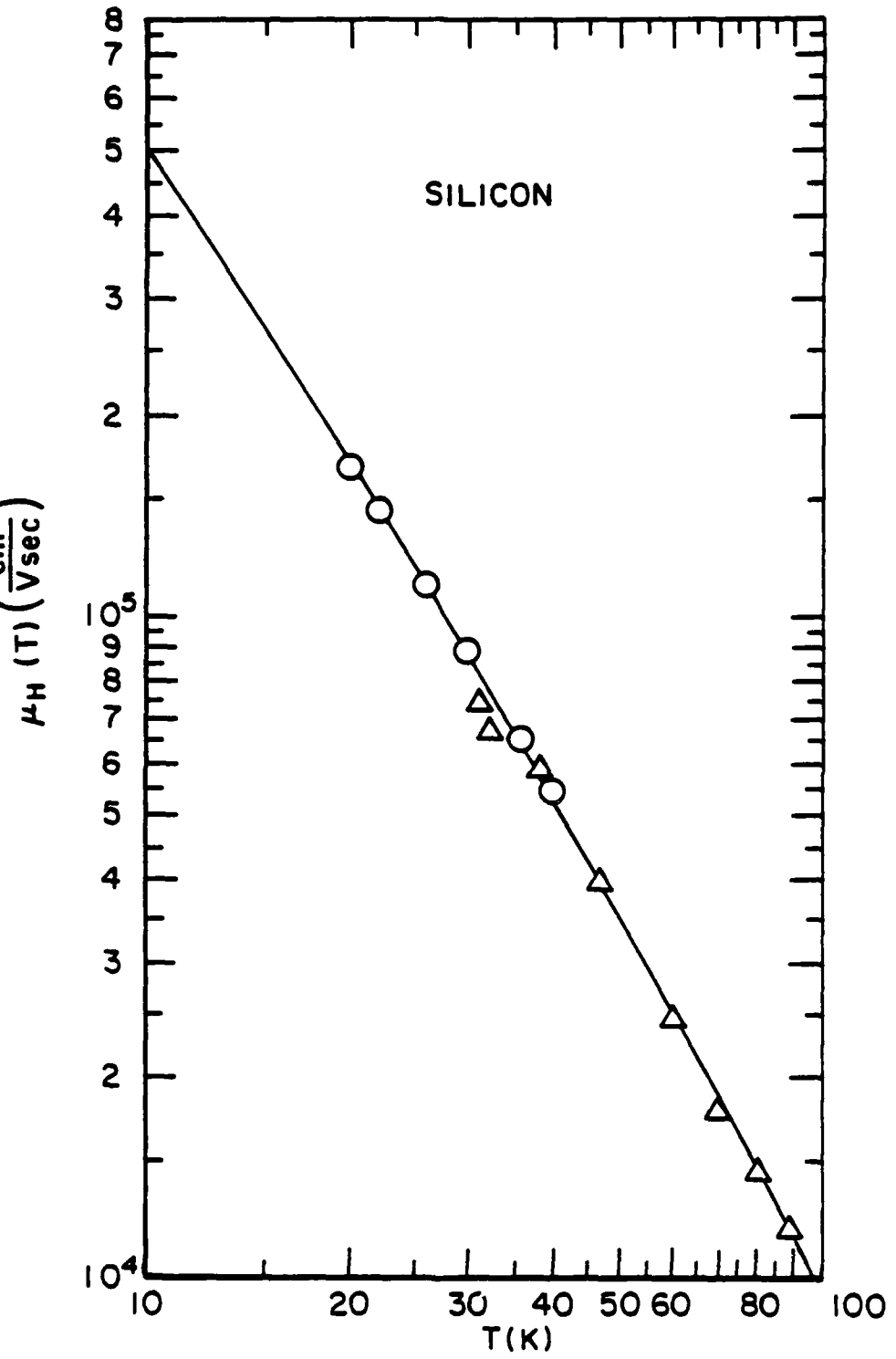

Fig. 28. Calculated Hall mobility for silicon (solid line) and the experimental data for sample 1202-H (circles), and the data of Elstner[66] (triangles, acceptors $1.0 \times 10^{13} cm^{-3}$, donors $6.5 \times 10^{10} cm^{-3}$).

as was done for Ge by Lawaetz[4]. Note that these two phonon scattering mechanisms are in competition with one another. Therefore, our S matrix, Eq. 24, will consist of two parts

$$S = S_{ac} + S_{opt} \quad , \tag{92}$$

for the acoustic and optical phonons. Clearly, to solve for the mobilities we need to invert S; e.g., Eqs. (29) and (43),

$$S^{-1} = (S_{ac} + S_{opt})^{-1} \tag{93}$$

which is not the same as

$$S^{-1} = S_{ac}^{-1} + S_{opt}^{-1} \tag{94}$$

This last generally unacceptable approximatior leads to the often used expression

$$\mu^{-1} = \sum_i \mu_i^{-1} \quad , \tag{95}$$

where the inverse of mobilities for each scattering mechanism are added. We shall summarize results of this calculation and measurements in the next section.

SECTION VI
SUMMARY AND CONCLUSIONS

We have shown that the experimental Hall factor for acoustic phonon scattering in p-type silicon is very close to the simple, textbook value of $3\pi/8$. There is, however, a slight temperature dependence that is not predicted by theories that neglect the nonparabolic nature of the valence bands. This temperature dependent Hall factor has been shown to have a noticeable effect on the results of Hall effect analysis, affecting primarily the acceptor concentration. We used the experimentally determined r's to calculate the true conductivity mobility for acoustic phonon scattering as a function of temperature. These values were in turn compared with our calculations where agreement was found to be excellent. The experiment yields a temperature dependence of $T^{-1.75}$ for μ_c and $T^{-1.65}$ for $\mu_H(H\rightarrow 0)$.

The conductivity and Hall mobilities for silicon and germanium have been calculated using the deformation potential theory of Tiersten[3] and the formalism developed by Lawaetz[4]. We have solved the Boltzmann equation without recourse to the relaxation time approximation. The agreement between experimental and theoretical r-factors is on the order of 4% for silicon and 12% for germanium. The corresponding mobilities are generally in better agreement with the experiments than are the r-factors.

The results of our calculation of the conductivity and Hall mobilities for Si and Ge, together with the pioneering works of Tiersten and Lawaetz, indicate that phonon limited transport in nonpolar semiconductors can be quantitatively modeled within the framework of the first-principles deformation potential theory. It appears that the main limitation to the quantitative accuracy of the method is the precision with which the deformation potentials are known, other input parameters having already been determined with sufficient precision.

Elimination of a few approximations in our theoretical treatment can make the theoretical results more exact but that

might be beyond the resolution of present day experiments. These approximations, taken together with the inherent limitations of the deformation potential concept itself, can be estimated to produce a $\pm 10\%$ fundamental accuracy of the method employed here[3,4]. These approximations will produce worse agreement for progressively higher transport coefficients; e.g., longitudinal and transverse magnetoresistance, etc.

The lowest temperature results would be improved by retaining the phonon energy in the delta function argument, Eq. (3). Another improvement would result from the use of the dynamical matrix solutions for phonon energies and polarization vectors. By using a degenerate perturbation theory, one also should eliminate the ambiguity in defining the polarization vectors in the $\vec{q} \to 0$ limit for forward intraband hole scattering[3,4]. Finally, as Lawaetz has shown[67], the deformation potential scattering theory is only the first order long wavelength approximation to the full carrier-phonon interaction term. This approximation he shows is good to at least 5%, which provides the limit on the accuracy of the method itself.

APPENDIX A

SYMMETRY ANALYSIS FOR CONDUCTIVITY TENSORS

The most general form for the current density is[68]

$$J_\mu = \sigma_{\mu\nu}F_\nu + \sigma_{\mu\nu\lambda}F_\nu B_\lambda + \sigma_{\mu\nu\lambda\eta}F_\nu B_\lambda B_\eta + \ldots \quad , \tag{A1}$$

to terms linear in the electric field F, where the sums are to be performed over repeated indices which stand for x, y, and z. The first term in the sum can be written in terms of the conductivity tensor $\overleftrightarrow{\sigma}$ as

$$\vec{J} = \overleftrightarrow{\sigma} \cdot \vec{F} \quad , \tag{A2}$$

where both $\vec{J}$ and $\vec{F}$ transform like vectors

$$\overleftrightarrow{R} \cdot \vec{J} = \vec{J}' \qquad \overleftrightarrow{R} \cdot \vec{F} = \vec{F}' \quad , \tag{A3}$$

when operated on by one of the 48 rotations R of the cubic point group O_h. In the rotated coordinate system the conductivity tensor $\overleftrightarrow{\sigma}$ becomes $\overleftrightarrow{\sigma}'$, where

$$\vec{J}' = \overleftrightarrow{\sigma}' \cdot \vec{F}' \quad , \tag{A4}$$

so that from (A2), (A3), and (A4)[69]

$$\overleftrightarrow{\sigma}' = \overleftrightarrow{R} \cdot \overleftrightarrow{\sigma} \cdot \overleftrightarrow{R}^{-1} \quad , \tag{A5}$$

for all $R \varepsilon O_h$. Since $\overleftrightarrow{\sigma}$ is a macroscopic property of the material, it is invariant under all rotations, so that

$$\overleftrightarrow{\sigma}' = \overleftrightarrow{\sigma} \quad . \tag{A6}$$

Applying a few rotation matrices to the tensor $\overleftrightarrow{\sigma}$ in Eq. (A5) quickly establishes that

$$\sigma_{\mu\nu} = 0 \quad \text{for} \quad \mu \neq \nu \quad , \tag{A7a}$$

and

$$\sigma_{\mu\mu} = \sigma_o$$

so that the second rank conductivity tensor is diagonal.

A similar analysis for the third rank tensor yields[69]

$$J_\mu = \sigma_{\mu\nu\lambda}F_\nu B_\lambda \quad , \tag{A8}$$

$$RJ_\mu = \sigma'_{\mu\nu\lambda}(RF_\nu)(RB_\lambda) \quad . \tag{A9}$$

Vectors $\vec{J}$ and $\vec{F}$ transform according to the rows of the Γ_{15} representation whose matrix representation is given by the rotation matrices R themselves. The magnetic field B transforms like a pseudovector under rotations according to the rows of the Γ'_{15} representation. The matrix representation for Γ'_{15} is given by the rotation matrices R for the proper rotations and (-IR) for improper rotations, where I is the inversion matrix. Again, the σ' tensor is invariant under rotations to that

$$\sigma'_{\mu\nu\lambda} = \sigma_{\mu\nu\lambda} \tag{A10}$$

which leads via Eqs. (A8) and (A9) to the condition

$$\sigma'_{\mu\nu\lambda} = \sum_{\mu'\nu'\lambda'} R_{\mu\mu'} R_{\nu\nu'} \Gamma^{m}_{\lambda\lambda'}(R) \sigma_{\mu\nu\lambda} ,$$

where $\Gamma^{m}(R)$ are the matrices for the Γ'_{15} representation. Performing the indicated operations in Eq. (A11), with a few rotation operators, shows that

$$\sigma_{\mu\nu\lambda} = \epsilon_{\mu\nu\lambda}\alpha \tag{A11}$$

where $\epsilon_{\mu\nu\lambda}$ is the Levi-Cevita symbol. Altogether, we obtain to first order in $\vec{F}$ and $\vec{B}$

$$\vec{J} = \sigma_c \vec{F} + \alpha(\vec{F}\times\vec{B}) \quad . \tag{A12}$$

Clearly, $\sigma_c = ep\mu_c$, and

$$\vec{J} = ep\langle\vec{V}\rangle = ep(\langle\vec{V}_{10}\rangle F + \langle\vec{V}_{11}\rangle FB + \ldots) \quad , \tag{A13}$$

so that

$$\mu_c = \langle\vec{V}_{10}\rangle \cdot \hat{F} \quad , \tag{A14}$$

$$\alpha = \frac{\hat{F}\times\hat{B}}{|\hat{F}\times\hat{B}|^2} \cdot \langle\vec{V}_{11}\rangle \quad . \tag{A15}$$

The coefficient α is related to the Hall mobility, μ_H. The Hall mobility is defined as

$$\mu_H = \frac{(F_y)_H}{B_z F_x} \quad , \tag{A16}$$

where F_x is the electric field in direction of the applied voltage, $(F_y)_H$ the field in direction of the Hall voltage, and B_z is the applied magnetic field. More generally, the Hall electric field is given by

$$\vec{F}_H = \mu_H(\vec{F}x\vec{B}) \quad , \tag{A17}$$

so that

$$\vec{J} = ep\mu_c[\vec{F}+\vec{F}_H]$$

$$= ep[\mu_c\vec{F}+\mu_c\mu_H(\vec{F}x\vec{B})] \quad . \tag{A18}$$

By comparison with (A12)

$$\alpha = \mu_c\mu_H = \mu_c(r\mu_c) = r\mu_c^2 \quad . \tag{A19}$$

It should be said that the above proof implicitly uses the Neumann theorem which states that macroscopic physical properties of a crystal are invariant under point group operations of the crystal's space group. In case of the diamond structure, fractional translations in a unit cell are too small on the macroscopic scale to influence the results of experimental measurements.

APPENDIX B

COUPLING COEFFICIENTS FOR THE MAGNETIC FIELD TERM, EQ. 64

An alternative technique for dealing with the operations indicated by Eq. (64) are provided in this Appendix. It is necessary to work with the expression

$$\vec{h}^N(E,\hat{k})K_\lambda^{\delta\mu}(\hat{k}) = [\vec{\nabla}_{\vec{k}}E_N(\vec{k})\times\vec{\nabla}_{\vec{k}}]_E K_\lambda^{\delta\mu}(\hat{k}) \quad . \tag{B1}$$

We recast the energy gradient into the form of Eq. (62b) and obtain

$$h_q^N(E,\hat{k})K_\lambda^{\delta\mu}(\hat{k}) = \epsilon_{qpr}\left(\frac{\partial E_N}{\partial k_p}\frac{\partial}{\partial k_r}\right)_E K_\lambda^{\delta\mu}(\hat{k}) =$$

$$2\gamma_N^{-\frac{1}{2}}\,\epsilon_{qpr}\left[\left(x_p\Pi_4+x_p^3\Pi_5+x_p^5\Pi_6\right)\frac{\partial}{\partial k_r}\right]_E K_\lambda^{\delta\mu}(\hat{k}) \quad , \tag{B2}$$

where x_q are direction cosines, $x_q=k_q/k$. Typical terms in Eq. (B2) are

$$h_q^{(1)}K_\lambda^{\delta\mu} \equiv \left[\epsilon_{qpr}\,x_p\,\frac{\partial}{\partial k_r}\right] K_\lambda^{\delta\mu} \quad , \tag{B3a}$$

$$h_q^{(3)}K_\lambda^{\delta\mu} \equiv \left[\epsilon_{qpr}\,x_p^3\,\frac{\partial}{\partial k_r}\right] K_\lambda^{\delta\mu} \quad , \tag{B3b}$$

$$h_q^{(5)}K_\lambda^{\delta\mu} \equiv \left[\epsilon_{qpr}\,x_p^5\,\frac{\partial}{\partial k_r}\right] K_\lambda^{\delta\mu} \quad . \tag{B3c}$$

The operations in Eqs. (B3) can be expressed as a sum of cubic harmonics with coupling coefficients defined by

$$kh_q^{(n)}K_\lambda^{\delta\mu} = \sum_{j\nu\lambda'} C_{q\mu}^{j\nu\lambda'}(n,\lambda)K_{\lambda'}^{j\nu} \quad . \tag{B4}$$

We have worked out a number of tables for the coupling coefficients C defined by Eq. (B4). Some of the tables are provided below in the VdLB notation[46]:

$$kh_q^{(1)}\delta_{1p} = \begin{pmatrix} 0 & -\delta_{1z} & \delta_{1y} \\ \delta_{1z} & 0 & -\delta_{1x} \\ -\delta_{1y} & \delta_{1x} & 0 \end{pmatrix} \quad , \tag{B5}$$

$$kh_q^{(1)}\delta_{3p} = \frac{3}{2}\begin{pmatrix} 0 & \delta_{3z} & -\delta_{3y} \\ -\delta_{3z} & 0 & \delta_{3x} \\ \delta_{3y} & -\delta_{3x} & 0 \end{pmatrix} + \frac{\sqrt{15}}{2}\begin{pmatrix} 0 & \varepsilon'_{3z} & \varepsilon'_{3y} \\ \varepsilon'_{3z} & 0 & \varepsilon'_{3x} \\ \varepsilon'_{3y} & \varepsilon'_{3x} & 0 \end{pmatrix} \tag{B6}$$

$$kh_q^{(1)}\delta_{5p} = \frac{15}{8}\begin{pmatrix} 0 & -\delta_{5z} & \delta_{5y} \\ \delta_{5z} & 0 & -\delta_{5x} \\ -\delta_{5y} & \delta_{5x} & 0 \end{pmatrix} + \frac{3\sqrt{5\cdot 7}}{8}\begin{pmatrix} 0 & -\delta_{5z} & \delta'_{5y} \\ \delta'_{5z} & 0 & -\delta'_{5x} \\ -\delta'_{5y} & \delta'_{5x} & 0 \end{pmatrix}$$

$$- \frac{\sqrt{3\cdot 5\cdot 7}}{4}\begin{pmatrix} 0 & \varepsilon'_{5z} & \varepsilon'_{5y} \\ \varepsilon'_{5z} & 0 & \varepsilon'_{5x} \\ \varepsilon'_{5y} & \varepsilon'_{5x} & 0 \end{pmatrix} \tag{B7}$$

$$kh_q^{(1)}\delta'_{5q} = 2\begin{pmatrix} \sqrt{3}\left(\gamma'_5\right)_1 + \left(\gamma'_5\right)_2 & 0 & 0 \\ 0 & -3\left(\gamma'_5\right)_1 + \left(\gamma'_5\right)_2 & 0 \\ 0 & 0 & -2\left(\gamma'_5\right)_2 \end{pmatrix} \tag{B8}$$

$$+ \frac{11}{8}\begin{pmatrix} 0 & \delta'_{5z} & -\delta'_{5y} \\ -\delta'_{5z} & 0 & \delta'_{5x} \\ \delta'_{5y} & -\delta'_{5x} & 0 \end{pmatrix} + \frac{3\sqrt{5\cdot 7}}{8}\begin{pmatrix} 0 & -\delta_{5z} & \delta_{5y} \\ \delta_{5z} & 0 & -\delta_{5x} \\ -\delta_{5y} & \delta_{5x} & 0 \end{pmatrix}$$

$$+ \frac{3\sqrt{3}}{4}\begin{pmatrix} 0 & \varepsilon'_{5z} & \varepsilon'_{5y} \\ \varepsilon'_{5z} & 0 & \varepsilon'_{5x} \\ \varepsilon'_{5y} & \varepsilon'_{5x} & 0 \end{pmatrix}$$

We note that these matrices are traceless and that the matrices with δ's inside are antisymmetric, while those with ε' are symmetric. Although we have a number of other matrices for these tables, our tables for $h_q^{(3)}$, $h_q^{(5)}$ are not complete enough to warrant their reporting. We would encourage other workers to complete these tables. They have the potential of simplifying the computational effort in an elegant manner. This will be especially true in calculations of higher magnetoresistance coefficients.

REFERENCES

1. D. K. Schroder, T. T. Braggins, and H. M. Hobgood, "The Doping Concentrations of Indium-Doped Silicon Measured by Hall, C-V, and Junction-Breakdown Techniques," Journal of Applied Physics, October 1978, pp. 5256-5265.

2. F. Mousty, P. Ostoja, and L. Passari, "Relationship Between Resistivity and Phosphorus Concentration in Silicon," Journal of Applied Physics, October 1974, pp. 4576-4580.

3. M. Tiersten, "Acoustic-Mode Scattering of Holes," IBM Journal of Research and Development, April 1961, pp. 122-131; "Acoustic-Mode Scattering Mobility of Holes in Diamond Type Semiconductors," Journal of Physics and Chemistry of Solids, January 1964, pp. 1151-1168.

4. P. Lawaetz, "Low-Field Mobility and Galvanomagnetic Properties of Holes in Germanium with Phonon Scattering," Physical Review, October 1968, pp. 867-880.

5. G. E. Pikus and G. L. Bir, "Effect of Deformation on the Hole Energy Spectrum of Germanium and Silicon," Soviet Physics-Solid State, 1960, pp. 1502-1517; "Theory of Deformation Potential for Semiconductors with a Complex Band Structure," Soviet Physics-Solid State, 1960, pp. 2039-2051.

6. G. I. Bir, E. Normantas, and G. E. Pikus, "Galvanomagnetic Effects in Semiconductors with Degenerate Zones," Soviet Physics-Solid State, November 1962, pp. 867-877.

7. C. Herring and E. Vogt, "Transport and Deformation-Potential Theory for Many-Valley Semiconductors with Anisotropic Scattering," Physical Review, February 1956, pp. 944-961.

8. W. P. Dumke, "Deformation Potential Theory for n-Type Ge," Physical Review, January 1956, pp. 531-536; "High-Field Conductivity of the (111) Valleys of Ge," Physical Review B, August 1970, pp. 987-996.

9. P. P. Debye and E. M. Conwell, "Electrical Properties of n-Type Germanium," Physical Review, February 1954, pp. 693-707.

10. H. Nakagawa and S. Zukotynski, "The Valence Bandstructure and the Hole Mobility in Silicon," Canadian Journal of Physics, 1977, pp. 1485-1491; "Drift Mobility and Hall Coefficient Factor of Holes in Germanium and Silicon," Canadian Journal of Physics, 1977, pp. 364-372.

11. Sheng S. Li, "The Dopant Density and Temperature Dependence of Hole Mobility and Resistivity in Boron Doped Silicon," Solid-State Electronics, 1978, pp. 1109-1117.

12. L. C. Linares and S. S. Li, "An Improved Model for Analyzing Hole Mobility and Resistivity in p-Type Silicon Doped with Boron, Gallium, and Indium," Journal of the Electrochemical Society, December 1981, pp. 601-608.

13. J. F. Lin, S. S. Li, L. C. Linares, and K. W. Teng, "Theoretical Analysis of Hall Factor and Hall Mobility in p-Type Silicon," Solid-State Electronics, 1981, pp. 827-833.

14. M. Costato, S. Fontanesi, and L. Reggiani, "Electron Energy Relaxation Time in Si and Ge," Journal of Physics and Chemistry of Solids, 1973, pp. 547-564.

15. M. Costato and L. Reggiani, "Scattering Probabilities for Holes (I)," Physica Status Solidi B, 1973, pp. 471-482.

16. G. Ottaviani, L. Reggiani, C. Canali, F. Nava, and A. Alberigi-Quaranta, "Hole Drift Velocity in Silicon," Physical Review B, 1975, pp. 3318-3329.

17. L. Reggiani, C. Canali, F. Nava, and G. Ottaviani, "Hole Drift Velocity in Germanium," Physical Review B, September 1977, pp. 2781-2791.

18. G. Gagliani and L. Reggiani, "Nonparabolicity and Intrinsic Carrier Concentration in Si and Ge," Il Nuovo Cimento, December 1975, pp. 207-216.

19. C. Canali, C. Jacoboni, F. Nava, G. Ottaviani, and A. Alberigi-Quaranta, "Electron Drift Velocity in Silicon," Physical Review B, September 1975, pp. 2265-2284.

20. S. Bosi, C. Jacoboni, and L. Reggiani, "Acoustic Scattering in a Two-Band System and its Application to Hole Transport Properties in Cubic Semiconductors," Journal of Physics C, 1979, pp. 1525-1531.

21. M. Costato, G. Gagliani, C. Jacoboni, and L. Reggiani, "Ohmic Hole Mobility in Cubic Semiconductors," Journal of Physics and Chemistry of Solids, 1974, pp. 1605-1614.

22. M. Asche and J. von Borzeszkowski, "On the Temperature Dependence of Hole Mobility in Silicon," Physica Status Solidi, 1970, pp. 433-438.

23. J. von Borzeszkowski, "On the Electric Field Dependence of the Conductivity of Holes in Si at Low Temperatures," Physica Status Solidi, 1976, pp. 607-614.

24. A. Hackmann, D. Neubert, V. Scherz, and R. Schlief, "Determination of Carrier Densities in Lightly Doped Silicon Crystals from the Hall Effect," Physical Review B, October 1981, pp. 4666-4683.

25. K. Takeda, K. Sakui, and M. Sakata, "Temperature Dependence of Mobility and Hall Coefficient Factor for Holes of Highly Pure Silicon," Journal of Physics C, 1982, pp. 767-776.

26. D. L. Rode, "Theory of Electron Galvanomagnetics in Crystals: Hall Effect in Semiconductors and Semimetals," Physica Status Solidi B, 1973, pp. 687-696; "Electron Mobility in Direct Gap Polar Semiconductors," Physical Review, August 1970, pp. 1012-1024.

27. J. D. Wiley and M. DiDomenico, "Lattice Mobility of Holes in III-V Compounds," Physical Review B, July 1970, pp. 427-433.

28. J. D. Wiley, "Polar Mobility of Holes in III-V Compounds," Physical Review B, 1971, pp. 2485-2493.

29. L. J. Challis and S. C. Haseler, "The Effect of Uniaxial Stress on the Thermal Conductivity of p-Ge," Journal of Physics C, 1978, pp. 4681-4694.

30. J. C. Merle, M. Capizzi, P. Fiorini, and A. Frova, "Uniaxially Stressed Silicon: Fine Structure of the Exciton and Deforma-p tion Potentials," Physical Review B, June 1978, pp. 4821-4834, see Table III.

31. K. Suzuki and J. C. Hensel, "Quantum Resonances in the Valence Bands of Germanium. I. Theoretical Considerations," Physical Review B, May 1974, pp. 4184-4218.

32. J. C. Hensel and K. Suzuki, "Quantum Resonances in the Valence Bands of Germanium. II. Cyclotron Resonances in Uniaxially Stressed Crystals," Physical Review B, May 1974, pp. 4219-4257.

33. T. Fjeldly, Ishiguro, and C. Elbaum, "Heat-Pulse Propagation in p-Type Si and Ge Under Uniaxial Stress," Physical Review B, February 1973, pp. 1392-1410.

34. K. Hess, "Effect of Uniaxial Stress on Energy Loss and Scattering Mechanism in p-Type Silicon," Journal of Physics and Chemistry of Solids, 1972, pp. 139-143.

35. M. Costato and L. Reggiani, "On the Effect of Pressure on the Band Extrema of Covalent Semiconductors," Lettere al Nuovo Cimento, October 1970, pp. 848-857.

36. I. Balslev, "Influence of Uniaxial Stress on the Indirect Absorption Edge in Silicon and Germanium," Physical Review, March 1966, pp. 637-647.

37. R. H. Parmenter, "Uniform Strains and Deformation Potentials," Physical Review, September 1955, pp. 1767-1776.

38. H. R. Chandrasekhar, P. Fischer, A. K. Ramdas, and F. Rodriguez, "Quantitative Piezospectroscopy of the Ground and Exciton States of Acceptors in Silicon," Physical Review B, October 1973, pp. 3836-3851.

39. E. B. Hale and T. G. Castner, Jr., "Ground-State Wave Function of Shallow Donors in Uniaxially Stressed Silicon: Piezohyperfine Constants Determined by Electron-Nuclear Double Resonance," Physical Review B, June 1970, pp. 4763-4783.

40. Evan O. Kane, "Energy Band Structure in p-Type Germanium and Silicon," Journal of Physics and Chemistry of Solids, 1956, pp. 82-99.

41. G. D. Whitfield, "Theory of Electron-Phonon Interactions," Physical Review, February 1961, pp. 720-734.

42. P. J. Price, "The Linear Hall Effect," IBM Journal, July 1957, p. 239; "The Lorenz Number," April 1957, p. 147; "The Physical Interpretation of Mean Free Path and the Integral Method," July 1958, p. 200.

43. Frank L. Madarasz and Frank Szmulowicz, "Transition Rates for Acoustic-Phonon—Hole Scattering in p-Type Silicon with Nonparabolic Bands," Physical Review B, October 1981, pp. 4611-4622.

44. Frank Szmulowicz and Frank L. Madarasz, "Angular Dependence of Hole—Acoustic-Phonon Transition Rates in Silicon," Physical Review B, August 1982, pp. 2101-2112.

45. J. F. Cornwell, Group Theory and Electronic Energy Bands in Solids, John Wiley & Sons, New York, 1969.

46. Fred C. Von der Lage and H. A. Bethe, "A Method for Obtaining Electronic Eigenfunctions and Eigenvalues in Solids with an Application to Sodium," Physical Review, May 1947, pp. 612-622.

47. Frederick Seitz, "Note on the Theory of Resistance of a Cubic Semiconductor in a Magnetic Field," Physical Review, July 1950, pp. 372-375.

48. Frank L. Madarasz, Joseph E. Lang, and Patrick M. Hemenger, "Effective Masses for Nonparabolic Bands in p-Type Silicon," Journal of Applied Physics, July 1981, pp. 4646-4648 (Eq. (10a) of this reference should read, $\eta = \sqrt{2} \sin \phi$.)

49. Daniel D. McCracken, Fortran With Engineering Applications, John Wiley & Sons, New York, 1967.

50. A. H. Stroud and Don Secrest, Gaussian Quadrature Formulas, Prentice-Hall, New Jersey, 1966.

AD-A130 021 MEASUREMENT AND THEORY OF THE HALL SCATTERING FACTOR AND THE CONDUCTIVITY..(U) DAYTON UNIV OH RESEARCH INST F SZMULOWICZ ET AL. APR 83 AFWAL-TR-83-4043 2/2

UNCLASSIFIED F33615-81-C-5095 F/G 20/12 NL

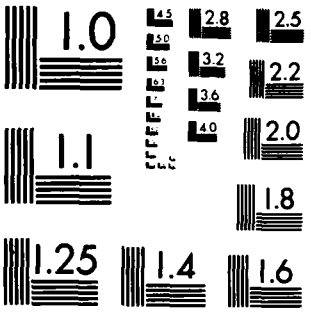

51. Philip J. Davis and Ivan Polonsky, in Handbook of Mathematical Functions With Formulas, Graphs, and Mathematical Tables, U.S. Government Printing Office, Washington, D.C., 1972.

52. J. D. Wiley, "Valence-Band Deformation Potentials for the III-V Compounds," Solid State Communication, 1970, pp. 1865-1868.

53. A. C. Beer and R. K. Willardson, "Hall and Transverse Magnetoresistance Effects for Warped Bands and Mixed Scattering," Physical Review, June 1958, pp. 1286-1294.

54. C. Goldberg, E. N. Adams, and R. E. Davis, "Magnetoconductivity in p-Type Germanium," Physical Review, February 1957, pp. 865-876.

55. F. J. Morin, "Lattice Scattering Mobility in Germanium," Physical Review, January 1954, pp. 62-63.

56. G. Ottaviani, C. Canali, F. Nava, and J. W. Mayer, "Hole Drift Velocity in High-Purity Ge Between 8° and 220°K," Journal of Applied Physics, June 1973, pp. 2917-2918.

57. D. M. Brown and R. Bray, "Analysis of Lattice and Ionized Impurity Scattering in p-Type Germanium," Physical Review, September 1962, pp. 1593-1602.

58. Patrick M. Hemenger, "Measurement of High Resistivity Semiconductors Using the van der Pauw Method," The Review of Scientific Instruments, June 1973, pp. 698-700.

59. Albert C. Beer, Solid State Physics, Supplement No. 4, Academic Press, New York, 1963.

60. H. P. Frederikse and W. R. Hosler, "Galvanomagnetic Effects in n-Type Indium Antimonide," Physical Review, December 1957, pp. 1136-1151.

61. A. C. Beer and R. K. Willardson, "Hall and Transverse Magnetoresistance effects for Warped Bands and Mixed Scattering," Physical Review, June 1958, pp. 1286-1297.

62. R. A. Smith, Semiconductors, 2nd Edition, Cambridge University Press, 1976.

63. Benjamin Lax and J. G. Mavroides, "Statistics and Galvanomagnetic Effects in Germanium and Silicon with Warped Energy Sources," Physical Review, December 1955, pp. 1650-1657.

64. J. G. Mavroides and Benjamin Lax, "Magnetoresistance of Holes in Germanium and Silicon with Warped Energy Sources," Physical Review, September 1957, pp. 1530-1534.

65. R. Baron, M. H. Young, J. K. Neeland, and O. J. Marsh, "A New Acceptor Level in Indium-Doped Silicon," Applied Physics Letters, 1977, p. 594. Also appeared in Semiconductor Silicon 1977, H. R. Huff and E. Sirtl, eds., The Electrochemical Society, Princeton, 1977.

66. L. Elstner, "Die Temperaturabhangigkeit der Defektelektronenbeweglichkeit in Siliziumkristallen," Physica Status Solidi, 1966, pp. 139-150.

67. P. Lawaetz, "Long-Wavelength Phonon Scattering in Nonpolar Semiconductors," Physical Review, July 1969, pp. 730-739.

68. Melvin Lax, Symmetry Principles in Solid State and Molecular Physics, John Wiley & Sons, New York, 1974.

*USGPO: 1983-659-062-953


TE
MED